Oklahoma Department of Transportation
200 NE 21st Street, Oklahoma City, OK 73105-3204

FINAL REPORT ~ FHWA-OK-15-04

THE EFFECTS OF SOIL SUCTION ON SHALLOW SLOPE STABILITY

Gerald A. Miller, Ph.D., P.E.
Amy B. Cerato, Ph.D., P.E.
Arash Hassanikhah, Ph.D. Student
Maryam Varsei, M.Sc.
Roy Doumet, M.Sc.
Céline Bourasset, M.Sc.
School of Civil Engineering and Environmental Science
Gallogly College of Engineering
The University of Oklahoma
Norman, Oklahoma

Rifat Bulut, Ph.D., P.E.
School of Civil and Environmental Engineering
College of Engineering, Architecture and Technology
Oklahoma State University
Stillwater, Oklahoma

December 2015

Oklahoma Department
of Transportation

Transportation Excellence through
Research and Implementation

ODOT-spr@odot.org

Office of
Research & Implementation

THE EFFECTS OF SOIL SUCTION ON SHALLOW SLOPE STABILITY

FINAL REPORT ~ FHWA-OK-15-04
ODOT SP&R ITEM NUMBER 2160

Submitted to:
John R. Bowman, P.E.
Director of Capital Programs
Oklahoma Department of Transportation

Submitted by:
Gerald A. Miller, Ph.D., P.E.
Amy B. Cerato, Ph.D., P.E.
Arash Hassanikhah, Ph.D. Student
Maryam Varsei, Ph.D. Student
Roy Doumet, M.S. Student (Graduated)
Céline Bourasset, M.S. Student (Graduated)
School of Civil Engineering and Environmental Science (CEES)
The University of Oklahoma
Rifat Bulut, Ph.D., P.E.
School of Civil and Environmental Engineering
Oklahoma State University

Oklahoma Department of Transportation

December 2015

TECHNICAL REPORT DOCUMENTATION PAGE

1. REPORT NO. **FHWA-OK-15-04**	2. GOVERNMENT ACCESSION NO.	3. RECIPIENTS CATALOG NO.
4. TITLE AND SUBTITLE **The Effects of Soil Suction on Shallow Slope Stability**		5. REPORT DATE **December 2015** 6. PERFORMING ORGANIZATION CODE
7. AUTHOR(S) **Gerald A. Miller, Amy B. Cerato, Arash Hassanikhah, Maryam Varsei, Roy Doumet, Céline Bourasset, Rifat Bulut**		8. PERFORMING ORGANIZATION REPORT
9. PERFORMING ORGANIZATION NAME AND ADDRESS **University of Oklahoma, School of Civil Engineering and Environmental Science, 202 West Boyd Street, Room 334 Norman, OK 73019**		10. WORK UNIT NO. 11. CONTRACT OR GRANT NO. **ODOT SP&R Item Number 2160**
12. SPONSORING AGENCY NAME AND ADDRESS **Oklahoma Department of Transportation, Materials and Research Division, 200 N.E. 21st Street, Room 3A7 Oklahoma City, OK 73105**		13. TYPE OF REPORT AND PERIOD COVERED **Final Report** **Oct. 2011-Dec. 2015** 14. SPONSORING AGENCY CODE
15. SUPPLEMENTARY NOTES		

16 . ABSTRACT

Research work described in this report was undertaken to improve understanding of desiccation cracking and shallow slope failures in clayey slopes subjected to seasonal variations in weather. Research involved field and laboratory testing and computer modeling. Two test sites where shallow slope failures had occurred were instrumented with weather monitoring equipment and sensors to measure variations in soil moisture. The purpose was to examine the variations in soil moisture, and hence shear strength, as a function of time and depth. A primary goal was to evaluate two commercially available computer programs with respect to their ability to predict soil moisture changes and suction. Results of the study indicated that reasonable predictions of soil moisture changes due to weather are possible with commercial software but considerable effort is needed for parameter determination, model calibration and validation. Unsaturated seepage analyses provided insight into pore water pressure development in the slopes considering the impact of desiccation cracking. The results suggest that desiccation cracks may increase the mass hydraulic conductivity of the near surface soils by one to two orders of magnitude. Further, results of seepage analyses suggest that upper layers of the slope soil profile may become nearly saturated in some areas with positive pore water pressure developing over a significant portion of the failure surface. Unsaturated slope stability analyses were conducted using the predicted pore pressure distributions from unsaturated seepage models and unsaturated strength parameters determined from suction-controlled direct shear tests on compacted soil. In addition, traditional slope stability analyses were conducted using drained shear strength parameters and assumed positive pore pressures. Both methods provided reasonable predictions of the failure conditions (factor of safety of 1) for the two sites; however, both have advantages and disadvantages relative to one another. A simple method of predicting the depth of desiccation cracks in compacted soil was developed based on linear elastic theory and shows promise relative to observations at one of the test sites. Tensile strengths used in crack depth predictions were based on measurements in a new apparatus developed and manufactured at the University of Oklahoma. Theoretical predictions of tensile strength based on a micro-structural effective stress model compared favorably to measured strengths.

17. KEY WORDS **slope stability, suction, unsaturated seepage, tensile strength, desiccation cracks, weather, climate**	18. DISTRIBUTION STATEMENT **No restrictions. This publication is available from the Materials and Research Div., Oklahoma DOT.**		
19. SECURITY CLASSIF. (OF THIS REPORT) **Unclassified**	20. SECURITY CLASSIF. (OF THIS PAGE) **Unclassified**	21. NO. OF PAGES **191**	22. PRICE **N/A**

SI* (MODERN METRIC) CONVERSION FACTORS

APPROXIMATE CONVERSIONS TO SI UNITS				
SYMBOL	**WHEN YOU KNOW**	**MULTIPLY BY**	**TO FIND**	**SYMBOL**
		LENGTH		
in	inches	25.4	millimeters	mm
ft	feet	0.305	meters	m
yd	yards	0.914	meters	m
mi	miles	1.61	kilometers	km
		AREA		
in^2	square inches	645.2	square millimeters	mm^2
ft^2	square feet	0.093	square meters	m^2
yd^2	square yard	0.836	square meters	m^2
ac	acres	0.405	hectares	ha
mi^2	square miles	2.59	square kilometers	km^2
		VOLUME		
fl oz	fluid ounces	29.57	milliliters	mL
gal	gallons	3.785	liters	L
ft^3	cubic feet	0.028	cubic meters	m^3
yd^3	cubic yards	0.765	cubic meters	m^3
		NOTE: volumes greater than 1000 L shall be shown in m^3		
		MASS		
oz	ounces	28.35	grams	g
lb	pounds	0.454	kilograms	kg
T	short tons (2000 lb)	0.907	megagrams (or "metric ton")	Mg (or "t")
		TEMPERATURE (exact degrees)		
°F	Fahrenheit	5 (F-32)/9 or (F-32)/1.8	Celsius	°C
		ILLUMINATION		
fc	foot-candles	10.76	lux	lx
fl	foot-Lamberts	3.426	candela/m^2	cd/m^2
		FORCE and PRESSURE or STRESS		
lbf	poundforce	4.45	newtons	N
lbf/in^2	poundforce per square inch	6.89	kilopascals	kPa

APPROXIMATE CONVERSIONS FROM SI UNITS				
SYMBOL	**WHEN YOU KNOW**	**MULTIPLY BY**	**TO FIND**	**SYMBOL**
LENGTH				
mm	millimeters	0.039	inches	in
m	meters	3.28	feet	ft
m	meters	1.09	yards	yd
km	kilometers	0.621	miles	mi
AREA				
mm^2	square millimeters	0.0016	square inches	in^2
m^2	square meters	10.764	square feet	ft^2
m^2	square meters	1.195	square yards	yd^2
ha	hectares	2.47	acres	ac
km^2	square kilometers	0.386	square miles	mi^2
VOLUME				
mL	milliliters	0.034	fluid ounces	fl oz
L	liters	0.264	gallons	gal
m^3	cubic meters	35.314	cubic feet	ft^3
m^3	cubic meters	1.307	cubic yards	yd^3
MASS				
g	grams	0.035	ounces	oz
kg	kilograms	2.202	pounds	lb
Mg (or "t")	megagrams (or "metric ton")	1.103	short tons (2000 lb)	T
TEMPERATURE (exact degrees)				
°C	Celsius	1.8C+32	Fahrenheit	°F
ILLUMINATION				
lx	lux	0.0929	foot-candles	fc
cd/m^2	candela/m^2	0.2919	foot-Lamberts	fl
FORCE and PRESSURE or STRESS				
N	newtons	0.225	poundforce	lbf
kPa	kilopascals	0.145	poundforce per square inch	lbf/in^2

*SI is the symbol for the International System of Units. Appropriate rounding should be made to comply with Section 4 of ASTM E380.

TABLE OF CONTENTS

LIST OF TABLES

LIST OF FIGURES

SUMMARY

Shallow slope failures in roadway cuts and embankments are frequent problems along Oklahoma highways and many other States; they represent a significant burden on maintenance budgets. Often these failures are associated with clayey soils having relatively high plasticity. Generally, during construction these soils have high shear strength, a stiff consistency, and produce stable slopes. However, over time the soils experience cyclic wetting and drying resulting in a net increase in soil moisture content and corresponding decrease in shear strength due to softening and loss of suction. Eventually, the reduction in shear strength results in a slope failure usually after a period of significant wetting. Exacerbating the problem are desiccation cracks that develop during extreme drying periods allowing water to penetrate the soil deeper and faster. Shallow slope failures in clayey soils are widespread and poorly understood and very little research has been conducted to provide guidance on how to address desiccation cracking in slope stability analyses.

Research work described in this report was undertaken to improve understanding of desiccation cracking and shallow slope failures in clayey slopes subjected to seasonal variations in weather. Research involved field and laboratory testing and computer modeling. Two test sites where shallow slope failures had occurred were instrumented with weather monitoring equipment and sensors to measure variations in soil moisture. The purpose was to examine the variations in soil moisture, and hence shear strength, as a function of time and depth. A primary goal was to evaluate two commercially available computer programs with respect to their ability to predict soil moisture changes and suction. Understanding how soil moisture changes in shallow slopes in response to weather is critical to predicting temporal variations in stability.

Results of the study indicate that reasonable predictions of soil moisture changes due to weather are possible with commercial software but considerable effort is needed for parameter determination, model calibration and validation. Unsaturated seepage analyses provided insight into pore water pressure development in the slopes considering the impact of desiccation cracking. The results suggest that desiccation cracks may increase the mass hydraulic conductivity of the near surface soils by one to two orders of magnitude. Further, results of seepage analyses suggest that upper layers of the slope soil profile may become nearly saturated in some areas with positive pore water pressure developing over a significant portion of the failure surface.

Unsaturated slope stability analyses were conducted using the predicted pore pressure distributions from unsaturated seepage models and unsaturated strength parameters determined from suction-controlled direct shear tests on compacted soil. In addition, traditional slope stability analyses were conducted using drained shear strength parameters from triaxial testing on field samples and direct shear testing on fully softened compacted specimens, and assumed positive pore pressures (based on pore pressure ratio). Both methods provided reasonable predictions of the failure conditions (factor of safety of 1) for the two sites; however, both have advantages and disadvantages relative to one another.

A simple method of predicting the depth of desiccation cracks in compacted soil was developed based on linear elastic theory. The method allows one to estimate the change in suction required to cause cracking at a particular depth based on the tensile strength of the soil. By comparing the expected changes in suction within the active zone of a soil profile to the suction changes required to cause cracking at each depth, reasonable estimates of the depth of cracking may be obtained. The method shows promise relative to observations at one of the test sites where sufficient field measurements of soil moisture content were available to reasonably establish the active depth. The thickness of the surface soil layer with enhanced hydraulic conductivity used in seepage analyses was based in part on the crack depth predictions.

Tensile strengths used in crack depth predictions were based on measurements in a new apparatus developed and manufactured at the University of Oklahoma. This first generation device is unique in that it allows for the determination of tensile strength while the soil is desiccating. It was used to study the influence of dry density and moisture content on the tensile strength of composite soil samples obtained from the two test sites. Theoretical predictions of tensile strength based on a micro-structural effective stress model compared favorably to measured strengths.

Chapter 1 INTRODUCTION

1.1 Problem Statement

Shallow slope failures in roadway cuts and embankments are frequent problems along Oklahoma highways and many other States; they represent a significant burden on maintenance budgets. Often these failures are associated with clayey soils having relatively high plasticity. Generally, during construction these soils have relatively high shear strength, a stiff consistency, and produce stable slopes. However, over time the soils experience cyclic wetting and drying resulting in a net increase in soil moisture content and corresponding decrease in shear strength. Eventually, the reduction in shear strength results in a slope failure usually after a period of significant wetting. Exacerbating the problem are desiccation cracks that develop during extreme drying periods allowing water to penetrate the soil deeper and faster.

The loss of shear strength in clayey soils due to wetting is associated with two inter-related phenomena. First, as the moisture content is increased the matric suction is reduced, which reduces the intergranular or effective stress in the soil. Decreasing effective stress equates to reduced shear strength. Second, as the moisture content increases the diffuse double layers surrounding clay particles expand and take on water with a corresponding increase in soil void ratio. Reduced dry density and increased water content results in softening and substantially lower shear strength. An additional consequence of wetting is that the driving mass of the soil increases with increased moisture content. Thus, while shearing resistance (or strength) is decreasing, imposed gravitational shearing stresses and cumulative strain are increasing, further reducing the slope stability.

Shallow slope failures in clayey soils are widespread and poorly understood and very little research has been conducted to provide guidance on how to address desiccation cracking in slope stability analysis. Research work described in this report was undertaken to improve understanding of desiccation cracking and shallow slope failures in clayey slopes subjected to seasonal variations in weather.

1.2 Overview of Research

Research described in this report was conducted to help engineers better understand and predict shallow slope stability to implement preventive measures if necessary. Research involved field and laboratory testing and computer modeling. Two test sites where shallow slope failures had occurred were instrumented with weather monitoring equipment and sensors to measure variations in soil moisture. The purpose was to examine the variations in soil moisture, and hence shear strength, as a function of time and depth. A primary goal was to evaluate two commercially available computer programs with respect to their ability to predict soil moisture changes. Understanding how soil moisture changes in shallow slopes in response to weather is critical to predicting temporal variations in stability.

Laboratory testing focused on basic soil characterization, evaluating shear strength, hydraulic conductivity and soil water characteristic behavior of the soil. The purpose was to provide the necessary parameters to populate models for predicting climate variation induced changes in soil moisture and slope stability. In addition, an in depth investigation of tensile strength associated with desiccation cracking was conducted in a newly developed apparatus for studying crack development under drying conditions.

Modeling was conducted using software to predict variations in soil moisture content and stability. Two commercially available programs were used for soil moisture modeling: Vadose/W and SVFlux. Limit equilibrium slope stability analyses were conducted using the software SVSlope. Slope stability analyses were conducted to examine how factors of safety vary in response to moisture content and suction changes, and under different hydrologic and drainage conditions. Additionally, the governing shear strength corresponding to different soil states was investigated through slope stability analyses.

1.3 Research Objectives and Tasks

Three primary objectives of the research were: 1) To provide geotechnical engineers with recommendations for predicting stability of cut slopes and embankment slopes composed of unsaturated soil, incorporating soil moisture condition and suction into the analysis. 2) To provide geotechnical engineers with recommendations for predicting changes in soil moisture conditions and suction in slopes as a function of expected weather/climate conditions so that a proper "design moisture condition" can be selected. This will also allow for predicting the slope stability over time based on predicted moisture content changes. 3) To provide recommendations to minimize the climate impacts on slope stability including, as necessary, reducing adverse impacts of desiccation cracking in clayey materials.

Results of this research provide engineers with tools for improved analysis of shallow slope stability and recommendations for preventing failures. To achieve the project objectives many tasks were completed as follows.

1. An extensive search of the literature was conducted to gather published information relevant to shallow slope stability, desiccation cracking, and modeling of soil moisture variations in the vadose zone.
2. Two test sites were identified with assistance of ODOT personnel. Instrumentation was installed to monitor primary weather parameters and soil moisture content at different depths. Instruments were monitored for two years while numerous site visits occurred to collect soil samples, make observations, download data and conduct site maintenance.
3. Basic soil testing was conducted to determine engineering properties of the soils needed for classification and phase relationship calculations.
4. Soil Water Characteristic Curve Testing was performed to determine the relationship between suction and water content for samples from different depths at each test site.
5. Moisture flow testing via one dimensional diffusion and back-pressure saturated flexible wall hydraulic conductivity testing was carried out.
6. Testing was conducted to determine soil shear strength including back-pressure saturated triaxial compression tests, direct shear tests, saturated and unsaturated conditions, undisturbed and remolded samples, and fully softened soil states.

7. Development of a new device to study desiccation crack development. The new device was used to determine the tensile strength of the soil under drying conditions. Effects of initial dry density and initial water content were investigated using the device for soils obtained from the two test sites.
8. Extensive modeling of soil moisture profiles using weather data as input was conducted to evaluate the predictive capability of two commercially available software programs Vadose/W and SVFlux.
9. Numerous slope stability analyses were conducted for the two test sites using SVSlope software to evaluate the most appropriate strength parameters and hydraulic assumptions for modeling shallow slope stability.
10. Recommendations for predicting design moisture conditions in slopes and for determining governing strengths and hydraulic conditions for slope stability analysis were developed. Preliminary recommendations for addressing the influence of desiccation cracking were included among suggestions for modeling shallow slope stability.

1.4 Organization of Report

In Chapter 2 results of the literature review are presented. Chapter 3 contains descriptions of the two tests sites, instrumentation installed to monitor weather and soil moisture, soil sampling and field measurements, laboratory testing methods and software used to model soil moisture variations and slope stability. The development of the desiccation test box is described in Chapter 4 along with details of the testing procedure and results for soils obtained from the two test sites. Chapter 5 is used to present the weather and soil moisture instrumentation data obtained during the nearly two years of monitoring at each test site. In addition, results of soil moisture modeling are presented in Chapter 5. In Chapter 6 the results of laboratory testing are presented and in Chapter 7 are the results slope stability modeling. Finally, Chapter 8 provides conclusions and recommendations for additional research and recommendations for practice. Tables and Figures are placed at the end of corresponding chapters.

Chapter 2 LITERATURE REVIEW

2.1 Introduction

The literature presented in this chapter focuses on shallow slope stability, moisture flux modeling and desiccation cracking. There is vast amounts of information in the literature on these topics. Some of the more pertinent references are discussed in this Chapter.

2.2 Shallow Slope Stability

Stability of shallow slopes has been a particular focus of several researchers including Aubeny and Lytton 2004, Kim and Lee 2010, and Ray et al. 2011. Shallow landslides studied by Aubeny and Lytton 2004, were modeled considering seepage conditions with constant suction on the slope surface that produces a destabilizing hydraulic gradient with a component of flow in the upward direction. Since these slope failures occurred in soil with effective friction angles more than the natural slope angle, they reasoned that the slope failure may result from a destabilizing hydraulic gradient, which became critical after many years of infiltration. Aubeny and Lytton (2004) indicated that the shallow slope failures generally occurred after 12 to 31 years in the cases they studied and that the time required for failure depends on development of desiccation cracks and rate of moisture diffusion into the slope. Their conclusions were based on results of infinite slope analysis considering pore water pressure effects partly attributed to unsaturated seepage under the destabilizing hydraulic gradient.

The study by Kim and Lee (2010) involved a one-dimensional infiltration model and emphasized the importance of the wetting depth in analyzing the slope stability.

Ray et al. (2011) developed infinite slope stability methods that account for the effect of soil moisture changes on slope instability based on the unsaturated zone soil moisture, saturated soil thickness, and soil physical properties.

Studies conducted by Rahardjo et al. (2007) have emphasized the important role of permeability in high plasticity soils. In these soils where the permeability is very low, the infiltration of water is much slower so they are less sensitive to short rainfall events. However, the rate of recovery for the factor of safety is also slower for low permeability soils. As a result, long and/or repeated rainfall events may be necessary to fail the slope. The authors concluded their study by stating that the slopes with high permeability usually fail as a consequence of a rising of the water table while the low permeability soil would likely fail due to a reduction in matric suction of the soil located above the water table.

2.3 Shear Strength Governing Shallow Slope Stability

Slopes may fail under drained or undrained conditions depending on the rate of loading and importance of shear induced excess pore water pressures. Thus, slope stability analyses are typically conducted using effective stress strength (“drained strength”) parameters for the drained case or undrained shear strength where shear-induced excess pore water pressures are important. It is also possible to analyze the undrained case using effective stress analysis with consideration of shear-induced excess pore water pressures in addition to the ambient pore water pressures normally considered in a drained scenario.

Undrained shear strength is represented by a single parameter (s_u or c_u), and used in a total stress analysis with an assumed total stress friction angle of zero. Hence, the failure envelope is independent of stress level and represented simply by the equation,

$$\tau_{ff}=c_u \tag{2.1}$$

where τ_{ff} is the shear stress on the failure plane at failure. Note that while the total stress analysis is performed without consideration of effective stresses, the value of s_u is strongly dependent on initial effective stress conditions and should be determined accordingly. On the other hand, the effective stress analysis requires the effective stress strength parameters (friction angle, ϕ', and cohesion, c') to be known as well as the effective stress normal to the failure plane at failure (σ'_{ff}). The effective stress analysis makes use of a failure envelope represented by the equation,

$$\tau_{ff}=\sigma'_{ff}\tan\phi'+c' \tag{2.2}$$

Shear strength, τ_{ff}, depends on the effective stress, which is equal to the total stress (σ_{ff}) minus the pore water pressure at failure (u_f); or

$$\tau_{ff}=(\sigma_{ff}-u_f)\tan\phi'+c' \tag{2.3}$$

Thus, u_f in a “drained analysis” would be equal to the ambient, steady state, pore water pressure in the slope at the time of failure. However, if the effective stress analysis is used to model an undrained problem, then u_f must also include shear-induced excess pore water pressures.

There are basically three representations of shear strength associated with drained strength failure envelopes that have traditionally been used in slope stability analyses: the peak shear strength, the residual shear strength and the fully softened shear strength (Duncan et al. 2011). These strengths are represented by effective stress friction angle and cohesion intercepts corresponding to different soil states that may exist under field conditions. These strengths do not account for the influence of matric suction on shear strength of unsaturated soils. Thus, an implicit assumption in the use of these strengths for clayey soils is that the soil is saturated. A fourth approach is to use an unsaturated shear strength model that accounts for the strength contribution from soil suction.

2.3.1 Peak Shear Strength

The peak shear strength is also called “intact strength” and corresponds to the maximum strength a soil can reach for a given initial moisture content and dry density. It essentially represents an upper bound shear strength relative to existing soil conditions in the field. The peak shear strength is time-dependent and occurs before the fully softened condition is reached (Mesri and Shahien 2003). Mesri and Shahien (2003) showed that there can be a wide variation in the shear strength under the same effective normal stress, as the soil may have experienced different degrees of softening during its history. Existing shear strength can be obtained by conducting triaxial tests on undisturbed samples. For compacted soils, the peak shear strength can be obtained by running triaxial or direct shear tests that recreate the moisture content and compaction (i.e., dry density) used on-site.

2.3.2 Fully Softened Shear Strength

The soil softens as a result of external factors, such as weather. The infiltration and loss of water due to wetting/drying is responsible for the swelling/shrinking of the soil and these variations of volume soften the soil. The phenomenon of softening leads to a decrease in the initial as-compacted shear strength (i.e., the peak shear strength) to the fully softened shear strength (Skempton 1970). Recent studies have shown that slope failures occurring in compacted fill are mostly shallow failures due to a softening of the soil. This is especially true for high plasticity clay embankments in regions where weather can induce desiccation cracks. Because of these cracks, water is able to enter deeper and faster into the soil.

Fully softened shear strength is stress-dependent and is a function of the type of clay mineral and quantity of clay size particles. Field observations indicate that the fully softened strength can be mobilized around excavations in fissured clays (Skempton 1977) and in desiccated, cracked, and weathered compacted clay embankments, where infiltration of water along cracks results in higher water contents and void ratios (Wright et al. 2007).

The fully softened shear strength corresponds to a new failure envelope, which seems to be similar to the failure envelope for normally consolidated clays (Skempton 1970). It can be estimated from the peak strength obtained from shear tests run on reconstituted normally consolidated specimens (Mesri and Shahien 2003). In their study, Stark and Duncan (1991) showed that compacted, wetted soils have a behavior very similar to normally consolidated soils, as wetting tends to erase the stress history of soil. The friction angle of a soil subjected to wetting and drying cycles tends to be similar to the shear strength of normally consolidated clay. Observed failure envelopes are curved, which means that the friction angles vary with normal stress. There is no cohesion and the friction angle is higher for extremely low stresses (Kayyal and Wright 1991).

Different procedures have been proposed to create fully softened specimens. Kayyal and Wright (1991) subjected remolded specimens to cycles of wetting and drying before shearing using a triaxial apparatus. Another procedure consisting of preparing specimens at water contents equal to the liquid limit was also proposed (Castellanos et al. 2013). In this procedure, the soil is soaked in distilled water before being processed through a sieve. As the water content is very high at this point, the soil is air-dried to its liquid limit before being poured in the shear box. In the present research, these two methods were tried to assess the fully softened shear strength. It is a variation of the first procedure that gave the most satisfactory results.

The tests necessary to assess the shear strength of a soil are time consuming and expensive. As a result, efforts have been made to correlate the fully softened and residual shear strengths with basic soil properties. Stark and Eid (1997) found that the secant fully softened shear strength decreases with an increasing liquid limit and clay size fraction. A higher clay size fraction results in particles that are more prone to face to face interaction, resulting in lower shear strength. Stark and Hussain (2012) proposed empirical correlations for the drained shear strength for slope stability analyses as a function of effective normal stress, liquid limit and clay size fraction. They classify the soil into three different groups using clay size fractions (less than 20%, between 25% and 45% and more than 50%).

The fully softened shear strength is usually used for analyzing stability of first time slope failures, as prescribed by Wright et al (2007). However, studies conducted on first-time slope failures suggest that the strength can be lower than the fully softened shear strength (Stark and Eid 1997). Similar observations have been made by Mesri and Shahien (2003) who suggested that the fully softened shear strength should be used for most of first time slope failures; however, in some cases part of the slip surface of these slopes at failure may already be at residual conditions resulting from rather small displacements.

2.3.3 Residual Shear Strength

The residual shear strength is considered the lowest shear strength a soil can reach under field conditions through degradation by environmental factors and shearing. It corresponds to a state were the particles are reoriented parallel to the direction of shearing, which offers the least resistance. Residual conditions are associated with existing failure surfaces where shearing has produced a nearly parallel alignment of particles. However, in the aforementioned study, Mesri and Shahien 2003 explain that residual conditions may be present on part of the slip surface for first time slope failures due to the geological history of the soil. The presence of structural discontinuities tends to localize shear strains (Mesri and Shahien 2003). In these specific zones, only small shear displacements may be necessary to fail the soil to residual conditions. The residual condition corresponds to a state where the plate-shaped and elongated particles are oriented in the direction of shearing. A predominantly face to face interaction results in a decrease in shear resistance (Mesri and Cepedia-Diaz 1986).

In summary, it is often difficult to know with certainty which shear strength, peak, fully softened or residual should be used to run stability analyses. The infiltration of water leads to changes in volume that soften the soil and potential displacements and/or discontinuities in the soil lead to a rearrangement of the particles. As it is not possible to know with certainty everything the soil has been subjected to, these different values of shear strength should be obtained and their pertinence and use should be evaluated in light of the geologic history and expected changes of the soil under field conditions. While the peak, fully softened and residual shear strength provide a means of bounding the slope stability problem, they represent fully saturated conditions and do not account for the possibility of failure under unsaturated conditions.

2.3.4 Unsaturated Shear Strength

Embankment and cut slopes are often in an unsaturated state prior to wetting events leading up to failure. While it may be reasonable to evaluate long term stability by assuming saturated conditions, to accurately determine the existing stability of a slope or the evolution of stability over time, it is necessary to consider shear strength of the soil under unsaturated conditions. Additionally, it is possible that slopes may fail when significant portions of the failure surface are in an unsaturated condition. There are various models proposed to represent the strength envelope of unsaturated soil, but most are of the form:

$$\tau_{ff}=(\sigma_{ff}-u_{af})\tan\phi'+f(u_{af}-u_{wf})+c' \qquad \textbf{(2.4)}$$

where σ_{ff} is the total normal stress on the failure plane at failure, u_{af} is the pore air pressure on the failure plane at failure, $\sigma_{ff}-u_{af}$ is the net normal stress, u_{wf} is the pore water pressure at failure, u_{af}-u_{wf} is the matric suction on the failure plane at failure, f(u_{af}-u_{wf}) is the component of shear strength that depends on matric suction, and, ϕ' and c' are effective stress strength parameters as defined previously. Models for the suction dependent component of strength, f(u_{af}-u_{wf}), are generally non-linear functions of suction on account of the variation in liquid-solid-air interfacial areas in the unsaturated soil (e.g. Vanapalli et al. 1996, Hamid and Miller 2009, Khoury and Miller 2012). A simple bilinear model was presented by Fredlund and Rahardjo (1993):

$$\tau_{ff}=(\sigma_{ff}-u_{af})\tan\phi'+(u_{af}-u_{wf})\tan\phi^b+c' \qquad \textbf{(2.5)}$$

$$\text{for } (u_{af}-u_{wf})\leq(u_a-u_w)_b; \qquad \tan\phi^b=\tan\phi'$$

$$\text{for } (u_{af}-u_{wf})>(u_a-u_w)_b; \qquad \tan\phi^b=\text{constant}<\tan\phi'$$

where $(u_a-u_w)_b$ is the air entry suction for the soil, which corresponds to the point at which the soil begins to desaturate (i.e. S<100%). The friction angle, ϕ^b, determines the contribution of shear strength from matric suction; it is less than ϕ' on account of the decrease in solid-water interfacial area within the soil that occurs for degree of saturation (S) less than 100%. Equation 2.5 can be simplified for use in traditional limit equilibrium analyses of ϕ-c soils by combining the effective stress cohesion and suction dependent component of strength into a single cohesion term, c:

$$c=(u_{af}-u_{wf})\tan\phi^b+c' \qquad \textbf{(2.6)}$$

Thus, Equation 2.5 becomes,

$$\tau_{ff}=(\sigma_{ff}-u_{af})\tan\phi'+c \qquad \textbf{(2.7)}$$

Use of Equations 2.6 and 2.7 requires the suction on the failure surface be known as well as the pore air pressure at failure. For most slope stability problems it is reasonable to assume the pore air pressure remains at atmospheric pressure in the pores (i.e. u_{af}=0 gage pressure) of unsaturated soil. The suction at failure can be estimated by modeling moisture variations in the slope and utilizing a Soil Water Characteristic Curve (SWCC) to estimate suction.

2.4 Unsaturated Soil Slopes and Stability

As stated earlier, a decrease in effective stress occurs when water enters surface cracks and infiltrates unsaturated soil. This is attributed to the decrease of matric suction and results in a loss of shear strength. When this phenomenon happens in a slope, the driving forces may become greater than the resisting forces along some critical failure surface and a failure occurs. Suction is especially important in shallow slope stability because mechanical stresses are small, which means that effective stresses in the soil skeleton are mostly due to suction (Aubeny and Lytton 2002).

To evaluate stability, it is important to understand the mechanism of infiltration to estimate the time necessary for the moisture to diffuse into the soil. This phenomenon is influenced by the nature and structure of the soil. Studies conducted by Rahardjo et al. (2007) have emphasized the important role of permeability in high plasticity soils. In these soils where the permeability is very low, the infiltration of water is much slower so they are less sensitive to short rainfall events. However, the rate of recovery for the factor of safety is also slower for slopes composed of low permeability soils. As a result, long and/or repeated rainfall event(s) may be necessary to fail such slopes. The authors further concluded that slopes with high permeability usually fail as a consequence of a rising water table while the low permeability soil would likely fail due to a reduction in matric suction of the soil located above the water table.

Using a Mohr-Coulomb strength model that incorporates the influence of suction on shear strength, such as Equation 2.7, stability of unsaturated slopes is simply analyzed using any of the limit equilibrium methods for drained analysis of ϕ-c soils. The difficulty is in predicting appropriate values of suction. If suction is assumed to be zero or pore water pressures are assumed to be positive, the analysis is similar to a classical drained approach. Alternatively, suctions can be estimated using an unsaturated seepage model that incorporates the influence of climate; this is discussed in more detail throughout this report.

2.5 Influence of Desiccation Cracking on Shallow Slope Stability

The existence of desiccation cracks in soil has a crucial impact on geotechnical and geo-environmental structures such as dams, embankments, slopes and hydraulic barriers. Soil with cracks is more compressible than its flawless form at the same water content (Morris et al., 1992). The presence of cracks also increases the permeability and hydraulic conductivity of soil and consequently affects the strength of soil and stability of slopes. Existence of cracks, seasonal climate change and frequent occurrence of drying-wetting cycles can reduce the soil strength (Rayhani et al. 2007).

During wetting, desiccation cracks are flow channels that allow water to infiltrate into the soil layers easily and rapidly. This causes the soil suction to decrease and driving forces acting on the slope to increase. Matric suction (negative pore pressure) has a major role in soil strength and loss of suction results in decrease in shear strength and reduction of factor of safety (Aubeny and Lytton 2004; Kamal and Hossain 2010). As the crack depth increases, pore water pressure significantly increases and causes a dramatic reduction in slope stability (Wang et al. 2011).

Yuen et al. (1998) measured the hydraulic conductivity of undisturbed expansive clay using triaxial permeability tests. The specimens were subjected to drying-wetting cycles that produced fissures and cracks. The results showed that the drying-wetting cycles and presence of cracks would cause the hydraulic conductivity to increase approximately by one order of magnitude.

Albrecht and Benson (2001) and Rayhani et al. (2007) studied the effect of desiccation induced cracking on clayey soils by conducting flexible-wall permeameter and falling head tests, respectively. They found that the specimens having higher plasticity index experience higher volume shrinkage, larger number of cracks and therefore higher hydraulic conductivity. The first drying-wetting cycle is observed to have the greatest impact on increase in hydraulic properties and the largest increase occurs in specimens compacted to wet of optimum.

Aubeny and Lytton (2004) proposed two models of slope failure for high plasticity clays, a stability model and a moisture diffusion model, respectively. They suggested that slope failures are mainly associated with a destabilizing hydraulic gradient in the slopes that builds up over many years of infiltration. The primary “evidence” for this assertion is based on the observation that the assumed effective stress friction angle of the soil was greater than the majority of slope angles (inclinations) in the cases they studied. If this was true, then their infinite slope stability equation would in fact suggest that the slopes should be stable unless a “destabilizing hydraulic gradient” existed that caused the failures. The effective stress friction angle used in their analysis was 25 degrees, which as mentioned, is generally larger than most highway slope angles (typical 3H:1V slope has inclination of about 18 degrees measured from horizontal). This friction angle was assumed based on available correlations with plasticity index and is a reasonable normally consolidated friction angle. Based on some convincing evidence in the literature, the authors assumed that fully wetted compacted soils would have soil properties similar to normally consolidated soils. Finally, they suggest that it is unlikely that the friction angle degraded to a residual value because there is no compelling evidence that the large strains necessary to cause friction angle degradation existed for these shallow slopes.

Zhang et al. (2012) employed a centrifuge model to examine the stability of cracked slopes under rainfall conditions. Two crack configurations, one vertical and one inclined, with a certain width and depth were used to investigate the effect of different cracks. Concentrated infiltration through the crack due simulated rainfall of three different intensities was used to study the slope deformation due to seepage of water through the crack. It was concluded that the rainfall penetration intensified in the presence of the crack and decreased further from the crack. The vertical displacements of the slope near the vertical crack were significantly larger than the horizontal displacements due to the significant infiltration, while the difference between the horizontal and vertical displacements were relatively small at the zones far from the crack. The inclined crack induced a larger displacement of the slope than the vertical crack near the slope surface because the inclined crack was closer to the slope surface.

Wang et al. investigated the effects of crack location and depth and rainfall intensity on stability of the slope. They used “Seep/W” and “Slope/W” to analyze the saturated and unsaturated water flow in a cracked soil slope. The results showed that the pore pressure distribution and factor of safety were influenced by the presence of a crack; however, the changes in shallow slope stability were small since the cracks did not coincide with the slip surface. The intense rainfall was also observed to have a large impact in reducing the slope stability.

2.6 Modeling Moisture Variation in Shallow Slopes

Several research projects have studied the factors that cause soil moisture fluctuations in shallow slopes. Generally, these projects use numerical modeling programs that can predict moisture variation and slope failure.

Ram et al. (2011) used an infinite slope stability model and a hydrological model (VIC-3L) to estimate the soil moisture variation in unsaturated soils located in a land surface zone for a series of groundwater table positions, soil thicknesses, surface vegetation and climate conditions. The hydrological model of a soil column showed that the top and middle soil layers demonstrate the dynamic response of the soil to weather conditions and rainfall events, and that lower layers capture the seasonal soil moisture behavior. Results from the hydrological analysis, also showed a strong correlation between the groundwater and the soil moisture values. The predicted soil moisture values and groundwater levels obtained from VIC-3L, were used in the slope stability model to calculate the factors of safety. It was found that the possibility of a slope failing increases with the increase of soil moisture content, the presence of thicker unsaturated zone, and the rise of the ground water level.

Briggs (2010) studied the subject of the impacts of weather change on embankment hydrology. He used a hydrological model that incorporates daily weather data and soil properties to model the changes in pore water pressures in a railway embankment. He compared model predicted pore water pressure variation and site monitored data, and analyzed the distribution of pore water pressure during extreme wet and dry periods. Briggs (2010) noted that piezometer data did not show significant seasonal pore water pressure variation due to the localized effects influenced by vegetation cover and local permeability. These piezometers were located under a surface layer covered by trees where high negative pore water pressures were measured. He added at these locations matric suction in the soil could extend below the rooting zone due to a persistent soil moisture deficit.

A finite element model of the embankment was created using VADOSE/W, to monitor the changes in pore water pressure due to weather conditions. Briggs used the model to study the impact of an extremely dry summer and an extremely wet period on soil moisture near the surface of the embankment. Water input and removal from the surface layer of the model were calculated as a function of the water balance at the surface. Briggs (2010), noted that an extremely wet winter may cause hydrostatic pore water pressures to develop in grass covered areas, while in tree covered areas residual soil suctions may remain at depth. He concluded that weather conditions and slope vegetation cover have a significant impact on embankment pore water pressures.

Other researchers have studied moisture variation in shallow slopes and influence of soil water fluctuations on slope stability. For instance, Paolo et al. (2011), studied the effect of heavy rainfall on shallow landslides using a model called QD-SLaM (Quasi-Dynamic Shallow Landsliding Model). Similarly, Salciarini et al. (2006) used TRIGRS (Transient Rainfall Infiltration and Grid-Based Regional Slope-Stability) to model the distribution of shallow rainfall-induced landslides. This program computes the change in pore water pressure and approximates the effective stress in unsaturated soils. Jones et al. (2009) investigated the long term influence of climate conditions on slope stability by using two numerical models: SVFlux and SVSlope, to study the change in factor of safety over 25 years of flood conditions. However, Jones noted that due to the complexity of the software that was used, errors were found when coupling the two hydrological and geotechnical programs in the analysis.

Simoni et al. (2008), used a hydrological 3-D model, called GEOtop, which models the hydraulic properties of soil and soil moisture, and computes surface runoff and heat flux. These results were used in an infinite slope geotechnical model, called GEOtop-FS, along with the measured soil properties, slope inclination, and soil layer thicknesses. The factor of safety is computed by using the hydrological module, which accounts for 3D-water redistribution and radiation budget to simulate the water flow within the soil and the soil-atmosphere interface.

In addition to the previous modeling applications, Gonzalo el al. (2007), discussed the relationship between groundwater flow, soil, vegetation and the atmosphere through the use of a combined model called RAMS-Hydro. It consists of a climate model, RAMS (Regional Atmosphere Modeling System), and a hydrological model (LEAF2-Hydro). In their research project they highlighted the role of the water table in controlling soil moisture. Whenever the water table was shallow, the soil moisture, in the top layers near the surface and root zones, was high. They explained that the presence of the water table as the lower boundary resulted in upward capillary flux from the water table and was the primary source for dry-period evapotranspiration.

Paolo et al. (2004) used a quasi-dynamic model to simulate the transient hydrological and geotechnical processes responsible for slope stability. They examined the contribution of lateral flow to slope instability by simulating the time dependent formation of a groundwater table in response to rainfall. They noted that both lateral and vertical fluxes are responsible for landslide triggering and stressed the importance to use such models for hazard planning and land management.

Florinsky et al. (2001) used a modeling software called LANDLORD to predict soil properties by digital terrain modeling. They noted that the prediction of soil properties, such as soil moisture, while incorporating the concept of accumulation, transit and dissipation zones can be more successful and appropriate than the prediction based on linear regression. Qiu et al. (2000), on the other hand, used a non-linear analysis that was used in ecological studies and soil-environmental research and called DCCA (Detrended Canonical Correspondence Analysis) to model the profile distribution of time-averaged soil moisture content. They classified the soil moisture content into three types: decreasing-type, waving-type and increasing type, and grouped the temporal dynamics of soil moisture content based on topography.

Other types of soil moisture related projects such as ESTAR were also used to study the soil moisture variation by using remote sensing footprints with varying soil, slope and vegetation. Mohanty et al. (2001) used this method based on air-borne passive microwave remote sensors to measure soil moisture and other characteristics such as the topography, vegetation and climate at a scale of hundred square kilometers. Hong et al. (2015) developed a physical model named SLIDE to predict the rainfall-induced landslides using the remotely sensed and in-situ data. The model was able to predict a direct relationship between the factor of safety and rainfall depth using modified assumptions on water seepage.

2.7 Field Monitoring of Moisture Variation in Slopes

Li et al. (2005) worked on monitoring soil moisture and matric suction variations in a saprolite slope. They installed a full-scale data acquisition system to monitor the moisture content, matric suction, pore-water pressure, horizontal earth pressure, and rainfall. Several monitoring instruments were used such as: soil moisture probes, tensiometers, piezometers, inclinometers, earth pressures cells, and rain gauge (tipping bucket). A dipmeter and inclinometer were also used to measure, respectively, the groundwater levels and horizontal displacements. The purpose of their study was to reveal the surface infiltration process before and during the excavation of a cut. The movement of the wetting front was different depending on the rainfall pattern. They noted that the maximum wetting front during the wet season was limited to the upper 9 to 10 feet. Li et al. (2005) concluded that the wetting front analysis shows that Lumb's unsaturated wetting band theory could be used to assess the movement of the wetting front in the unsaturated profile.

Other advanced methods have been used for studying the near-surface moisture variation in shallow slope surfaces such as the work done by Yang et al. (2012) who used the microwave radiometry as a global remote sensing tool to study the distribution of vegetation, moisture, surface and canopy temperature. They noted that microwave brightness could be used to update the hydrological models, and to characterize the topographical variations of deep soil moisture. Yang et al. (2012) noted after comparing results of soil moisture dynamics in shallow and deep layers that topographic factors like slope position and aspect only affect the soil moisture content in shallow layers. Moreover, Yeakley at al. (1998), used a time domain reflectometry (TDR) network to study soil moisture gradients in a slope. They showed that both topography and soil properties play important roles in soil moisture dynamics.

Chapter 3 FIELD, LABORATORY AND ANALYSIS METHODS

3.1 Test Sites

Two tests sites were identified for field and laboratory investigations of shallow slope stability. On one site was an embankment slope while on the other was a cut slope. Both of these sites were selected with assistance from the Oklahoma Department of Transportation (ODOT) Materials Division and at both sites shallow slope failures had occurred in the past. The sites are located in central Oklahoma in Chickasha and southeast Oklahoma near Idabel.

The slope at the Chickasha site is part of a roadway embankment. The bedrock geology of this region is classified as middle Permian age and mostly consists of red-brown silty shale with some fine-grained sandstone. The soil of this region is primarily medium to highly plastic clay.

The Idabel site contains a cut slope. The soils of this region are formed of colluvial sediments over limestone and known as residual, highly plastic clay with a significant shrink-swell potential.

3.2 Test Site Field Instrumentation for Monitoring Weather and Soil Moisture

Initial field work at Chickasha began in August, 2012 and the fully functional weather station was installed and began collecting data on August 31, 2012. The weather station manufactured by Campbell Scientific instruments includes sensors to quantify rainfall, air temperature, relative humidity, wind speed, wind direction, solar radiation, and volumetric water content at three depths in the soil profile. This weather station was installed on the slope face about half-way between the toe and the crest.

A similar weather station was installed at the Idabel Site, except that the location was at the top of the slope. This installation occurred on October 19, 2012 at which time data collection began. A remote access modem was installed on the data logger in Idabel so that data could be retrieved on computers in Norman. A photograph of the weather station installed at Idabel is shown in Figure 3.1. A list of sensors and measurement ranges is provided in Figure 3.2.

3.3 Soil Sampling and Field Testing

Hand auger borings were performed to depths of 6.0 ft. and samples were collected for moisture content determination and soil property tests. In addition, Shelby tubes were driven in the slope from the ground surface to depths of 4.0 ft. to provide samples for determining shear strength, hydraulic conductivity and moisture diffusion properties. Bulk samples were collected in 5-gallon buckets for compaction and desiccation testing.

3.4 Laboratory Testing Methods

3.4.1 Basic Soil Properties

Laboratory testing has been conducted to determine basic physical and index properties. Grain-size distribution and liquid and plastic limit tests were conducted in general accordance with ASTM standards (D422, D4318) on samples obtained at depths down to 6.0 ft. Results of these tests were used to classify the soils making up the embankment slope. Bar linear shrinkage tests were conducted to determine the shrinkage limit and linear shrinkage (B.S. 1377). Standard compaction tests were conducted on samples obtained from depths up to 6.0 ft. to determine maximum dry density and optimum water content in accordance with ASTM Standard D698. Specific gravity was determined on selected samples in accordance with ASTM Standard D854.

3.4.2 Soil Water Characteristic Curve (SWCC) Testing

Two testing devices were used to produce soil water characteristic curves (SWCC) of test soils: the WP4 Dewpoint Potentiometer manufactured by Decagon and a custom made axis translation test cell (shown in Figure 3.3) designed and built at the University of Oklahoma (Khoury 2010).

The WP4 measures total water potential (total suction) using the chilled mirror method to determine the relative humidity of the air above a sample in a closed chamber. The relative humidity above the sample is assumed to be at equilibrium with the air in the sample. At temperature equilibrium, relative humidity is directly related to water potential. Total suctions in a range of about 1 to 450 MPa (145 to 65,265 psi) can be practically determined with this method.

In the axis translation method, the pore water and pore air pressures are accurately controlled using two commercially available high precision motorized piston pumps. The computer controlled system of pumps and sensors can determine pressure and volume changes to a resolution on the order of 1 kPa (0.145 psi) and 1 mm^3 (6.102×10^{-5} $in.^3$), respectively. The water is transmitted to the soil via a high air entry porous disc (HAEPD) having an air entry value of 3 bar. The test cell was fabricated to fit into a one dimensional consolidation apparatus as shown in Figure 3.3, so that incremental vertical loading can be externally applied while independently controlling u_a

and u_w in the soil sample. The advantage of using this device is the ability to measure the volume change of a specimen during the test while controlling the vertical normal stress. In this method samples were compacted into the cell at the desired target unit weight and moisture content prior to testing. With the 3-bar HAEPD this method can be used to investigate the SWCC up to matric suctions of 300 kPa (43.5 psi).

3.4.3 Shear Strength

Shear strength testing was conducted to determine strength of the soil representing the soil in the failure zone of the slope. Testing was conducted to determine 1) saturated strength parameters from thin-walled samples obtained in situ, 2) fully softened strength from remolded representative compacted samples, and 3) saturated and unsaturated strength parameters of representative compacted samples. Thin-walled tube samples were tested in a conventional triaxial compression device. A conventional direct shear testing device was used to obtain the fully softened and saturated strength parameters for remolded compacted samples. Unsaturated shear strength parameters were determined using a modified direct shear apparatus with provisions for controlling pore air and pore water pressure.

3.4.3.1 Isotropically Consolidated Undrained Triaxial Compression (CIUC) Tests on Thin-Walled Tube Samples

Thin-walled tube samples were collected on site by manually driving Shelby tubes into the face of the slope at various depths down to four feet. Within a few days of sampling, the specimens were extruded, weighed and measured, wrapped in plastic sheeting (cellophane) and stored in the moisture room. The specimens were handled with care and trimmed using a sharp stainless steel knife. These samples may have suffered some disturbance during sampling as since tubes were driven into the slope using a sledge hammer. However, since the soil being sampled was relatively stiff, the influence of disturbance is thought to be minimal.

Table 3.1 presents the site name, borehole number and sample depth as well as the cell pressure and back pressure used for each test. The same effective pressure range was used for each sample during multistage tests. The triaxial tests were consolidated undrained compression tests with measurement of pore-water pressure to assess both drained and undrained strength parameters, as prescribed by ASTM D4767. Samples were saturated under backpressure. The triaxial tests were run on specimens from five different depths in order to get a good estimation of the general profile and determine the properties of potentially different layers. As it is difficult to obtain identical specimens to run several tests, multistage tests were chosen and were conducted under confining pressures of 2, 5, 10, and 15 psi. The cell pressure in each stage is shown in Table 3.1.

3.4.3.2 Drained Direct Shear Tests on Fully Softened Samples

Two different procedures were investigated for determining the fully softened shear strength. For the first, the samples were prepared at liquid limit and consolidated in the direct shear device to recreate the normally consolidated state of the soil. However, the soil appeared to be overly soft and did not consolidate effectively, requiring excessive time in the direct shear cell. Thus, another procedure was developed to simulate field softening in manner that is more representative of the cycles of wetting and drying in the field.

The second procedure, which was adopted to obtain the fully softened shear strength involved subjecting compacted specimens to cycles of wetting and drying. Each sample was subjected to 10 cycles of wetting and drying plus one cycle of wetting and then trimmed for single stage direct shear test. A complete wetting-drying cycle consisted of 24-hours of wetting in a fully submersed condition and 24-hours of drying at 140^{o}F. Samples were tested at a shearing rate of 0.035 in/hour, which was assumed to allow the sample to drain during shear. This rate was selected based on rates used previously for similar soils and consolidation characteristics of the soil. Samples were inundated with water, subjected to vertical normal stress, and allowed to consolidate prior to shearing. A range of normal stress values from 2.0 to 15.0 psi was used for the single stage direct shear testing.

3.4.3.3 Drained Direct Shear Tests on Compacted Unsaturated Samples under Suction Control

A series of tests was conducted using the modified direct shear apparatus that allows for control of pore air pressure and pore water pressure. The single stage unsaturated direct shear tests were performed on compacted, remolded samples under a range of suction and net normal stress of 7.3 to 29.0 psi and 7.3-34.8 psi, respectively.

The procedure to prepare the specimens and to conduct the tests has been described by Miller and Hamid (2007). The soil sample was first compacted in the shear box at a target water content and dry density. After compaction, the shear box cell containing the test specimen was placed in the DST air pressure chamber. The drainage line from the pore water pressure controller was connected to the bottom platen inlet port of a high air entry porous disc (HAEPD) placed on the bottom of the shear box. It is important to note that the HAEPD is saturated with de-aired water prior to testing. A seating load of 1.5 to 2.2 psi was applied to the test specimen in order to stabilize the position of the upper half of the shear box when it was raised to introduce the gap needed before the shearing process. Approximately sixty minutes after the initial compression seating load, the two screws holding the two halves of the shear box together were removed. Water is not permitted to flow to/from the drainage system from/to the porous stone during this time to minimize sample wetting. A gap was created between the two halves of the shear box by turning the four raising screws, which were then reversed to eliminate any contact between the screws and the box. After creating a gap of about 0.04 in. (which is slightly greater than the recommended gap of 0.025 in. in ASTM D3080, and also falls in the range of 10 to 20 times of D50 of the soil), the air chamber lid was sealed with bolts. The target matric suction value (u_a – u_w) following was then applied to the specimen by increasing the air and water pressures simultaneously via the axis translation technique.

The test specimen was allowed to equilibrate under the applied suction value. Equilibrium was assumed when negligible change in the water volume was observed. The net normal stress (σ – u_a) was then increased in increments of 1.5 psi by applying a vertical load to reach the target net normal stress. After the specimen was consolidated under the target vertical stress, it was subjected to drained shearing while controlling both suction and net normal stress.

Shearing was applied at a displacement rate of 0.012 in./hr. up to about 0.4 in. displacement. The changes in the specimen height and water volume were measured and recorded during all stages of the test. The specimen height was measured using an

LVDT that was attached to the loading ram. During shearing, the horizontal load and the horizontal and vertical displacements were measured and recorded.

3.4.3.4 Drained Direct Shear Tests on Compacted Saturated Samples

A series of single stage tests was conducted using the conventional direct shear apparatus and three different vertical normal stresses (7.3, 14.5, and 21.8 psi). A soil sample was first compacted in the shear box at target water content and dry density. A seating load of 1.5 to 2.2 psi was applied for sixty minutes to the test specimen in order to stabilize the position of the specimen. After applying the seating load, water was added to the specimen to saturate it for 24 hours. After the process of saturation the target value of normal stress was applied. The process of consolidation was completed when negligible change in the specimen height was observed. Shearing proceeded in the manner previously described; however, the tests were terminated after 0.24 inches of displacement, which was sufficient to define the peak shear strength.

3.4.4 Hydraulic Conductivity

To determine the saturated hydraulic conductivity of the soil located at the test sites, Shelby tube samples were collected at different times during the project as described previously. After extruding, the soil samples were wrapped with plastic film and stored in a moisture room. The standard test method for measurement of hydraulic conductivity of saturated materials with a flexible wall permeameter was used as described in ASTM D5084 -10. Samples were back-pressure saturated and tested under effective confining pressures of 3 to 6 psi. The goal was to simulate the in situ effective stress while maintaining sufficient cell pressure to counter the head pressure while achieving the desired gradient. For soil with very low hydraulic conductivity, necessitating high gradients, it is impractical to use confining pressures less than about 5 psi.

3.4.5 Moisture Diffusivity

In a laboratory at Oklahoma State University, one-dimensional moisture diffusivity measurements were made on thin-walled soil samples obtained from each test site. The method involves installing thermocouple psychrometers in confined soil cores and measuring suction variations along the length of the core while drying is permitted from one end exposed to atmosphere. Testing is conducted in a specially fabricated test box in which the temperature and humidity are carefully controlled. This testing allows for the determination of the moisture diffusion coefficient, which can be used in predicting evaporative moisture losses from soil profiles.

3.5 Modeling Soil Moisture Changes in Response to Weather

Two computer programs were used to model the variation in soil moisture profiles over time at the test sites. Vadose/W and SVFlux are two computer programs used to model transient flow of water, heat and vapor in unsaturated soil. The programs are built around fundamental equations governing the exchange of water between the soil and atmosphere at the ground surface (e.g. Penman 1948, Wilson et al. 1994) and can account for variations in the soil state (dry, frozen, saturated, unsaturated), soil type, soil temperature, and extent and type of vegetative cover, among other things.

Basically, the user is required to input a number of different parameters that govern the movement and storage of heat and water (in liquid and vapor forms) within a soil profile as well as information about the type and temporal variation of vegetative cover at the site. In addition, the initial soil moisture conditions in the profile are required. Once the basic soil and vegetative material parameters are input, the desired climate data defining weather variations over some defined time period are provided as input. The program is then run and the output generated provides predicted moisture (and suction) profiles as a function of time.

In this research, Vadose/W and SVFlux were used to predict the variations in moisture content in the soil profiles at each test site for comparison to the actual moisture content variations observed. In addition, the variations in moisture content and suction at critical points in time were used as input in the slope stability analysis to examine how the factor of safety against slope failure varies with seasonal weather variations. The purpose of this modeling was to evaluate and compare the predictive capability of these programs for predicting moisture variations in slopes due to seasonal weather changes.

The required input parameters with respect to Vadose/W and SVFlux are summarized in Table 3.2. These parameters are divided into categories of climate data, vegetation data, and soil data. As indicated in Table 3.2, the required input data varies somewhat between the two programs. As for the output, the programs were used to provide variations in volumetric water content over time at specific depths in the soil profiles.

Aside from the similarities in the required input and output parameters, the primary differences between these two programs are as follows:

1. VADOSE/W (2007) solves 1D and 2D problems, whereas SVFlux (2009) solves 1D, 2D and 3D problems.
2. In VADOSE/W mesh properties are manually defined, whereas in SVFlux mesh properties are automatically defined.
3. Different infiltration rates are computed by SVFlux and VADOSE/W for high precipitation rates. For instance, VADOSE/W does not respond well to high positive pressure gradients. In fact, infiltration is underestimated, and runoff values are overestimated when compared to those predicted by SVFlux (Gitrana et al. 2005).
4. VADOSE/W predicts lower actual evaporation rates (AE) when compared to SVFlux (Gitrana et al. 2005).
5. VADOSE/W couples the thermal fluxes within the soil whereas SVFlux does not.
6. VADOSE/W (2007) has a feature that allows runoff to pond at the ground surface, and then infiltrate in the following time steps. To predict the surface infiltration and actual evaporation VADOSE/W requires adding a thin surface layer above the ground surface to deal with high changes in flow gradients. The solver computes the seepage flow through this layer, and allows the water that does not infiltrate immediately into the soil profile to build-up and become a positive head pressure in subsequent steps. This situation happens specifically whenever the soil goes from being very dry to very wet.

7. Table 3.3 summarizes the type of methods used by both programs to compute the potential and actual evaporation, transpiration, runoff and infiltration. The main differences between VADOSE/W and SVFlux are in the way the amount of runoff is calculated during a wetting period, and the meshing properties when high positive gradients are applied on the system.

3.6 Modeling Slope Stability

The SVSlope software was designed to be a comprehensive tool for slope stability analysis based on the limit equilibrium of slices. The factor of safety defined by the limit equilibrium method is a factor by which the shear strength must be reduced to bring a material mass into a state of limit equilibrium along a specified slip surface. In this study, the shape of the potential slip surface was assumed to be circular and non-circular. The most common trigger for slope failures is rainfall events, which tend to eliminate the negative water pressures (suctions) in the upper zone of the soil. The SVSlope software is able to implement three types of unsaturated soil strength models including linear model, non-linear model, and pore pressure coefficient model. The former and latter models were used to obtain the factor of safety for analysis in this study. In addition, a transient pore-water pressure distribution from the SVFlux software was used to implement the linear model. The daily pore water pressure variations throughout the slope soil profile were based on the moisture variation prediction using the SVFlux. The critical state was determined on the rainfall day when the factor of safety was at a minimum. Finding the critical value of factor of safety was possible through several trials using the link between SVSlope and SVFlux.

To run the stability analyses, a simple model was created. The geometry of the slopes was based on optical survey measurements taken at the sites. The moisture content and dry density of the soil at different depths required for slope stability were based on measurements from hand auger samples and thin-walled tube samples obtained at each test site. These values are summarized in the Figures 3.4 and 3.5.

For both sites, a homogeneous profile was assumed for the purpose of stability analysis. Drained analyses were conducted using shear strength parameters obtained from laboratory strength tests, as presented in Chapter 6. Two general approaches were used. First, stability analyses were conducted using a range of friction angles, encompassing the range obtained from laboratory tests, and using a range of pore pressure ratios typically encountered in practice. This first approach is essentially a saturated drained analysis with positive pore pressures. From this, one gets a sense of what friction angle and pore water pressure conditions seem most appropriate to model stability at each test site. Since both sites have experienced failures, it was expected that the best predictions would produce factors of safety close to one (1.0).

In the second approach, the SVFlux program was used to predict pore water pressures, both positive and negative (suction) within the slope due to weather variations, and then an analysis using SVSlope and the unsaturated strength parameters was conducted. The effect of desiccation cracking was simulated in the unsaturated seepage modeling (SVFlux) by enhancing the hydraulic conductivity of the upper layer of soil on the slope. This is described in more detail in Chapter 7. Both of these methods have advantages and disadvantages; however, the unsaturated seepage and slope stability analyses provide a more realistic simulation of actual weather events and soil conditions leading to slope failure.

Table 3.1. Summary of multistage triaxial compression test conditions for thin-walled tube samples Idabel and Chickasha sites.

Site	Bore hole #	Sample depth (in)	Back pressure (psi)	Cell pressure (psi)			
				Stage 1	Stage 2	Stage 3	Stage 4
Idabel	BH3	17 - 23"	50	52	55	60	65
	BH3	23 -31"	40	42	46	52	x
	BH3	33 -39"	55	57	60	70	x
	BH2	37 - 43"	38	40	43	x	x
	BH2	38 -44"	53	x	58	63	68
Chickasha	BH2	10 -16"	35	37	40	45	50
	BH1	16 - 23"	45	47	50	55	x
	BH1	24 -32"	40	42	45	50	55
	BH2	30-36"	43	45	48	53	x
	BH1	35 -45"	30	32	35	40	x
	BH2	38-44"	35	37	40	45	50

Note: “x” indicates the stage was not conducted.

Table 3.2. Summary of input parameters.

Input Parameters	SVFlux		Vadose/W	
	Idabel	Chickasha	Idabel	Chickasha
Coefficient of compressibility, m_v (psf^{-1})	6.3e-5	7.3e-5	4.8e-7	4.8e-7
Unsaturated permeability function	van Genuchten & Mualem function	van Genuchten & Mualem function	Fredlung & Xing	Fredlung & Xing
SWCC fitting curve	van Genuchten & Mualem fitting estimation	van Genuchten & Mualem fitting estimation	Spline Function	Spline Function
Actual evaporation method	Wilson Limiting Equation (1997)	Wilson Limiting Equation (1997)	Penman-Wilson (1990-1994)	Penman-Wilson (1990-1994)
Leaf Area Index	Constant	Constant	Tratch (1996)	Tratch (1996)
Plant Limiting Factor	SVFlux database	SVFlux database	User Input	User Input
Root depth (ft.)	0.01	0.01	Max of 0.5 ft.	Max of 0.5 ft.

Table 3.3. Differences and similarities between SVFlux and VADOSE/W.

<table>
<tr><th>Software Feature or Property Being Modeled</th><th>SVFlux
(SoilVision Ltd.,2009)</th><th>VADOSE/W
(GeoSlope, 2007)</th></tr>
<tr><td>Transpiration</td><td>Tratch (1995)</td><td>Tratch (1996)</td></tr>
<tr><td>Potential Evaporation
(PE)</td><td>Modified Penman method
Wilson (1990) and Gitrana (2005)</td><td>Penman-Wilson
(1990,1994)</td></tr>
<tr><td>Actual Evaporation</td><td>Improved Fredlund-Wilson Penman method
(1990) and Gitrana (2005)</td><td>Penman-Wilson
(1990)</td></tr>
<tr><td>Infiltration</td><td>Mansell (2002)
Based on the Theory of Soil Cover</td><td rowspan="2">If Precipitation-AE < 0 then:
Infiltration = Precipitation- AE

If Precipitation - AE > 0 *
Runoff = Precipitation - AE - Infiltration</td></tr>
<tr><td>Runoff</td><td>Gitrana (2005)</td></tr>
<tr><td>Precipitation Intensity
Application and Distribution</td><td>Flexible
Step-function</td><td>Fixed
Sinusoidal</td></tr>
<tr><td>Mesh Properties</td><td>Automatic adaptive mesh refinement</td><td>Manual and remains fixed</td></tr>
<tr><td>Time Stepping</td><td>Automatic time refinement</td><td>Adaptive time steps</td></tr>
</table>

Figure 3.1. Weather station installed at Idabel test site.

Figure 3.2. Type of sensors and their corresponding range of measurements.

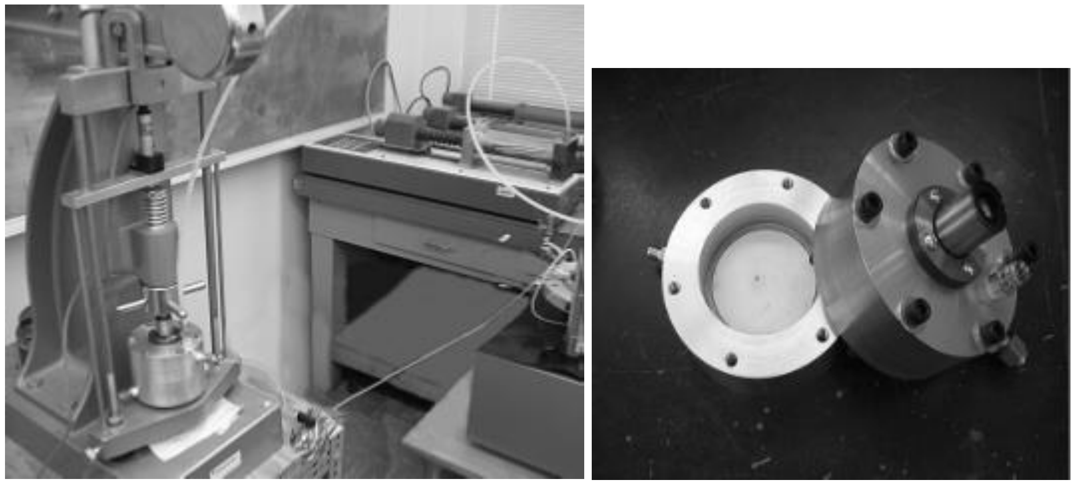

Figure 3.3. Custom device for determining the SWCC using axis translation under controlled net normal stress and matric suction.

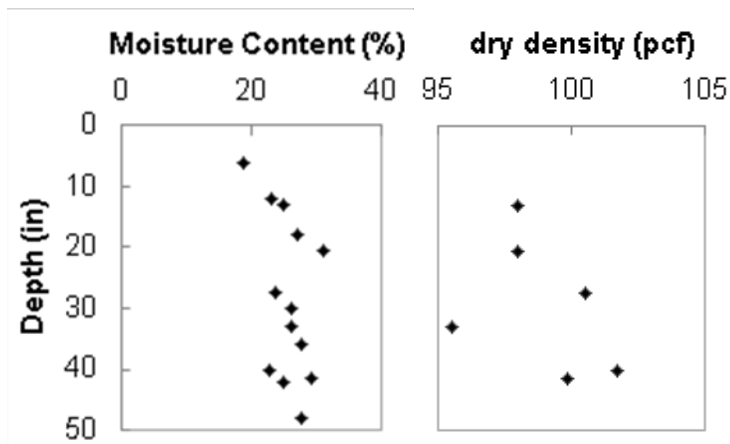

Figure 3.4. Chickasha: moisture content and dry density from field samples.

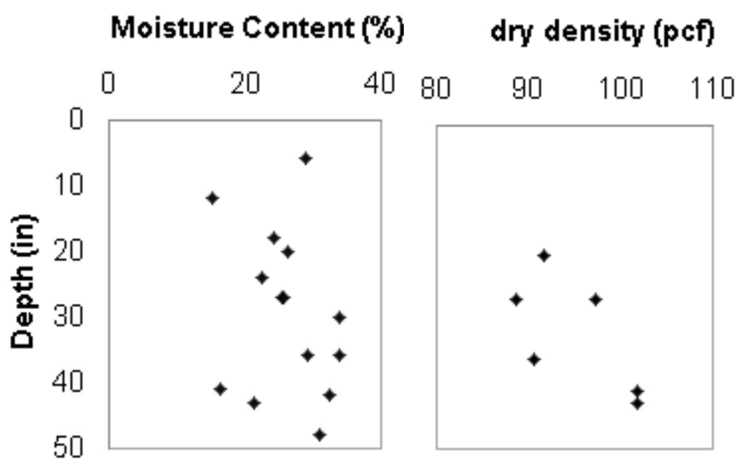

Figure 3.5. Idabel: moisture content and dry density from field samples.

Chapter 4 LABORATORY STUDY OF DESICCATION CRACKING

A unique desiccation box and testing apparatus was developed and fabricated at the University of Oklahoma. The device enables the direct determination of the uniaxial tensile strength of compacted soil during desiccation. The box was used to test composite samples of soil obtained from the Idabel and Chickasha test sites compacted to various densities and water contents. The composite soil properties are presented in Table 4.1.

For Chickasha, the composite soil properties are indicative of a lean clayey soil collected from the toe of the failed slope. Interestingly, this sample had lower plasticity than noted in the samples collected using a hand auger from the upper 5 feet of the profile (Chapter 6, Figure 6.2) in the vicinity of the weather station halfway up the slope. However, the PI of the composite sample is consistent with a mix of soil containing lower PI soils found below 5 feet in the hand auger boring. It seems during construction there was a wide range of soil types used in the embankment construction varying from lean to fat clay. The composite material collected from the toe in the slide area was likely a mix of soils from slide mass and the soils originally compacted at the base of the embankment.

Similarly, Idabel composite soil samples were collected from the toe of slope in the general vicinity of previous slides. The composite soil has a high plasticity and properties consistent with the samples collected from hand auger borings on the slope (Chapter 6, Figure 6.1). Generally, soil properties are fairly uniform with depth in the slope at the Idabel site. These observations are consistent with soil properties reported by Cerato and Nevels (2007).

4.1 Development of Soil Desiccation Test Box

One primary objective of this research was to develop a desiccation test apparatus to investigate the mechanism of desiccation cracking. Since a desiccation crack initiates when the tensile stress exceeds the tensile strength, determination of the tensile stresses in the soil is a necessary factor to understand the behavior of soil during desiccation. Therefore, a desiccation test apparatus was designed and developed in a way to be able to measure the tensile force produced in the soil bed while drying.

The preliminary bench scale tests started using a modified Teflon coated baking pan with roughened ends to constrain shrinkage of a soil bed allowing desiccation cracks to form while losing moisture content. In order to restrain the soil bed during shrinkage and cause the crack to form in the middle of the specimen, the bottom of the pan was roughened at each end as shown in Figure 4.1(a). The roughening was at first accomplished by scratching the pan and then by punching several holes within a 2-inch strip at each end to produce friction. However, this provided an inadequate restraining condition against shrinkage.

From additional trial versions of the desiccation tests, it was concluded that the most desirable constraining condition was achieved by placing sufficient screws in the end walls. Figure 4.1 shows the preliminary stage of bench scale desiccation testing device development. As illustrated in Figure 4.1(b), a small crack initiated near the mid-section of the pan; however, it was not developed across the width because the roughened bottom surface did not produce enough friction to prevent the soil bed from lateral shrinkage.

From Figures 4.1(c) and (d), it can be seen that several deep and large cracks occurred at the tip of the screws at the very early stage of drying due to the stress concentrations, which did not allow the tensile force to transfer to the center of the specimen. In order to solve this problem, the number of screws was reduced by half for the next test (Figure 4.1(e)). Figure 4.1(f) shows the most promising result that led to design and development of the new desiccation-tensile test apparatus

The newly developed device shown in Figure 4.2 and Figure 4.3 consists of a 10 in. x 12 in. rectangular shaped box with two separate halves. One half is fixed and there are some ball bearings under the other half to reduce the friction between the box and the surface below it. Where the two halves join, there are two load cells attached to the box to measure the tensile force generated in the specimen while it is drying. There is a small gap between the two box halves, which allows the tension in the soil to be transmitted to the load cells on either side. A constraining condition is applied to the specimen by placing screws in the end walls of the box and embedded in the soil within. This prevents the soil at the boundaries from pulling away from the ends during shrinkage and causes the desiccation crack to form at the mid-section of the box where the maximum tensile stress is expected to occur.

Teflon sheets shown in Figure 4.4 are used under the soil bed to minimize the friction between the box base and the specimen, such that the tensile stress developed in the soil is largely measured by the load cells. The apparatus sits upon a digital scale that monitors the moisture loss from the soil bed during drying. An overhead digital camera captures time-lapse photographs of the desiccation crack formation, moisture loss via scale readout, and load cell readouts. Load-cells are manufactured by OMEGA having a capacity of 100 lbf and an accuracy of ±0.03% full scale. It also has a peak detection feature that can display the maximum value of force at the end of the test. To get the time-lapse photography, an intervalometer manufactured by APUTURE (Figure 4.5) is connected to the camera. The generation of tensile stress and moisture loss can be monitored using the load cells and scale read-outs at a set interval during the desiccation process. A picture of the desiccation test apparatus including the desiccation box, load cell readouts, overhead camera and a scale to monitor the moisture loss is shown in Figure 4.6.

As previously mentioned, in almost all of the tensile strength testing methods described in the literature, the strength is measured by applying external load to the specimens to reach the tensile failure at constant water content. The newly designed apparatus is capable of measuring the tensile force developed during restrained shrinkage of soil bed under the desiccation process. This can provide a more realistic estimation of the tensile stress needed to form a desiccation crack in a natural compacted soil bed.

4.2 Desiccation Testing Procedures

To study the effect of initial water content, compaction effort and plasticity index on desiccation crack formation and tensile strength, two types of soil specimens were compacted to the target dry unit weights and various water contents. The compaction process improves the strength properties of soil by removing the air from voids. Dry unit weight (γ_d) increases with increase in water content up to the Optimum Moisture Content (OMC) and then decreases beyond that point. In the current study, an effort was made to study the tensile behavior of soil around optimum moisture content and maximum dry unit weight. Three different dry unit weights were picked for each type of soil to investigate the effect of compaction properties on tensile strength. Preparing the samples to water contents beyond optimum also provided for investigating the effect of a wider range of initial water content on tensile strength. Table 4.2 shows the test matrix for this study.

All test soils were processed to pass a No.4 sieve and wetted to different moisture contents mentioned in Table 4.2. The specimens were covered and left in a humid room for 24 hours to promote uniform distribution of moisture through the soil. The prepared soils were placed into the desiccation box and compacted in one layer to the target dry density to reach the 0.6 inch (≈1.5 cm) thickness. During compaction, an effort was made to uniformly distribute the soil and reach a uniform thickness. As shown in Figure 4.7, compaction was achieved by placing a steel plate on top of the specimen and striking it with a hammer. A piece of wax paper was placed on the top of the soil bed prior to compaction to prevent the wet surface of soil from adhering to the steel plate.

During compaction, the two halves of the box remained fixed to protect the load cells, and to achieve proper compaction. The surface of specimens was smoothed using a spatula to ease the observation of crack initiation. At this stage, the screws that attached the two halves of the box were loosened in order to release the force produced during the compaction process. Before starting the test, the two halves were attached in a fixed position through the load cells to allow the tensile force generated by the shrinking soil to transfer to the load cells during the test. The specimens were then allowed to air dry at 77^{o}F (room temperature). A camera was set up to produce time-lapse photos that captured both the desiccation crack development and weight loss of the desiccation box, by which the moisture content could be determined. The load cells were used to determine the tensile force developed in the soil during the drying process.

In this study, the tensile strength is defined as a highest value of tensile load that a specimen can withstand before it fails. It was observed in desiccation tests of this study that the failure corresponded to the point where the first crack initiated in the soil bed. It was assumed the soil bed was not cracked at the maximum tensile load and at this point, the load was carried by the full cross-sectional area of the soil bed. The amount of lateral shrinkage and change in thickness was judged to be insignificant from the start of the test until the time of failure; therefore, the tensile strength was calculated by dividing the average maximum tensile force measured by the load-cells by the initial cross sectional area of the soil bed.

4.3 Desiccation Test Results and Discussion

4.3.1 Chickasha: Overview of Tests and Observations

For Chickasha soil, three series of desiccation tests were performed on soil beds at various water contents and compacted at three constant dry unit weights of 110 pcf, 104.3 pcf and 92.3 pcf as indicated in Table 4.2. The results of desiccation tests on Chickasha soil are summarized in Table 4.3.

In almost all of the desiccation tests on Chickasha soil, a nearly linear crack was generated across the mid-section of the box when the tensile stress reached the peak value. The crack developed across the full width of the box and through the depth as shrinkage proceeded. Figure 4.8 shows the typical process of crack initiation and propagation during the desiccation process in a compacted bed of Chickasha Soil.

4.3.2 Idabel: Overview of Tests and Observations

Three sets of tests were conducted on compacted Idabel soil beds. The samples were wetted to several water contents and compacted to three different constant dry unit weights of 96.7, 82.7, and 73.2 pcf as indicated in Table 4.2. Table 4.4 presents the summary of desiccation test results from Idabel Soil.

The process of crack formation in a soil bed for Idabel Soil was the same as Chickasha Soil. Upon drying, tensile forces increased due to the presence of restrained ends, which led to crack formation at the mid-section of the soil bed where the tensile stress was expected to be maximum. Figure 4.9 shows a typical crack development during a desiccation test for Idabel soil.

4.3.3 Chickasha: Tensile Force and Water Content versus Time

In the first series, three tests were conducted on specimens compacted to the maximum dry unit weight at moisture contents that were 2% dry of optimum, optimum and 2% wet of optimum water content. It was desired to see how tensile strength changes around the optimum compaction conditions since these are representative of typical engineered highway embankments at the end of construction. Figure 4.10 shows the change in tensile force over time. It was observed that for all specimens the tensile force increased up to a point where the first crack appeared on the soil bed and then started to decrease as the crack kept propagating along the width and through the depth of the specimens. The greatest tensile strength was achieved for the specimen compacted to 2% wet of optimum.

In Figure 4.11 tensile force versus time for the third test series at the lowest dry density are shown. In the third series of desiccation tests, samples Ch-7 to Ch-12 were compacted to dry unit weight of 92.3 pcf and molded at water contents ranging from 16% to 34%; the latter being close to liquid limit. Compared to the first tests series, the tensile strength is clearly lower and times to reach failure increase with increasing water content. This latter point is emphasized in Figure 4.12, which shows tensile strength obtained from each test versus the time of cracking. Cracking time is the time required for the first crack to initiate in the soil bed and it corresponds to peak tensile force. Generally, it is seen that longer time was needed for crack initiation in specimens having higher initial water content. Data from the second test series exhibited similar behavior with strengths in between those obtained from the first and third series.

Variation of water content over time for Test Series 1 and 3 is illustrated in desiccation curves shown in Figures 4.13. All curves have a similar trend as the moisture content decreased more rapidly in the early stages of drying and then gradually approached an equilibrium state at the end of the test. The time needed to reach the equilibrium varied depending on initial water content of the specimens.

4.3.4 Chickasha: Tensile Strength

Figure 4.14 shows the effect of initial water content on tensile strength of Samples Ch-1, Ch-2 and Ch-3. The results indicate that at a constant dry unit weight of 110 pcf, which corresponds to the maximum compaction effort, the tensile strength increases for water contents ranging from -2% to +2% of optimum. Similar behavior was observed for samples Ch-4, Ch-5 and Ch-6 compacted to 104.3 pcf and wetted to OMC, 2% and 4% wet of optimum moisture content (Figure 4.15).

As presented in Table 4.2, Samples Ch-7 to Ch-12 were compacted to 92.3 pcf and various initial water contents to examine the tensile behavior of Chickasha Soil within a wider range of initial water contents. Note, it was not possible to use the larger range of water contents at the higher densities because of difficulties achieving the target density at high water contents. Figures 4.16 shows tensile strengths with respect to the corresponding cracking water content. The results show that tensile strength increased with increase in water content up to a peak value and then decreased with further increases in water content. Similar observations of strength increasing and then decreasing with water content at a given density were also made by Lakshmikantha et al. 2012. A possible explanation for this behavior is discussed in Section 4.4.

In Figure 4.17, plots of tensile strength versus cracking water content from each series are presented for a range of water content from about 15% to 25%. It is clear from this from this graph that for a given water content, greater tensile strength was achieved for the higher values of dry unit weight.

4.3.5 Idabel: Tensile Force and Water Content versus Time

Figures 4.18 and 4.19 show the variation of tensile force over drying time for Test Series 4 and 5. Similar to Chickasha soil, the rate of tensile force development is influenced by initial water content as the specimens tend to the saturated state. In specimens with initial water content closer to saturation, it takes more time for tensile forces to generate within the soil mass. Figure 4.20 also shows the effect of initial water content on cracking time.

In Figure 4.21 the change of water content with time is shown for each specimen of Test Series 4 and 5. The trend of desiccation curves was found to be similar for all tests. However, the time to approach an equilibrium water content at the end of drying tended to decrease with decreasing dry density and decreasing water content.

4.3.6 Idabel: Tensile Strength

Figure 4.22 presents the tensile strength versus cracking water content for Test Series 4. The results indicate that at an initial maximum dry unit weight of 96.7 pcf, the tensile strength increased with increase in initial water content for the specimens compacted at -2% to +2% of optimum moisture content.

Figures 4.23 to 4.24 present the results of Tests Series 5 and 6, respectively. These series encompass a much larger range of water content. Results are qualitatively analogous to those obtained for Chickasha Soil. The tensile strength increased with an increase in initial water content and then decreased after reaching a peak value. The peak tensile strength occurred around 70% to 80% degree of saturation for both sets of tests.

In Figure 4.25, a comparison of tensile strength for different dry densities and water contents in a range of 21% to 32% is shown. Similar to Chickasha Soil, the tensile strength of Idabel Soil increases with increasing dry density and increasing water contents near optimum. Figure 4.26 compares the tensile behavior of compacted Idabel soil within a wide range of initial water contents for two different dry densities of 82.7

and 73.2 pcf. Although the difference is not significant, the tensile strength is slightly greater for the set of tests having higher density. Similar to Chickasha soil, it was not practical to reach the maximum compaction density of 96.7 pcf for water contents far from optimum, which explains the lack of these data for the densest condition.

4.3.7 Effect of Soil Type on Tensile Strength of Soil

Figure 4.27 shows the variation of tensile strength as a function of water content for Chickasha and Idabel Soil at a relative compaction of 85%. The results show that Idabel Soil achieves greater tensile strength. These results support the notion that the tensile strength is expected to be higher for soils having higher plasticity index. This result is consistent with what has been reported by Al-Hussaini and Townsend (1974), Fang and Fernandez (1981), Barzegar et al. (1995), Kim and Hwang (2003), Tamrakar et al. (2005) and Kim et al. (2012).

4.3.8 Repeatability of Experiments

To investigate the repeatability of the results obtained from the desiccation box, three tests were carried out for Chickasha Soil at each of three different water contents (OMC and ±2% OMC). As shown in Figure 4.28, the results varied only slightly for the repeated tests. Since the desiccation process and generation of tensile stress is affected by environmental factors such as relative humidity and temperature, conducting the tests without controlling these factors can be considered a source of error. It was also challenging to stay consistent during the process of specimen compaction to reach a uniform thickness in the soil bed. Nevertheless, results in Figure 4.28 exhibit reasonably good repeatability and consistent trends.

4.4 Comparison of Experimental and Theoretical Estimates of Tensile Strength

There are various theoretical models for tensile strength of soils (e.g. Lu et al. 2009, Trabelsi et al. 2012). Following the work of Lakshmikantha et al. (2012), the theoretical tensile strength in the current study was determined using a Mohr-Coulomb type model developed by Alonso et al. (2010). This model was most effective at simulating the variation of tensile strength with water content observed from experiments in the current study. The model is particularly well suited to compacted clayey soils with dual porosity structures that vary with compaction water content. Influence of the soil structure is captured through the use of an effective stress model that incorporates an effective degree of saturation (S_r^e). As defined by Alonso et al. (2010), this effective degree of saturation is a measure of the water in the soil macropores, which is assumed to control the contribution of matric suction to the soil strength.

The effective degree of saturation is a measure of the degree to which the macropores in a dual porosity structure are filled with water. In this model, it is assumed that water volume held within micropores remains constant. In developing the equation for effective degree of saturation, the degree of saturation (as ordinarily defined) is separated into the macroscopic and microscopic degrees of saturation. The macroscopic degree of saturation (S_r^M) is associated with the water occupied in relatively large open pores, where the capillary forces govern the effective stress. The microscopic degree of saturation (S_r^m) is associated with the small pores in which physico-chemical bonds exists between the water and soil particles. These contributions are expressed in the following equation:

$$S_r = S_r^m + S_r^M \qquad \textbf{(4.1)}$$

where S_r is ordinary degree of saturation (i.e. volume of water divided by volume of voids). Effective degree of saturation is thus defined as:

$$S_r^e = \frac{S_r - S_r^m}{1 - S_r^m} \text{ for } S_r > S_r^m \text{ and } S_r^e = 0 \text{ for } S_r \leq S_r^m \qquad \textbf{(4.2)}$$

Equation 4.2 varies from 0 when there is no water in the macropores ($S_r = S_r^m$) to 1 when the soil is saturated. Because the distinction between micropores and macropores in soil is not entirely clear, and because Equation 4.2 discounts the contribution of water in the soil when ($S_r \leq S_r^m$), Alonso et al. (2010) proposed an alternative equation that is continuous for all values of S_r from 0 to 1 and provides a smooth transition at the point where $S_r = S_r^m$, while still retaining some essential features of Equation 4.2 (see Alonso et al. (2010) for more discussion). The proposed equation is:

$$S_r^e = (S_r)^\alpha \qquad \textbf{(4.3)}$$

where α (α≥ 1) is a material parameter. The α parameter is 1 for soils with uniform pore size distributions, such as for sands, and considerably larger for soils that develop distinct macropore and micropore structures, such as compacted clays.

Incorporating the effective degree of saturation, a general equation for effective stress based on the model proposed by Alonso et al. (2010) is:

$$\sigma' = \sigma - u_a + S_r^e(u_a - u_w) \qquad \textbf{(4.4)}$$

where σ' is the effective stress, σ is total stress, u_a is pore air pressure, u_w is pore water pressure, and u_a-u_w represents matric suction. Note, this is similar to the Bishop (1959) effective stress equation with the Bishop χ factor equal to S_r^e.

Incorporating this effective stress into the Mohr-Coulomb strength equation gives:

$$\tau = c' + \sigma' \tan\Phi'$$

$$\tau = c' + (\sigma - u_a)\tan\Phi' + S_r^e(u_a - u_w)\tan\Phi' \quad \textbf{(4.5)}$$

where τ is the shear strength on some plane, c' is the effective stress cohesion intercept, and Φ' is the effective stress friction angle. Equation 4.5 can be rearranged such that:

$$\tau = c + (\sigma - u_a)\tan\Phi' \quad \textbf{(4.6)}$$

and

$$c = c' + S_r^e(u_a - u_w)\tan\Phi' \quad \textbf{(4.7)}$$

The cohesion, c, represents the intercept when net normal stress equals zero in the net normal stress-shear stress ($\sigma - u_a$ vs τ) plane as shown in Figure 4.29. Under uniaxial tension with the major principal net normal stress equal to zero, the tensile strength (σ_{tu}) is equal to the minor principal net normal stress at failure as shown in Figure 4.29. The equation for the tensile strength is given by:

$$\sigma_{tu} = -\frac{2c\cos\Phi'}{1+\sin\Phi'} \quad \textbf{(4.8)}$$

or

$$\sigma_{tu} = -\frac{2c'\cos\Phi' + 2S_r^e(u_a - u_w)\tan\Phi' cos\Phi'}{1+\sin\Phi'} \quad \textbf{(4.9)}$$

Note that the tensile strength under isotropic tension (σ_t) can be determined from the intercept at shear stress equal zero as indicated on Figure 4.29. This formulation for tensile strength based on a Mohr-Coulomb model is similar to that given by others (e.g. Lu et al. 2009, Lakshmikantha et al. 2012).

The tensile strength calculated using Equation 4.9 was compared to the experimental results obtained from the desiccation box tests in this study. Soil parameters used in Equation 4.9 were obtained from experimental soil water characteristic curves and unsaturated strength parameters. Results of these tests are presented in Chapter 6. The best match between theoretical and measured tensile strengths was obtained using an effective degree of saturation (Equation 4.3) based on an α value equal to 8 for Chickasha and 7.5 for Idabel soil. Effective degrees of saturation are plotted against degree of saturation in Figure 4.30. Contrary to granular soils where the pores mostly consists of free water and α approaches 1, for the fine-grained soils that contain significant amounts of micropore and macropore structure, the difference between the apparent and effective degree of saturation can be significant. For selected α values in Figure 15, it is noted that the contribution of suction is relatively insignficant until the degree of saturation, S_r, exceeds about 0.6. Theoretically, this corresponds to the point at which the effective degree of saturation, S_r^e, rises from close to zero as capillary water begins filling the macropores.

Strength parameters were obtained from unsaturated and saturated direct shear tests, which provided ϕ' and c' values of 29.7° and 1.1 psi and 15.1° and 1.8 psi for Chickasha and Idabel soil, respectively. Suction in Equation 4.9 was obtained using the water content from experiments and experimentally determined soil water characteristic curve. The soil water charactristic curves were obtained by measuring the suction of several samples compacted at various water contents and densities matching those in the desiccation box tests. van Genuchten's model (1980) was used to plot the fitting curves for the SWCC obtained for the target dry unit weights used in the model as shown in Figures 4.31 and 4.32. Table 4.5 presents the SWCC model parameters obtanied for Chickasha and Idabel soils.

As shown in Figures 4.31 and 4.32, the predicted trends of tensile strength generally provide a reasonable match to the measured values. It is also clear that predicted values are very sensitive to value of the effective cohesion intercept (c'), as well other parameters including estimated suction, friction angle and effective degree of saturation. Predicted trends confirm that tensile strength does not necessarily increase with increasing suction and strongly depends on the pore structure and effective degree of saturation of the compacted clayey soil. Observed and predicted behavior is consistent with the different structure of compacted soil obtained on dry and wet sides of the optimum moisture content. Soil compacted at dry of optimum tends to have larger clods and larger macropores compared to the soil compacted at the wet side of optimum with smaller and more uniform pores. The presence of large macropores decreases the effect of suction and makes the soil structure brittle causing the tensile strength to decrease despite the existence of higher measured suction associated with the micropores.

4.5 Importance of Desiccation Box Test Findings

Desiccation cracks play an important role in failure of compacted embankment slopes. It is important to understand the behavior of desiccating soil to accurately analyze the stability of slopes and minimize the impact of desiccation cracks on slope failures in the design process. To this end, it is necessary to predict the depth and locations of desiccation cracks and assess their impact on hydraulic conductivity and suction decreases relative to significant wetting events. In order to predict the depth and locations of cracks, an accurate measurement of the tensile strength of soil is necessary. The desiccation box designed in this study is unique in that it permits direct measurement of approximate uniaxial tensile strength of soil during desiccation. Comparisons to theoretically estimated tensile strengths are quite favorable, which provides a measure of validation to both the experimental and theoretical methods. Continued research is focusing on improvements to the device and developing methods for predicting spatial variation of desiccation cracks in response to post-construction weather patterns. A preliminary method for predicting the depth and spacing of desiccation cracks was developed in this study and will be presented in Chapter 7 as part of the analysis of slope stability.

Table 4.1. Properties of the composite samples used for desiccation tests.

Property	Chickasha	Idabel
AASHTO Classification	A-6 (6)	A-7-6 (32)
USCS Symbol	CL	CH
USCS Group Name	Sandy Lean Clay	Fat Clay with Sand
Liquid Limit (%)	38	72
Plastic Limit (%)	20	26
Plasticity Index (%)	18	46
Specific Gravity	2.75	2.78
Gravel (%)	0	0
Sand (%)	11	3
Silt (%)	49	17
Clay Size (%)	40	80
Maximum Dry Unit Weight, (pcf)	110	96.7
Optimum Moisture Content (%)	18.0	24.0

Table 4.2. Test matrix of the desiccation tests.

Soil type	No. of series	Sample	Dry unit weight (pcf)	Water content (%)
Chickasha USCS symbol= CL	1	Ch-1	γ_{dmax}=110	-2%OMC=16
		Ch-2		OMC=18
		Ch-3		+2%OMC=20
	2	Ch-4	95%γ_{dmax}=104.5	18
		Ch-5		20
		Ch-6		22
	3	Ch-7	85%γ_{dmax}=93.5	16
		Ch-8		20
		Ch-9		23
		Ch-10		26
		Ch-11		30
		Ch-12		34
Idabel USCS symbol=CH	4	Id-1	γ_{dmax}=96.7	-2%OMC=22
		Id-2		OMC=24
		Id-3		+2%OMC=26
	5	Id-4	85%γ_{dmax}=82.2	15
		Id-5		18
		Id-6		20
		Id-7		24
		Id-8		26
		Id-9		34
		Id-10		42
		Id-11		60
	6	Id-12	75%γ_{dmax}=72.5	16
		Id-13		20
		Id-14		24
		Id-15		26
		Id-16		34
		Id-17		55

Table 4.3. Summary of Chickasha test results.

Dry Unit Weight (pcf)	No. of series	Test No.	Initial water content (w_i)(%)	Cracking water content (%)	Tensile strength (psi)
γ_d=110 pcf	1	Ch-1	16	15.8	1.8
		Ch-2	18	17.7	2.5
		Ch-3	20	19.6	3.35
γ_d=104.3 pcf	2	Ch-4	18	17.8	1.75
		Ch-5	20	19.4	2.6
		Ch-6	22	21.5	2.7
γ_d=92.3 pcf	3	Ch-7	16	15.4	0.5
		Ch-8	20	19.9	1.1
		Ch-9	23	22.6	1.3
		Ch-10	26	24.1	1.4
		Ch-11-1	30	25.1	1.75
		Ch-11-2	30	26.1	1.3
		Ch-12	34	31.4	0.9

Table 4.4. Summary of Idabel test results.

Dry Unit Weight (pcf)	No. of series	Test No.	Initial water content (w_i) (%)	Cracking water content (%)	Tensile strength (psi)
γ_d=96.7 (pcf)	4	Id-1	22	21.5	2
		Id-2	24	23.5	2.4
		Id-3	26	25.4	2.8
γ_d=82.7 (pcf)	5	Id-4	15	14.2	0.14
		Id-5	18	17.1	0.45
		Id-6	20	18	0.7
		Id-7	24	22.8	1.8
		Id-8	26	25.2	2.3
		Id-9	34	31.3	3
		Id-10	42	37.6	2.4
		Id-11	60	48.3	1.2
γ_d=73.2 (pcf)	6	Id-12	16	15.5	0.07
		Id-13	20	18.2	0.35
		Id-14	24	23.5	1.55
		Id-15	26	24.3	2
		Id-16	34	31.1	2.7
		Id-17	55	46.5	1.35

Table 4.5. Parameters of SWCCs using van Genuchten's model.

Soil	n	m	α_1(MPa)$^{-1}$
Chickasha	0.6	0.48	5
Idabel	1.1	0.28	10

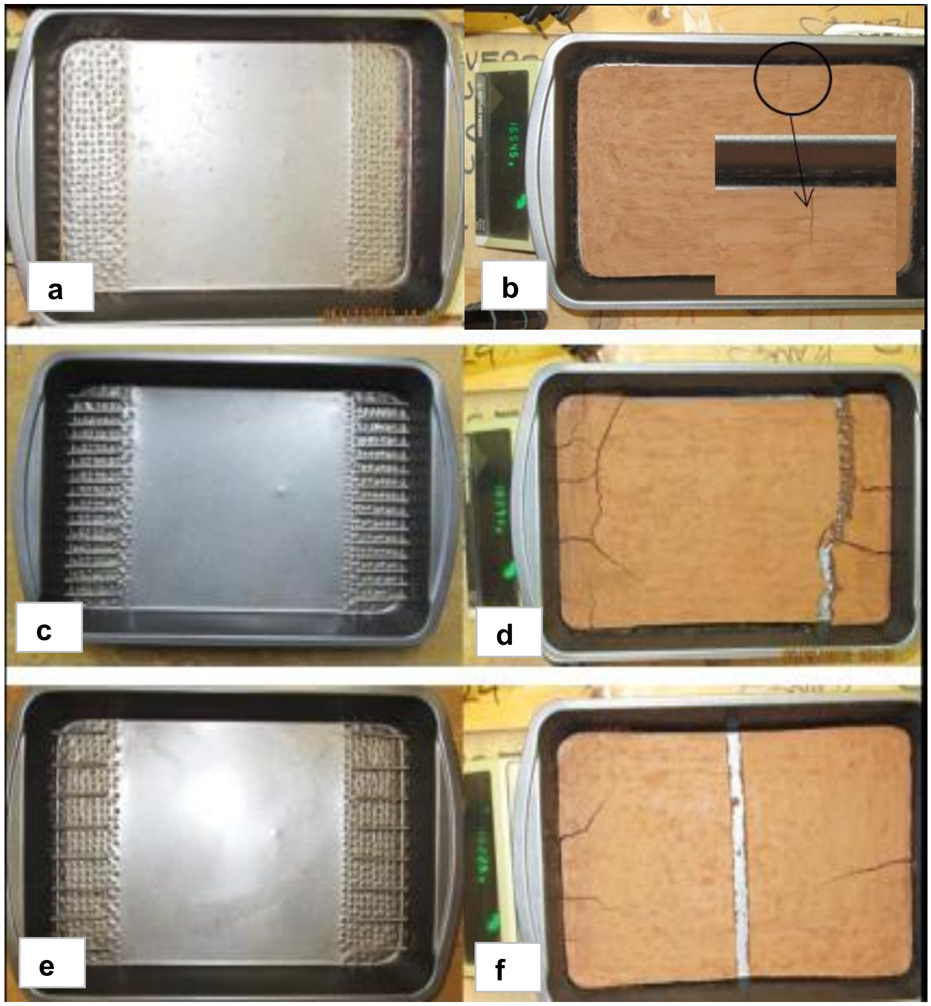

Figure 4.1. Development of desiccatoin box: roughened sides (a), formation of a small crack (b), screws used for constraning condition (c), stress concentration due to excessive friction (d), desired constraining condition (e), formation of crack in the middle of the drying soil bed (f).

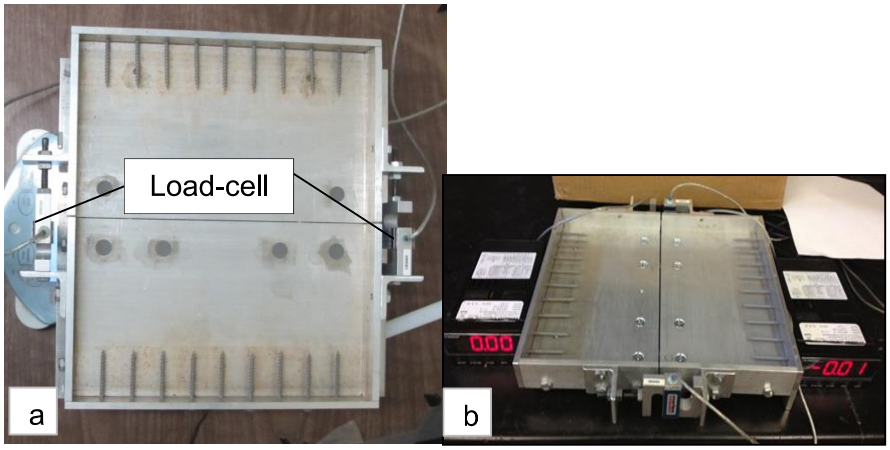

Figure 4.2. Newly developed desiccation box: top view (a) and side view (b).

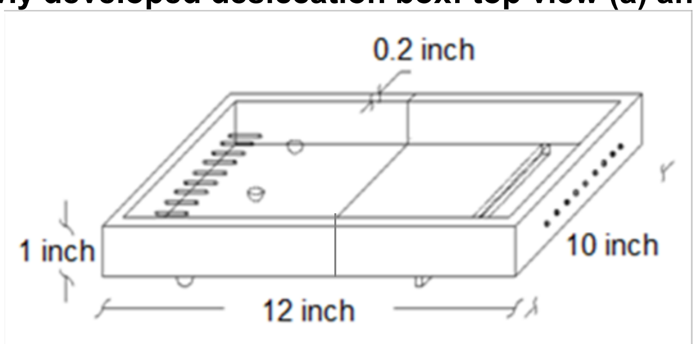

Figure 4.3. Schematic drawing of the desiccation box.

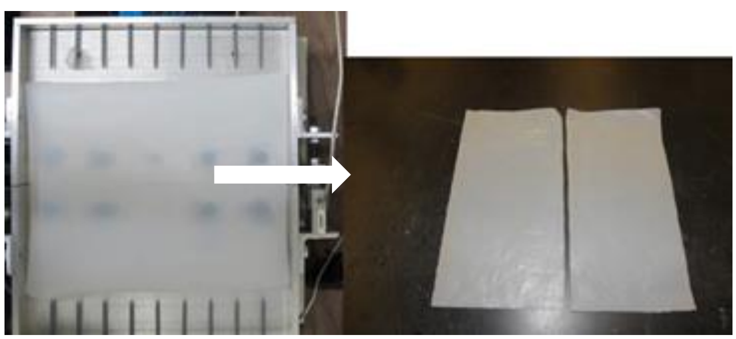

Figure 4.4. Teflon sheets placed beneath the soil bed.

Figure 4.5. Intervalometer used to capture time-lapse photos.

Figure 4.6. Desiccation box test apparatus.

Figure 4.7. Compaction process using a steel plate and a hammer.

Figure 4.8. Chickasha: typical process of desiccation cracking at the beginning of the test (a), 3 hours (b) and 12 hours (c) after starting the test.

Figure 4.9. Idabel: typical process of desiccation cracking at the beginning of the test (a), 4 hours (b) and 18 hours (c) after starting the test.

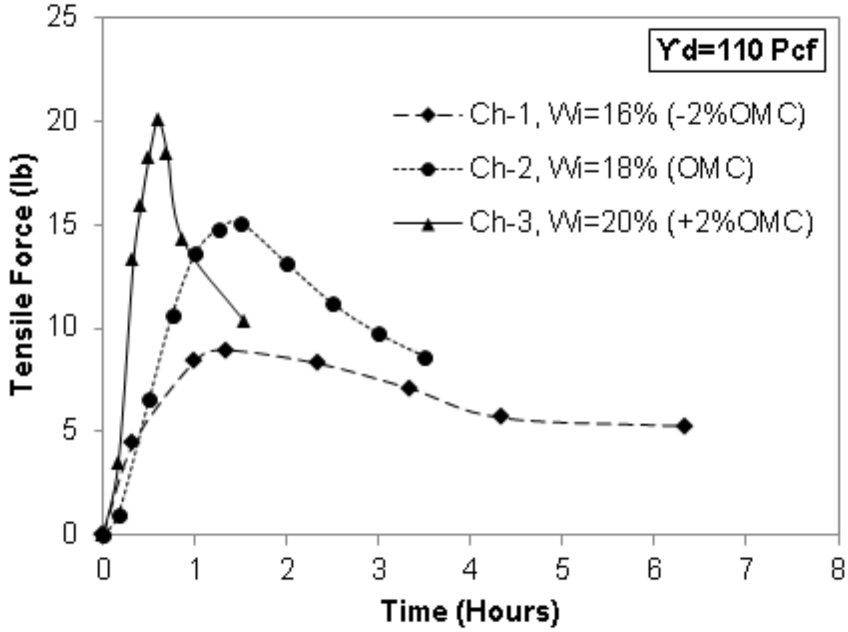

Figure 4.10. Chickasha: variation of tensile force over time for Test Series 1.

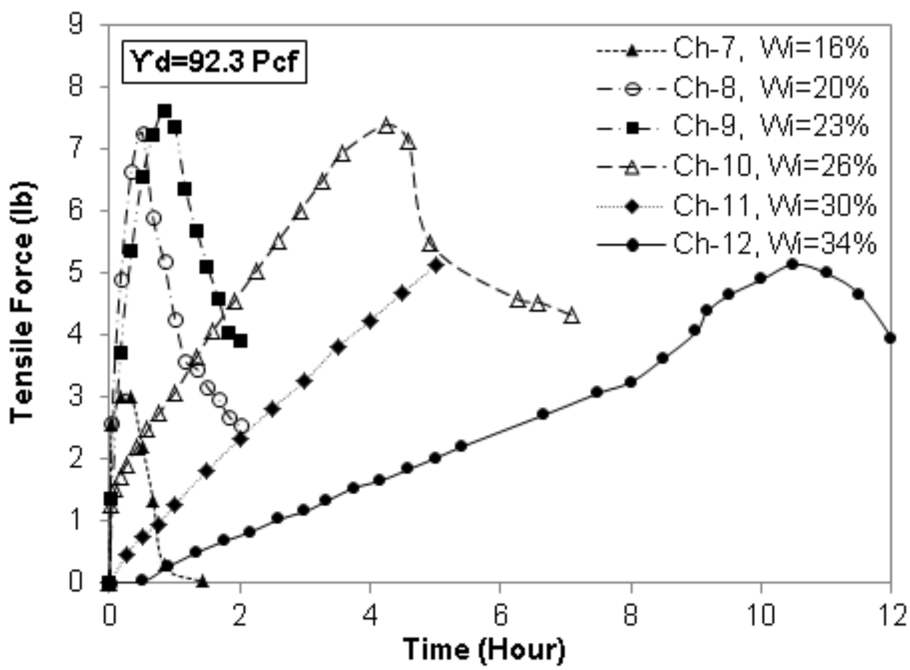

Figure 4.11. Chickasha: variation of tensile force over time for Test Series 3.

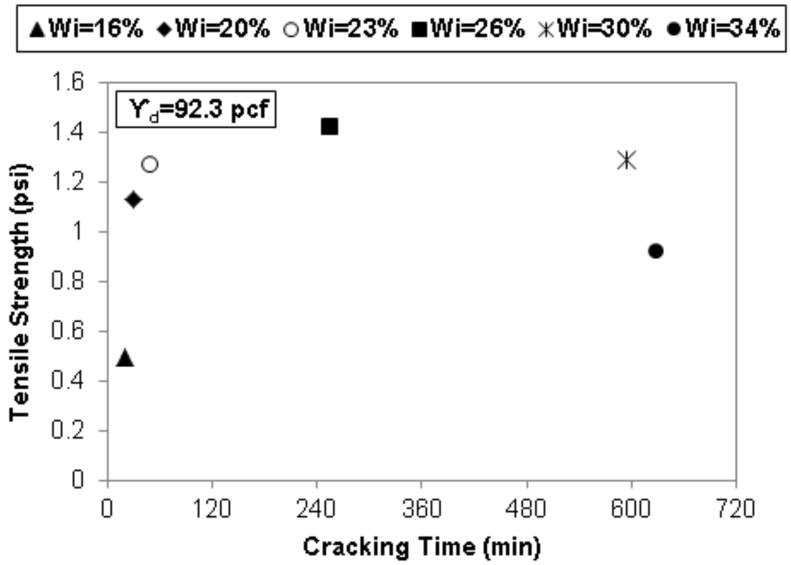

Figure 4.12. Chickasha: tensile strength versus cracking time for Test Series 3.

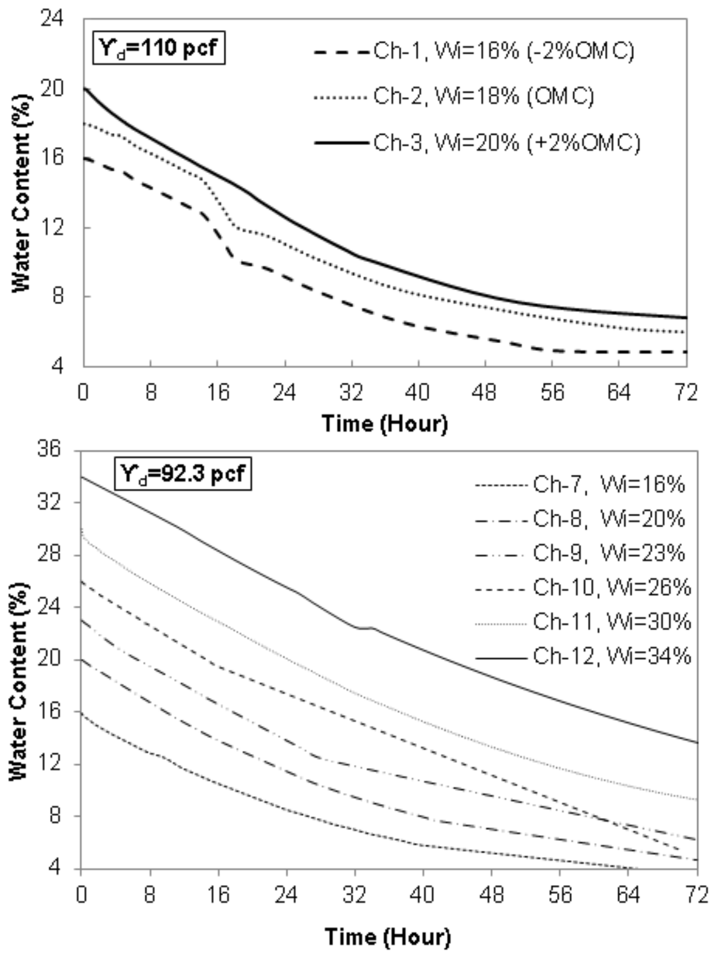

Figure 4.13. Chickasha: variation of water content over time for Test Series 1 (top) and 3 (bottom).

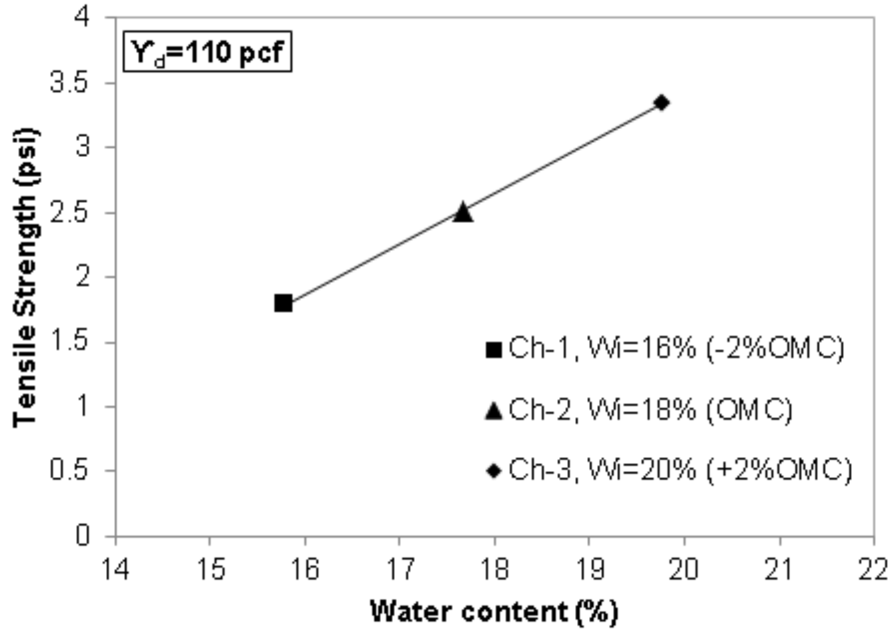

Figure 4.14. Chickasha: tensile strength versus cracking water content for Test Series 1.

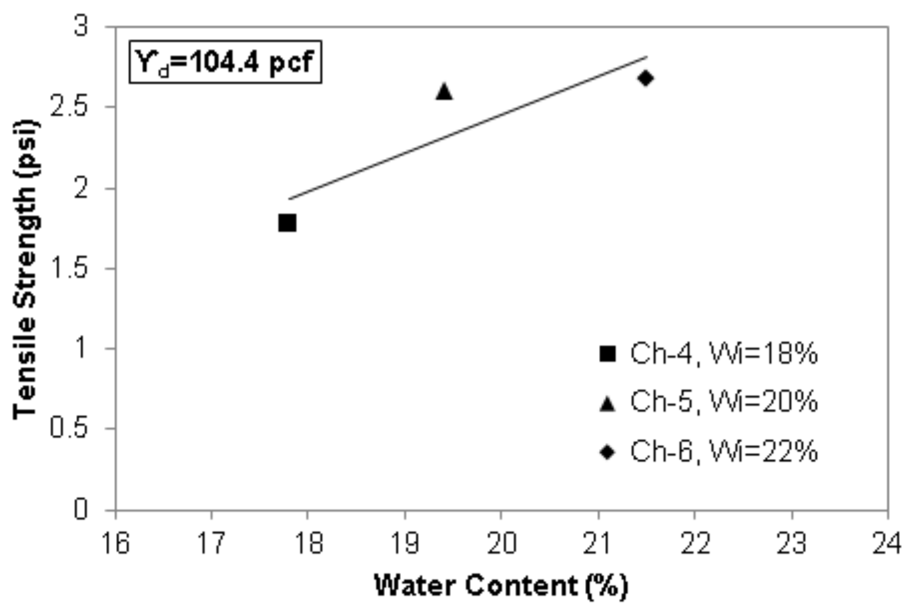

Figure 4.15. Chickasha: tensile strength versus cracking water content for Test Series 2.

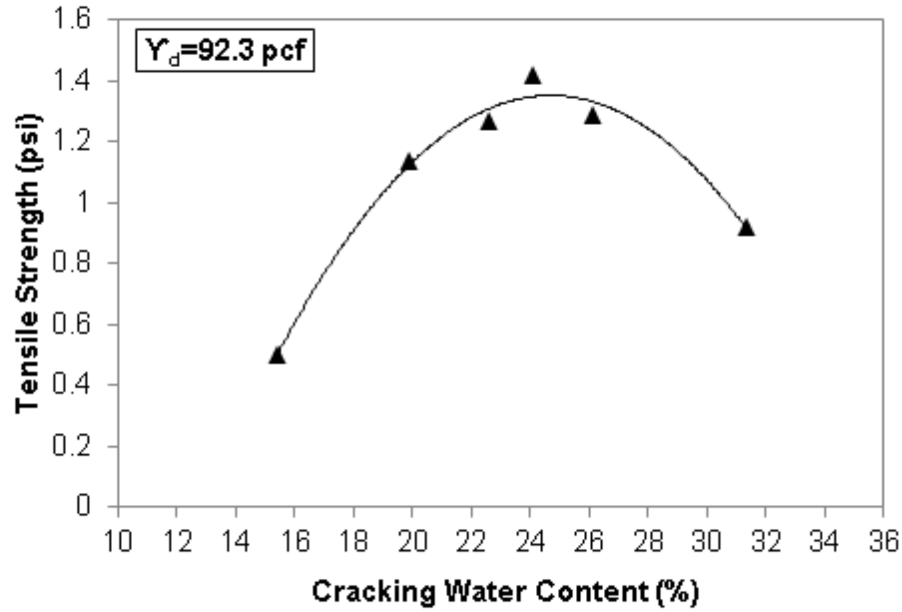

Figure 4.16. Chickasha: tensile strength versus cracking water content for Test Series 3.

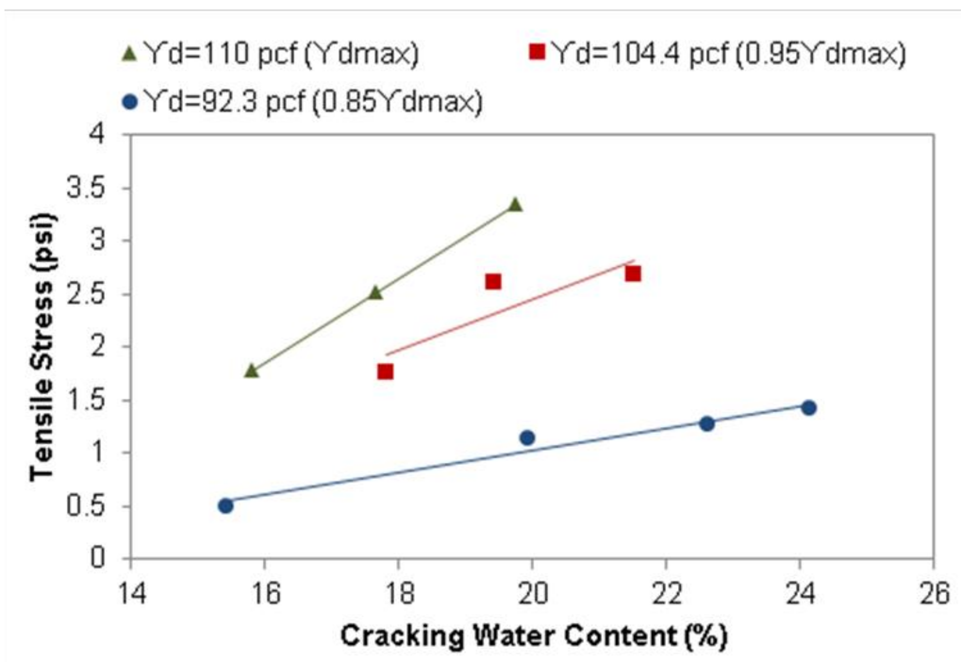

Figure 4.17. Chickasha: effect of dry unit weight on tensile strength.

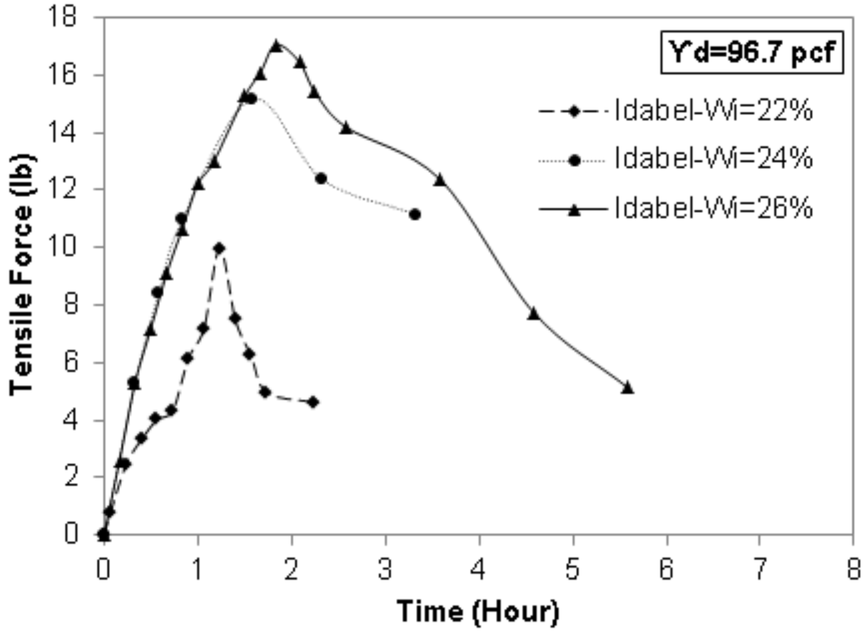

Figure 4.18. Idabel: variation of tensile force over time for Test Series 4.

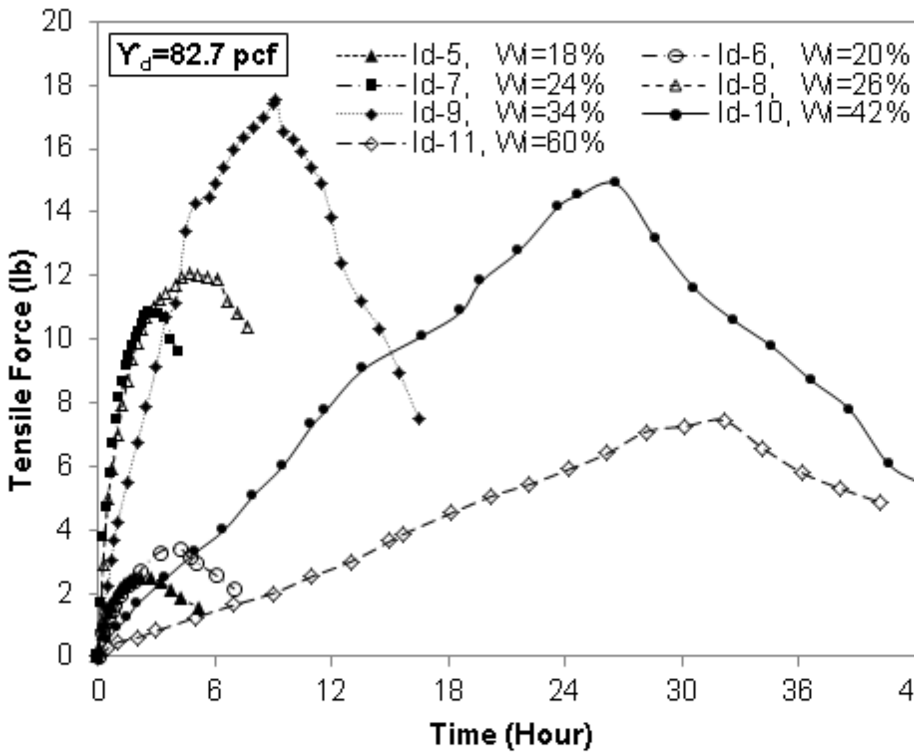

Figure 4.19. Idabel: variation of tensile force over time for Test Series 5.

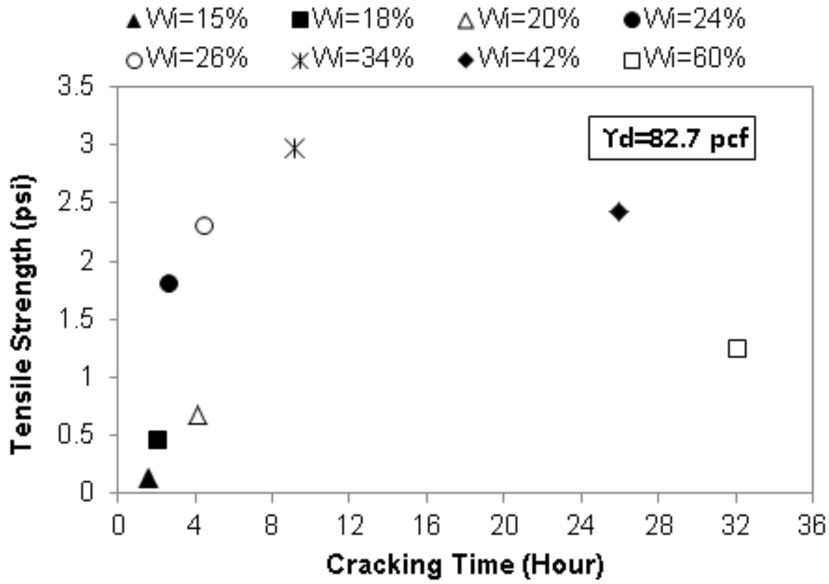

Figure 4.20. Idabel: tensile strength versus cracking time for Test Series 5.

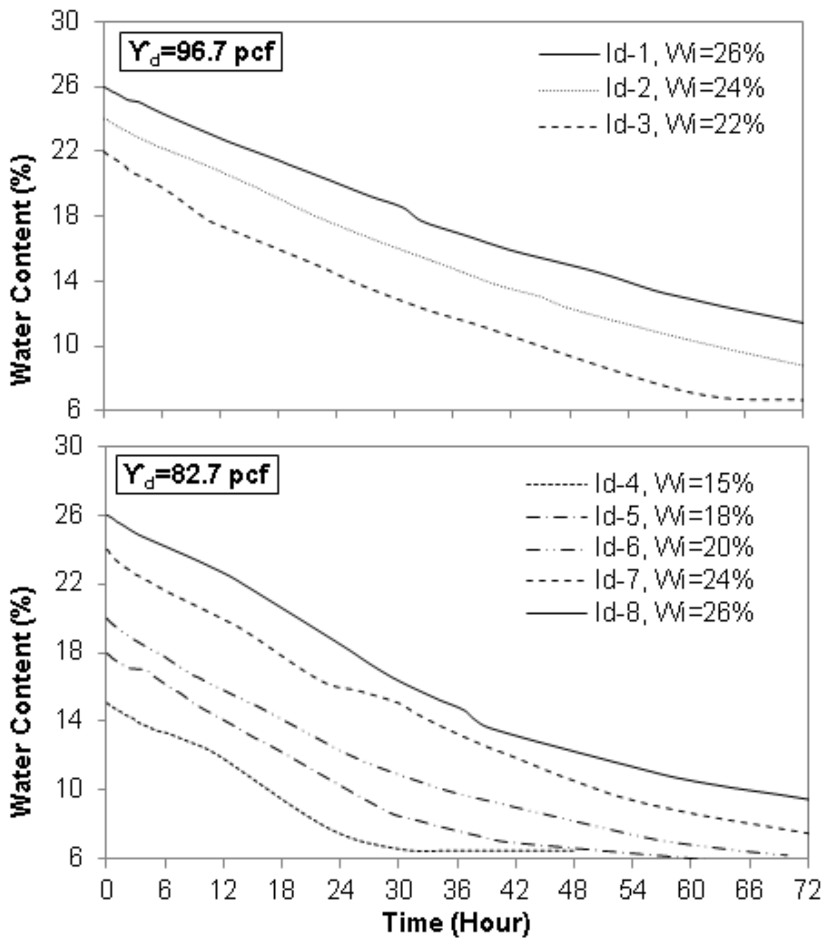

Figure 4.21. Idabel: variation of water content over time for Test Series 4 (top) and 5 (bottom).

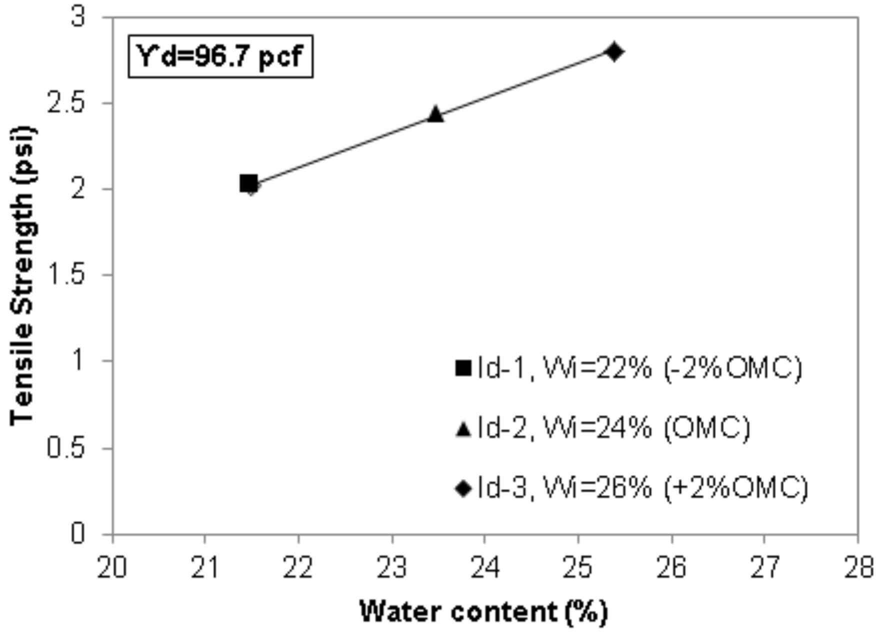

Figure 4.22. Idabel: tensile strength versus cracking water content for Test Series 4.

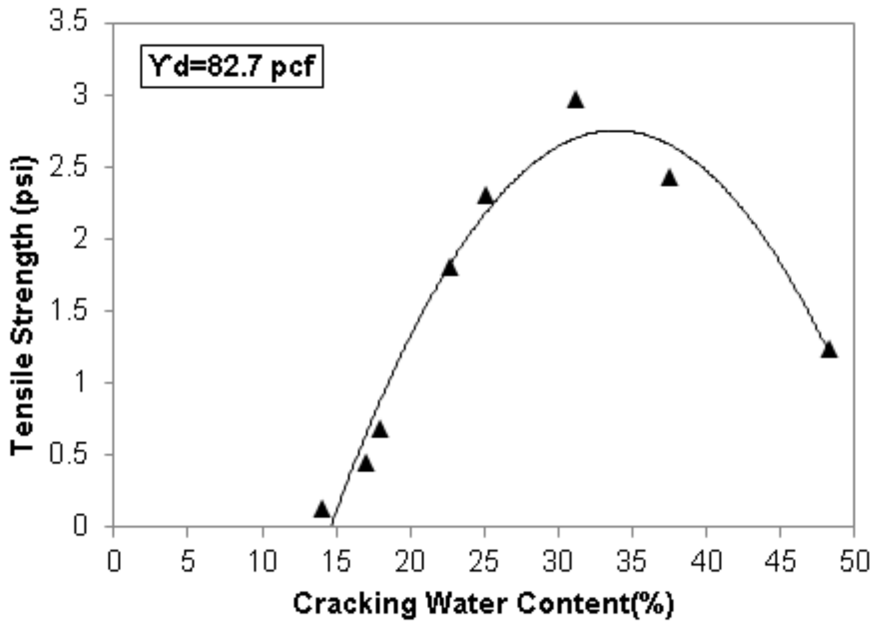

Figure 4.23. Idabel: tensile strength versus cracking water content for Test Series 5.

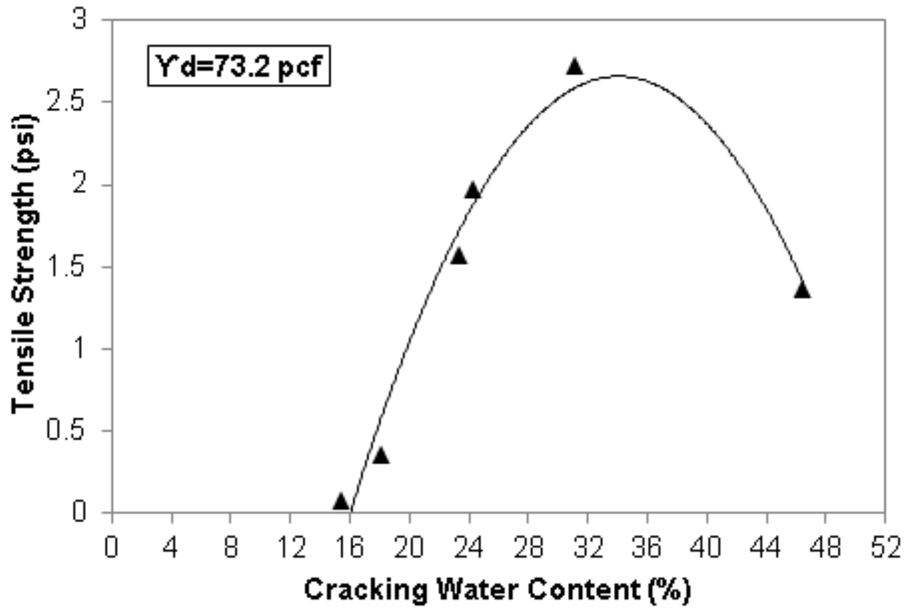

Figure 4.24. Idabel: tensile strength versus cracking water content for Test Series 6.

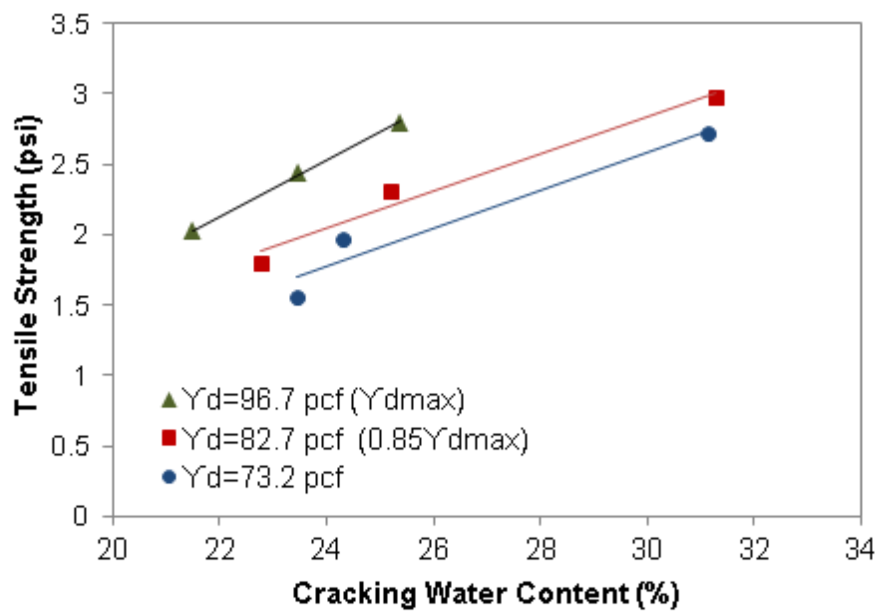

Figure 4.25. Idabel: effect of dry unit weight on tensile strength.

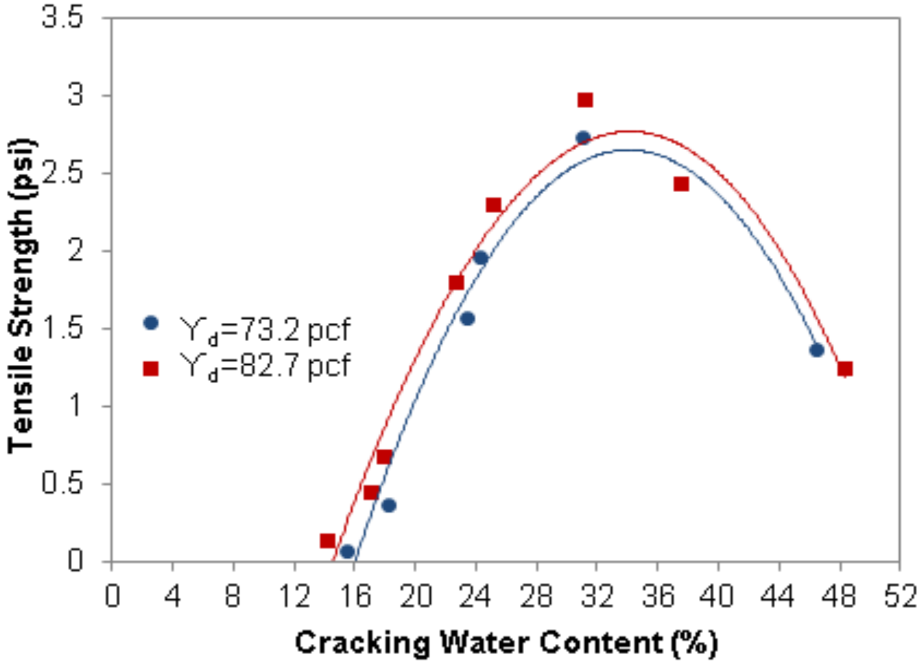

Figure 4.26. Idabel: effect of dry unit weight on tensile strength of Idabel Soil for Test Series 5 and 6.

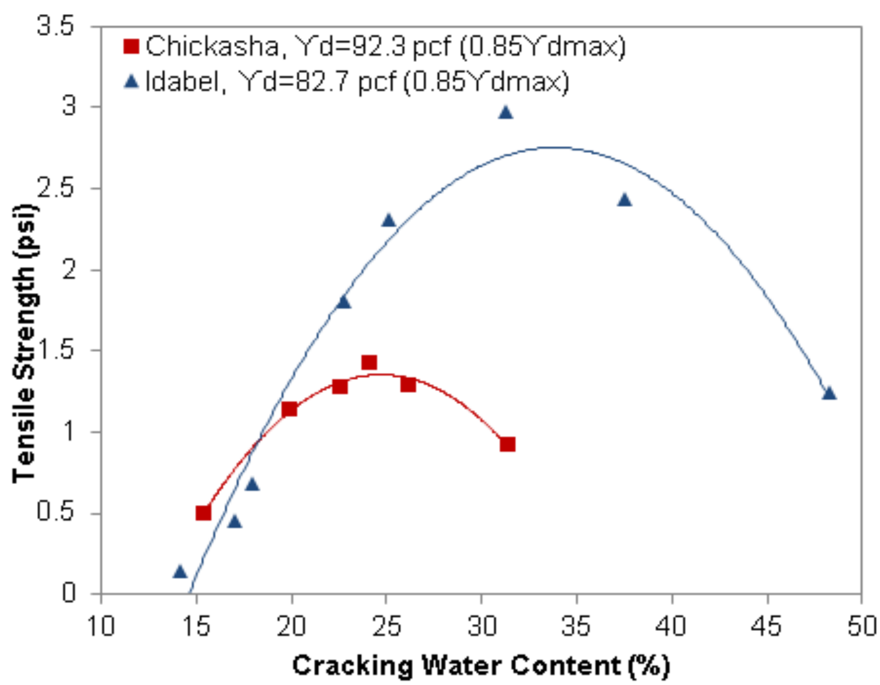

Figure 4.27. Effect of soil type on tensile strength of soil.

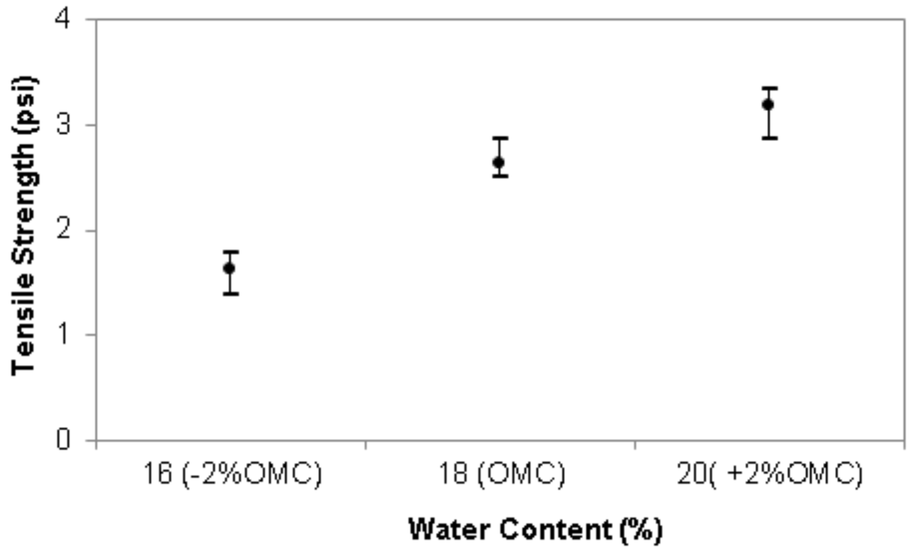

Figure 4.28. Repeatability of the test results (range bars shown for n=3 for each water content).

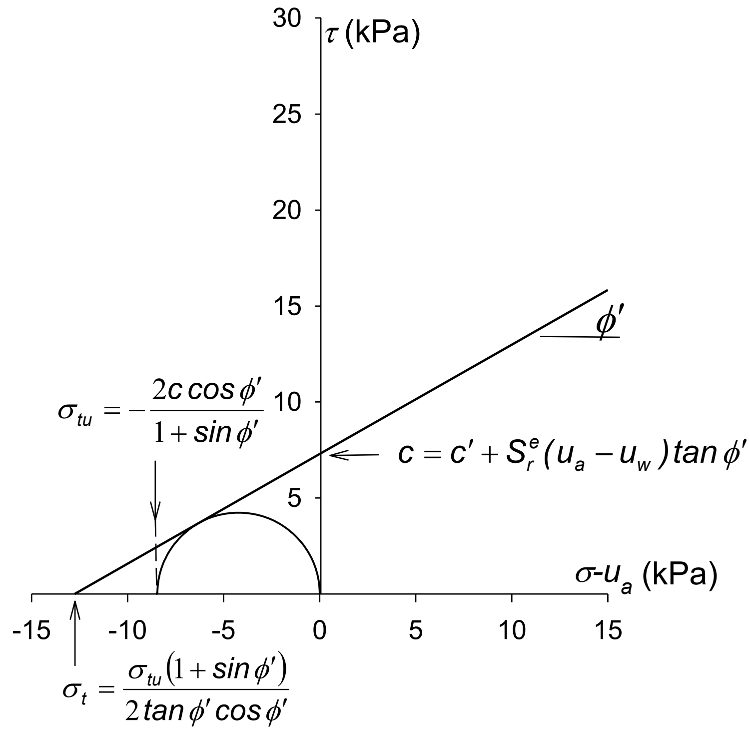

Figure 4.29. Tensile strength based on Mohr-Coulomb model.

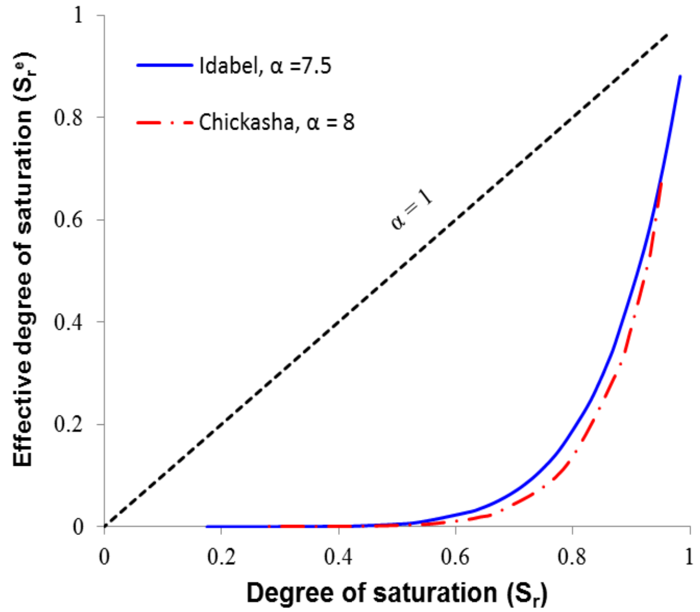

Figure 4.30. Plots from Equation 4.3 showing the variation of effective degree of saturation with degree of saturation.

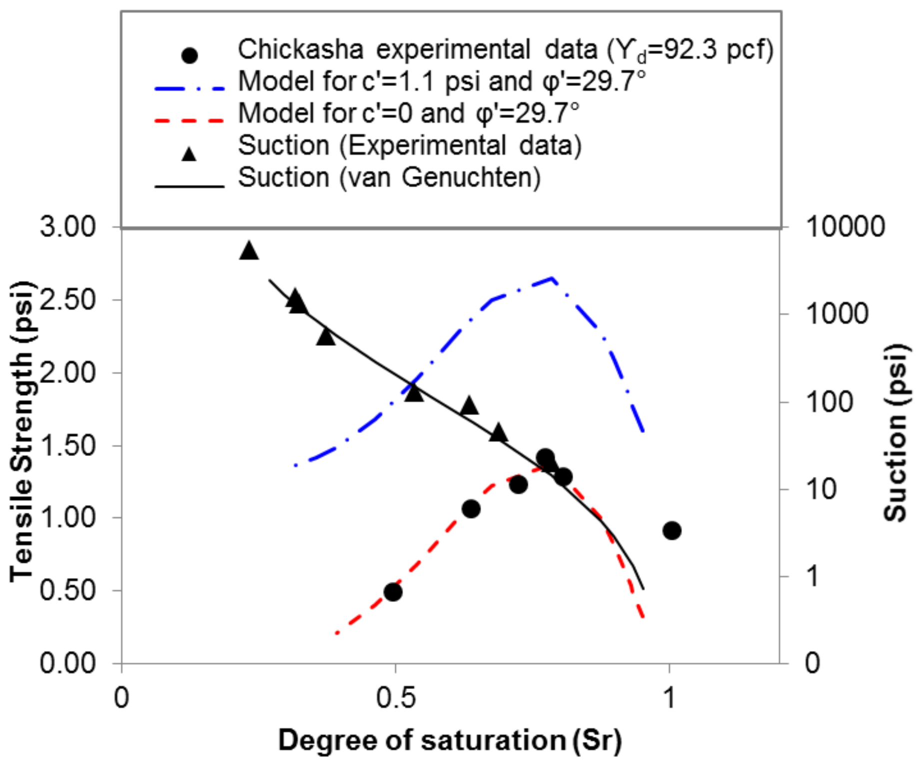

Figure 4.31. Chickasha: comparison of experimental results with the calculated tensile strength obtained from the theoretical model.

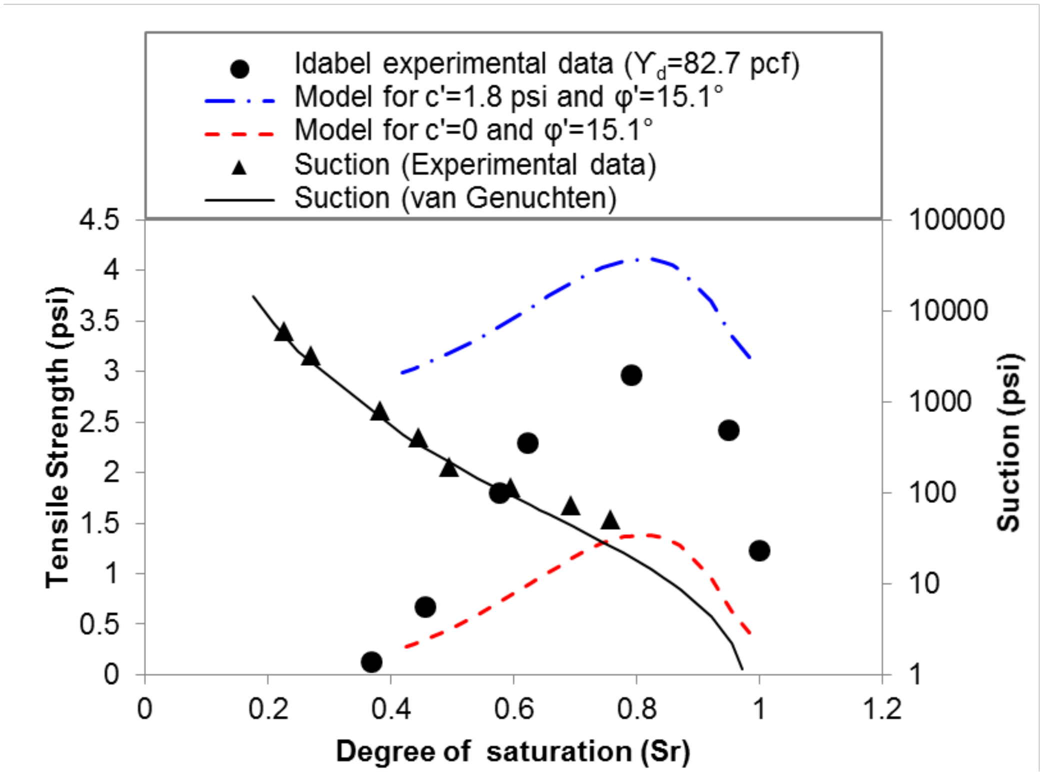

Figure 4.32. Idabel: comparison of experimental results with the calculated tensile strength obtained from the theoretical model.

Chapter 5 RESULTS FROM FIELD INSTRUMENTATION AND SOIL MOISTURE MODELING

5.1 Weather Data from the Chickasha Site

Data were collected from the weather monitoring station located in Chickasha, Oklahoma between August 31, 2012 and June 10, 2014. Figures 5.1, 5.2 and 5.3 show plots of the following information: 1) average daily air temperature, 2) wind speed, 3) maximum daily relative humidity, 4) maximum and minimum air temperature, 5) total daily solar radiation, 6) precipitation, and 7) average daily soil volumetric moisture content and temperature at depths of at 1, 3 and 6 ft.

The factors that most affect the air temperature are: the latitude, altitude and cloud coverage. The city of Chickasha is located at 35.03^o from the equator and at an elevation of about 1,093 ft. The average temperature ranges between a maximum of 105^{o}F to a minimum of 6^{o}F. Between December and January, it was noticed that the average air temperature drops to the minimum, and then increases gradually to its maximum between July and August. Similar factors also influence the total solar radiation. In fact, the highest value of solar radiation was recorded during the longest day in a calendar year which happens to be in June, when the duration of solar radiation is the longest and the solar angle of incidence is the greatest. Interestingly, the maximum recorded value of solar radiation equal to 2,581 BTU/ft^2 corresponds to June and not July or August when the atmospheric temperature is the highest. This is due to the fact that the amount of precipitation and water vapor increase at the end of the summer thus keeping the air temperature high but with reduced intensity of the solar radiation.

The soil temperature was measured at 1, 3 and 6 ft. The maximum soil temperature decreased from 81°F at 1 ft. to 76 °F at 3 ft. to 73 °F at 6 ft. below ground surface. The observed annual variation follows the pattern for air temperature rather than the solar radiation as shown in Figure 5.2. The highest recorded soil temperatures were between August and September, and the lowest were in between February and March. These values are mostly influenced by the soil moisture content, rainfall, net solar radiation, vegetation cover, soil texture, soil thermal and heat capacity.

The rainfall distribution during the monitoring period is shown in Figure 5.1 and tabulated for 2013 in Table 5.1. As the relative humidity increases in warm weather conditions, the chances for rainfall also increase. In fact, high precipitation occurred in April, July and August, and low precipitation occurred in February and December. Relative humidity is influenced mostly by air temperature and latitude.

The daily pattern of soil moisture content is not complete for the depths of 3.0 ft. and 6.0 ft. due to some equipment limitations. However, for a depth of 1.0 ft., the soil moisture content profile shows the seasonal variation with weather conditions. It can be noted that moisture content at a depth of 1 foot decreases significantly between July and October, and similarly rises in October and November. This relatively rapid drying results from the grater solar radiation and higher temperatures during these months. Desiccation cracks likely enhance the rate of drying and wetting during these months.

Similar types of weather data were also collected from the Oklahoma Mesonet monitoring station located in Chickasha, obtained using the daily data retrieval website tool (http://www.mesonet.org/index.php/weather/daily_data_retrieval). The data were collected for the same period of time, starting from August 31, 2012 and ending on June 10, 2014. Comparisons of data obtained from the test sites and Mesonet stations are shown in Figures 5.4 to 5.7.

The comparison between the two sets of data indicates some slight differences between the total daily solar radiation, wind speed, and relative humidity. These differences are similar in all three graphs, in that the data obtained from Mesonet are higher than that of the weather station. It is believed the differences are the result of the fact that the test site weather station is somewhat protected on the north slope of the embankment whereas the Mesonet monitoring station in Chickasha (35.03236°N, 97.9145°W) is located in an open farm field. On the other hand, the average air temperature and total amount of rainfall are relatively close at the two sites.

5.2 Weather Data from the Idabel Site

Similar weather data was collected from the weather station installed at the second test site located in Idabel, McCurtain County, Oklahoma. Because it was difficult to install sensors at greater depths due to the presence of frequent limestone cobbles and boulders, at this site the soil temperature and volumetric water content measurements were obtained at depths of 0.5, 1, and 1.5 ft. Weather data for the Idabel Site are presented in Figures 5.8, 5.9 and 5.10.

Compared to the Chickasha Site, data from the Idabel Site showed slightly higher amounts of rainfall, relative humidity and subsurface soil temperature variation (at 1-foot depth). These differences can be attributed to the Idabel Site: being located at a lower elevation than the Chickasha Site (361 feet above mean sea level, versus 1,076 feet), being at a different latitude (33^{o} 49’ 48” N, versus 35^{o} 1’ 56” N), and having greater percentage of active fine soil particles.

Table 5.1 shows a summary of the total monthly rainfall distribution during 2013. It shows that total rainfall was similar in Idabel and Chickasha during that year. Nevertheless, soil volumetric water contents generally reached higher values (e.g. 0.67 ft^3/ft^3 at a depth of 1.5 ft.) compared to Chickasha. This is attributed to the greater plasticity and swelling potential of the Idabel soil.

The comparisons between the weather data obtained from the Idabel site and the nearest Mesonet station are shown in Figures 5.11, 5.12 and 5.13. Generally, the comparison was favorable between the measured solar radiation, daily temperature, and wind speed. However, comparison for the rainfall data and relative humidity show some slight differences. The comparison indicates that on average it rained slightly more southwest of Idabel where the Mesonet station is located.

5.3 Modeling Moisture Variations in Soil Profiles using SVFlux

Extensive modeling of soil moisture profiles using weather data as input was conducted to evaluate the predictive capability of two commercially available software programs Vadose/W and SVFlux. This section presents results from SVFlux followed by Vadose/W results in the next section.

5.3.1 SVFlux: Chickasha Site

For the purpose of modeling, the depth of active zone was assumed to be within a depth of 10 feet. The layers assumed in the model are as shown in Figure 5.14. The precipitation pattern used in the modeling, shown in Figure 5.15, was based on onsite weather station measurements and supplemented with Mesonet station data as needed. The soil water characteristic curve (SWCC) and unsaturated hydraulic conductivity function used for modeling are shown in Figures 5.16 and 5.17.

The evaporation parameters including air temperature, air relative humidity, solar radiation, and wind speed were collected from the onsite weather station and entered as a climate boundary condition on the ground surface. The quality of the grass used in SVFlux as an input parameter is reflected by the Leaf Area Index (LAI) and was based on observations at the test site. An LAI of 3 was used indicating excellent grass coverage (LAI =3.0). The Plant Moisture Limiting factor (PML) was based on a typical function built into the software and shown in Figure 5.18.

The predicted and measured volumetric water content variations for three different depths at the site are shown in Figures 5.19 (a), (b), and (c). It is evident that higher fluctuations in volumetric water content occurred close to the surface and these fluctuations decreased with depth. This behavior can be attributed to the low hydraulic conductivity of clayey soils and longer durations needed to affect soils at greater depth. It is noted that the average trends of predicted moisture content variations are consistent with measured variations, however, more abrupt changes in measured values occur for some wetting and drying events. This may be in part due to desiccation cracks in the vicinity of moisture sensors which allow for more rapid drying and wetting at these locations.

5.3.2 SVFlux: Idabel Site

A similar approach to modeling moisture variations due to weather changes was used for the Idabel site. Similar to Chickasha, the geometry of the model assumed the active zone was limited to 10 feet as shown in the soil profile of Figure 5.20. The precipitation data recorded and at the local weather station is shown in Figure 5.21.

The evaporation parameters including air temperature, air relative humidity, net radiation, and wind speed were collected from the local weather station. Leaf Area Index (LAI) and Plant Limiting Factor were applied to the model procedures similar to those selected for Chickasha site. The soil water characteristic curves and hydraulic conductivity functions are shown in Figures 5.22 and 5.23.

The predicted and measured moisture contents for three different depths at the site are shown in Figure 5.24. The average trends of predicted moisture contents tended to be larger than measured values and similar to Chickasha, changes between drying and wetting cycles were more pronounced for the measured water contents. Considering all of the parameters required to model moisture variations in a soil profile and the numerous uncertainties and assumptions associated with laboratory testing, field measurements, and influence of desiccation cracks, the SVFlux predictions seem reasonably good, especially for the Chickasha site.

5.4 Modeling Moisture Variations in Soil Profiles using VADOSE/W

5.4.1 VADOSE/W: Chickasha

The program VADOSE/W was also used to model moisture variations at the test sites using basically the same input parameters, with few exceptions, used to model soil-atmosphere interaction with SVFlux. One exception is that VADOSE/W uses a variable Leaf Area Index (LAI) depending on the time of year whereas SVFLux uses a constant value. The numerical results generally under predicted the moisture content. This is attributed to two main factors. First, the runoff was not properly modeled to account for presence of the slope. Second, unlike SVFlux, VADOSE/W does not adjust the meshing properties during the change from a high negative to a high positive gradient. The predicted versus measured values are shown in Figure 5.25 for the sensor depths of 1, 3 and 6 ft. Results from Idabel were similar in that predicted moisture contents were well below those measured at sensor locations.

Table 5.1. Total monthly rainfall during 2013 for Chickasha and Idabel Sites.

Chickasha		Idabel	
Month	**Total Rainfall (in)**	**Month**	**Total Rainfall (in)**
Jan	1.99	**Jan**	3.36
Feb	2.53	**Feb**	1.98
Mar	0.71	**Mar**	3.18
Apr	9.01	**Apr**	1.15
May	3.92	**May**	6.5
Jun	4.34	**Jun**	4.5
Jul	5.53	**Jul**	5.72
Aug	2.53	**Aug**	0.01
Sep	1.85	**Sep**	2.55
Oct	2.06	**Oct**	4.47
Nov	0.83	**Nov**	2.65
Dec	0.33	**Dec**	1.93
Total	35.63	**Total**	36.07

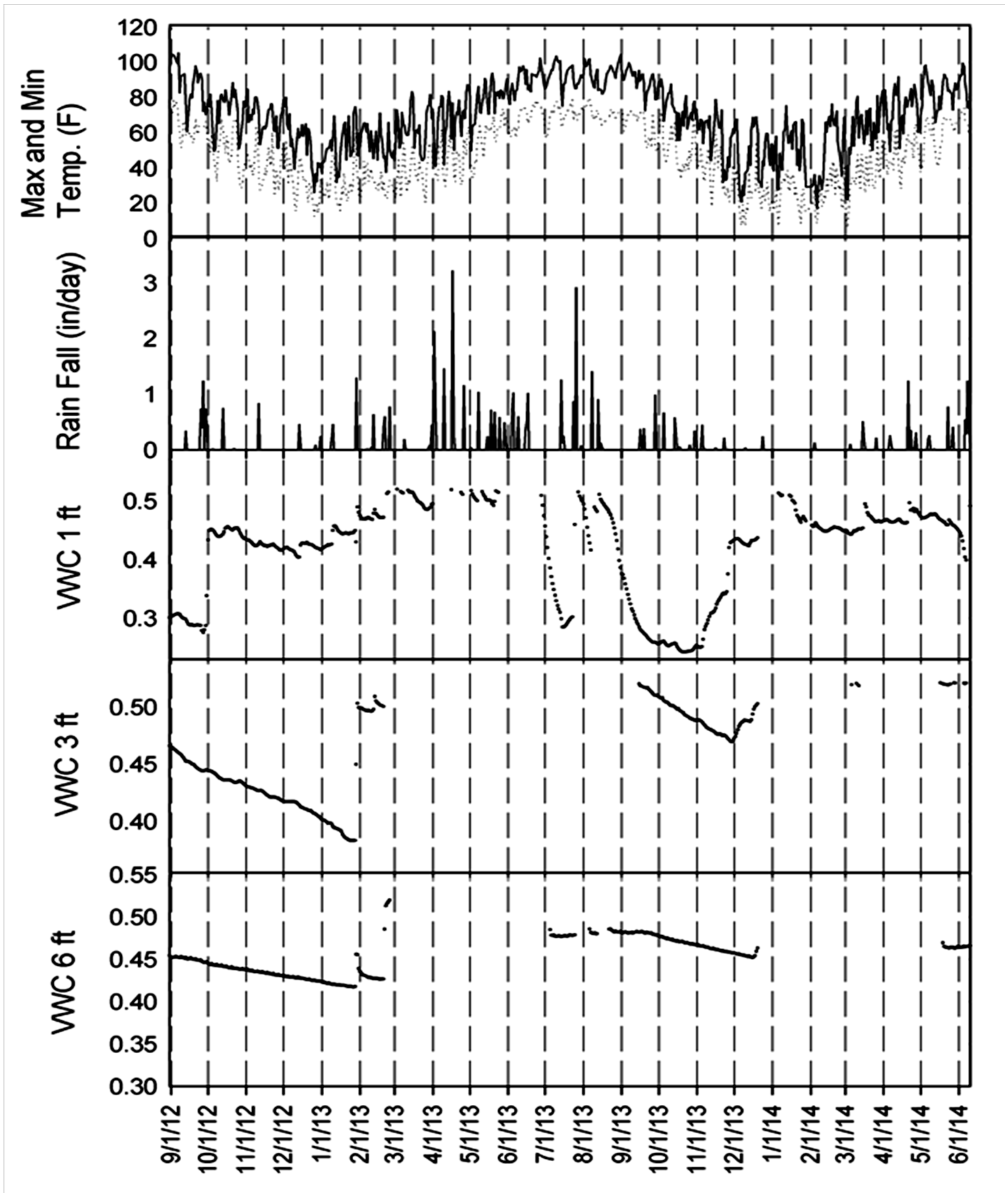

Figure 5.1. Chickasha: maximum and minimum daily temperature, total rainfall, and volumetric water content at the test site.

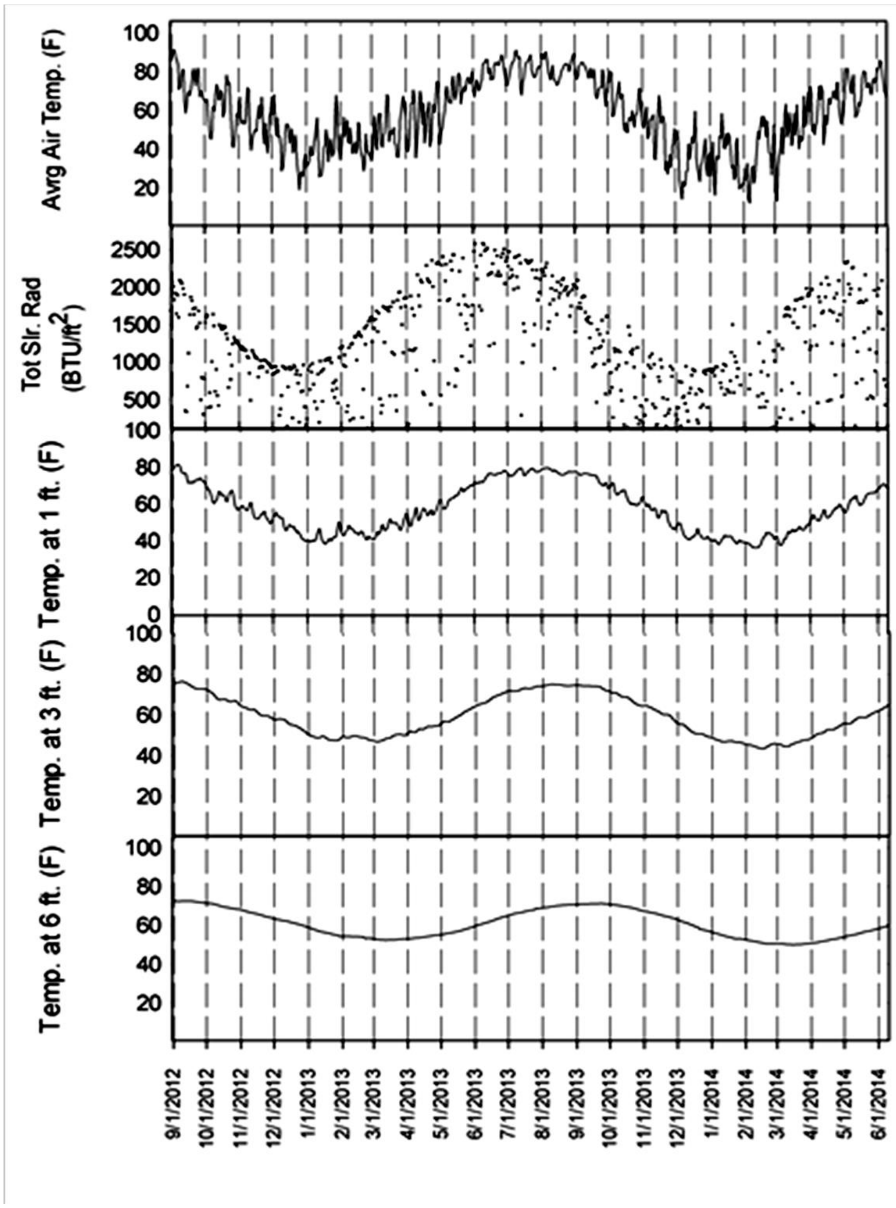

Figure 5.2. Chickasha: daily average temperature, total solar radiation, and subsurface soil temperature at the test site.

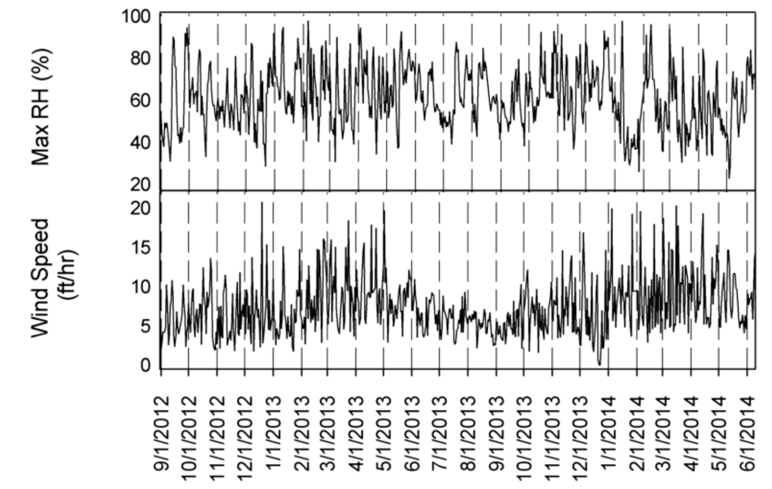

Figure 5.3. Chickasha: daily maximum relative humidity and average wind speed at the test site.

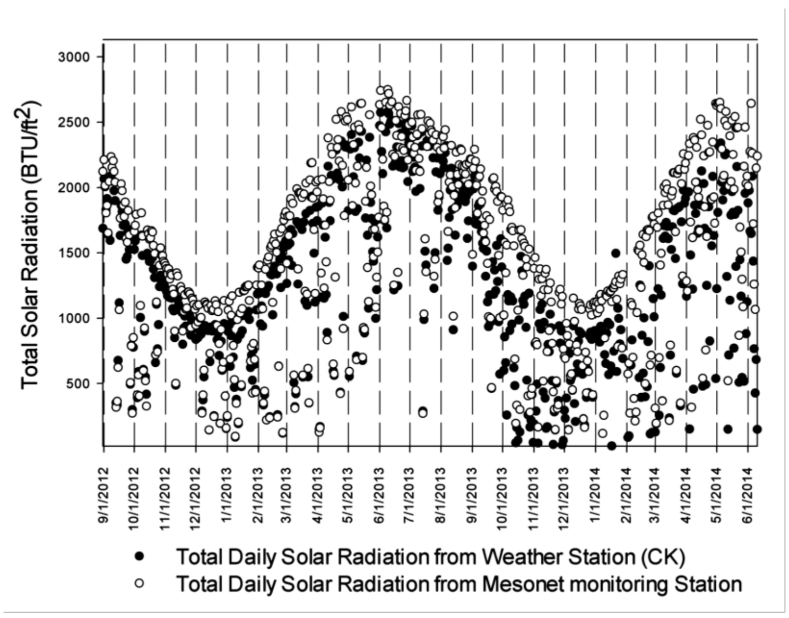

Figure 5.4. Chickasha: total daily solar radiation data from the test site and nearest Mesonet station.

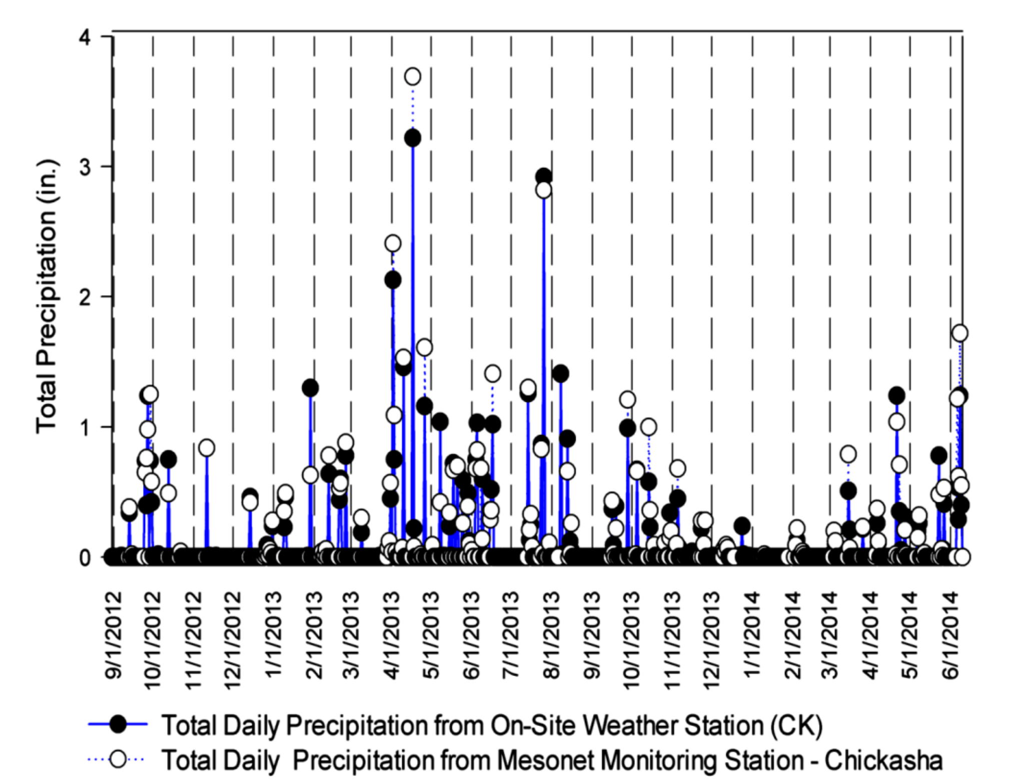

Figure 5.5. Chickasha: total daily precipitation from the test site and nearest Mesonet station.

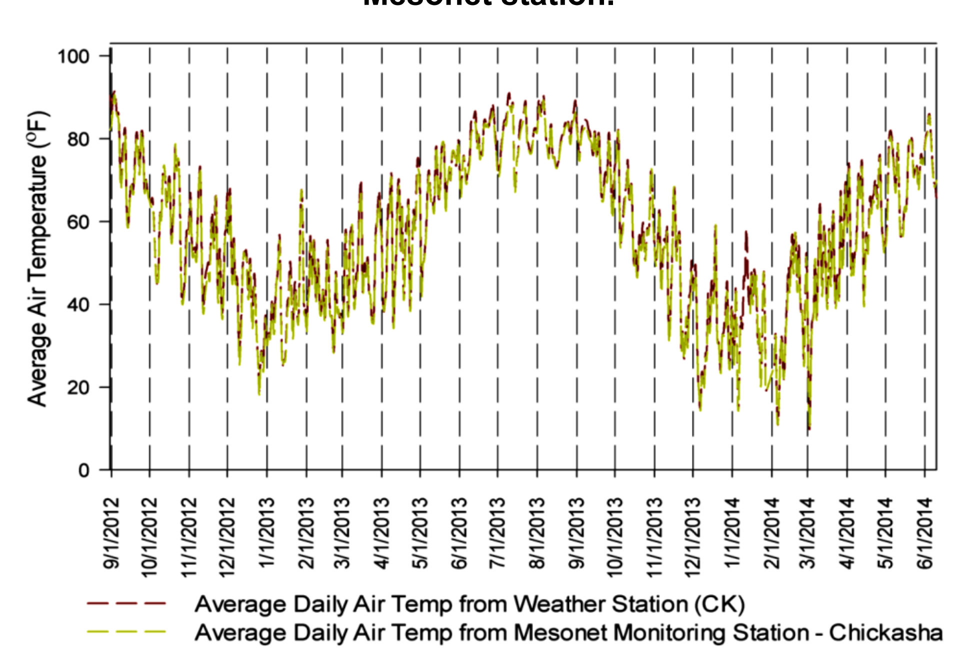

Figure 5.6. Chickasha: average daily air temperature from the test site and nearest Mesonet station.

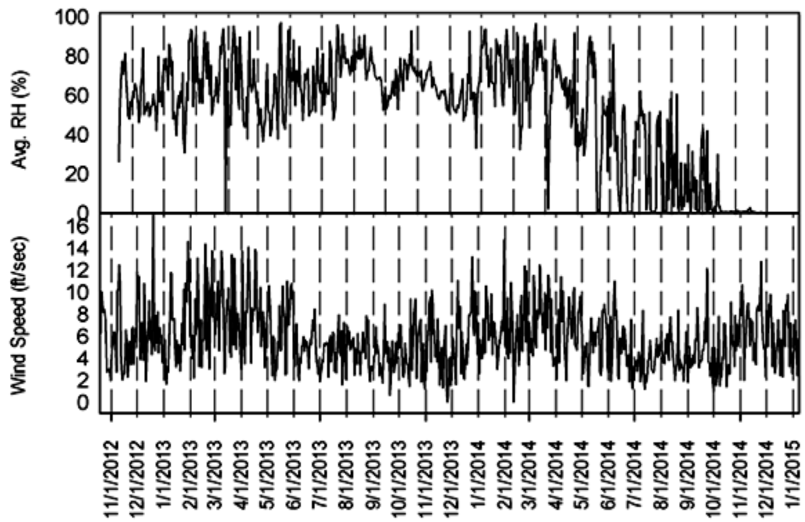

Figure 5.7. Idabel: daily maximum relative humidity and average wind speed at the test site.

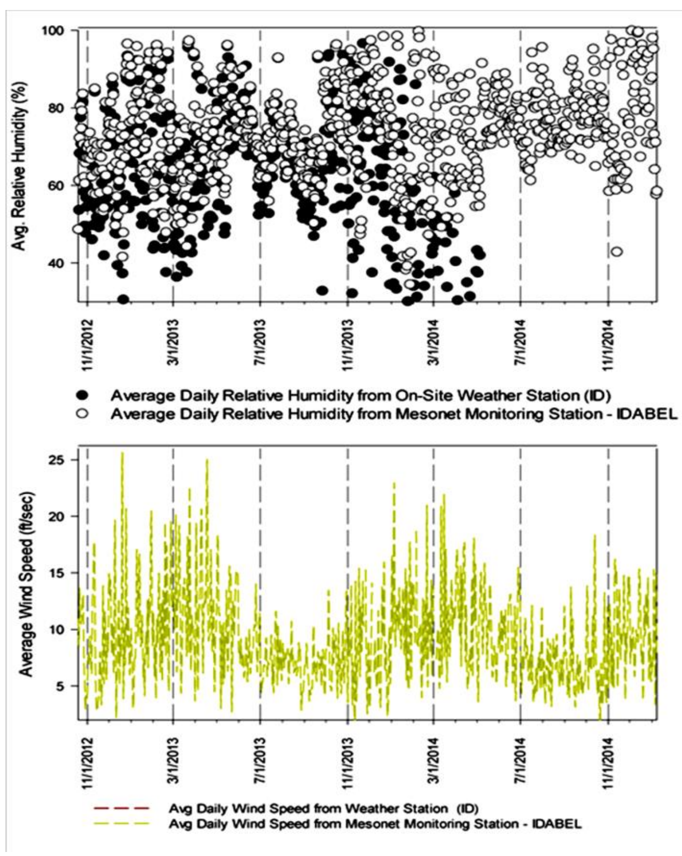

Figure 5.8. Idabel: average daily relative humidity and wind speed from the test site and nearest Mesonet station.

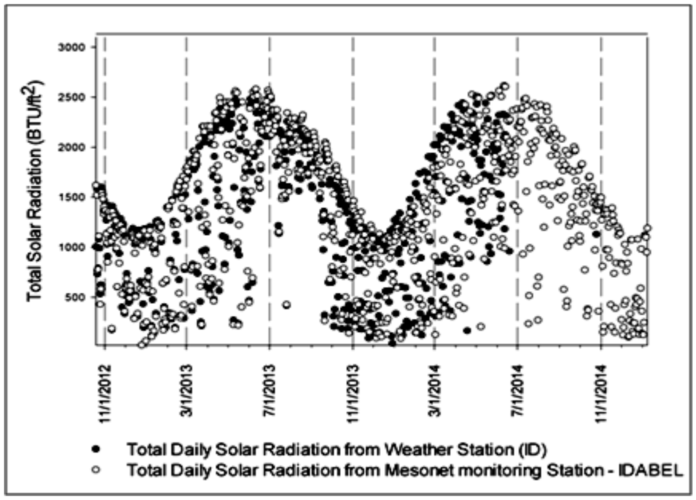

Figure 5.9. Idabel: total daily solar radiation data from the test site and nearest Mesonet station.

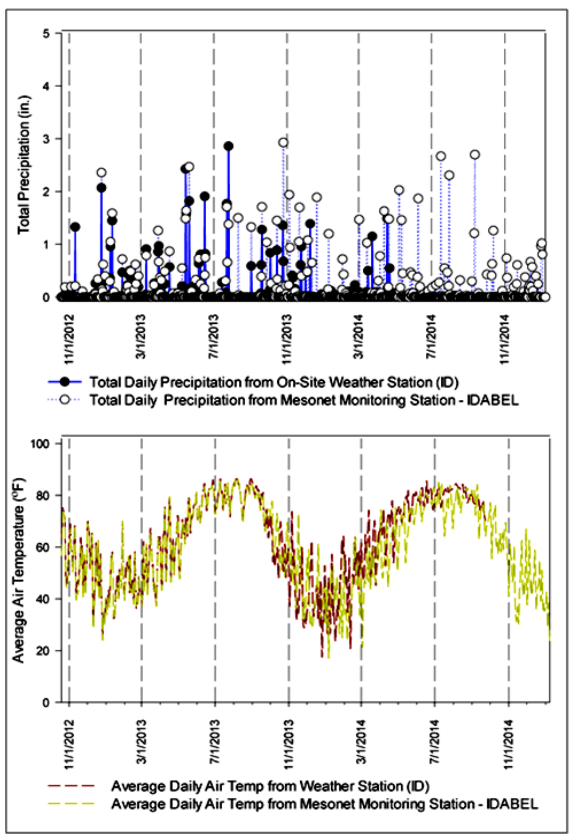

Figure 5.10. Idabel: total daily precipitation and air temperature from the test site and nearest Mesonet station.

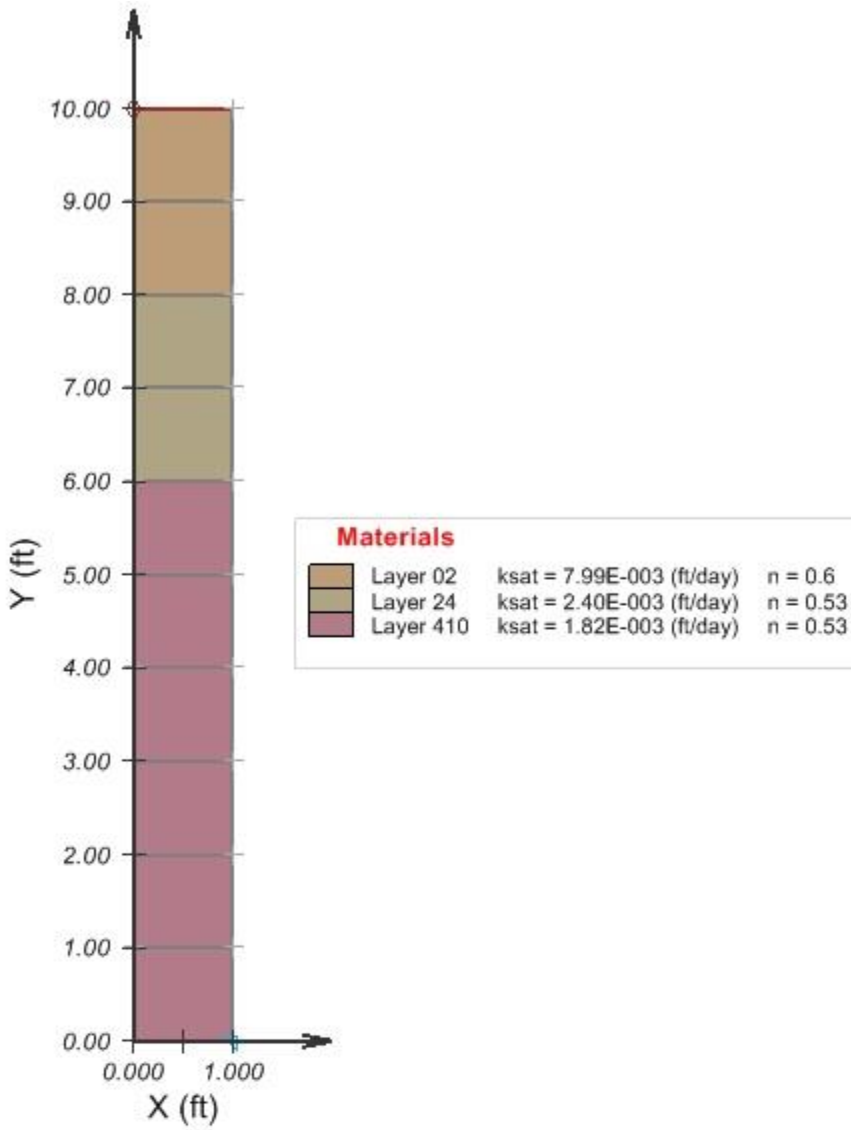

Figure 5.11. Chickasha: SVFlux model soil profile.

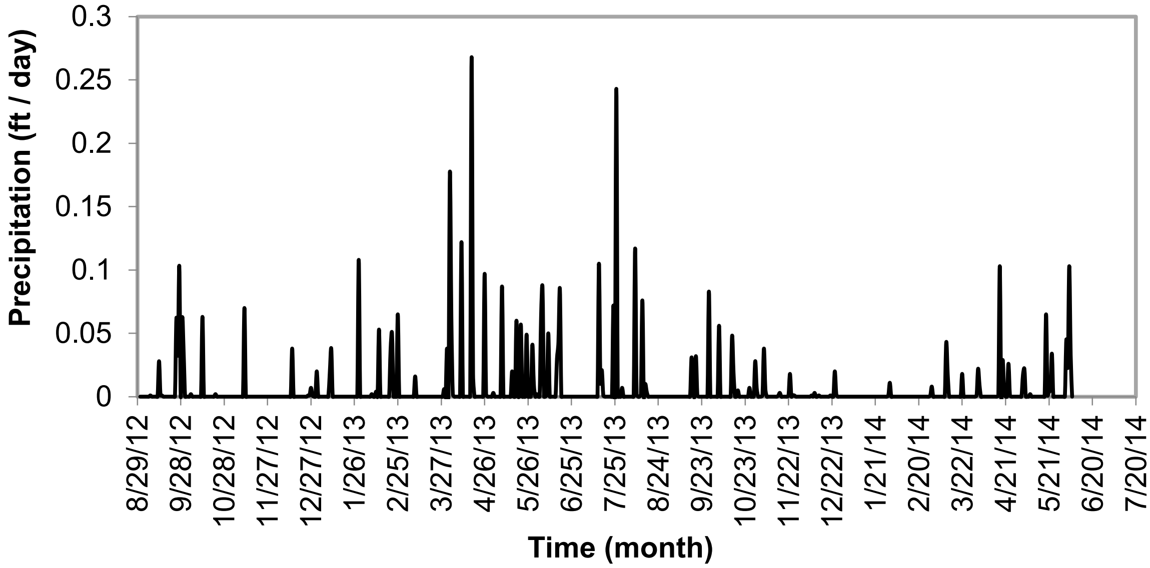

Figure 5.12. Chickasha: rainfall data.

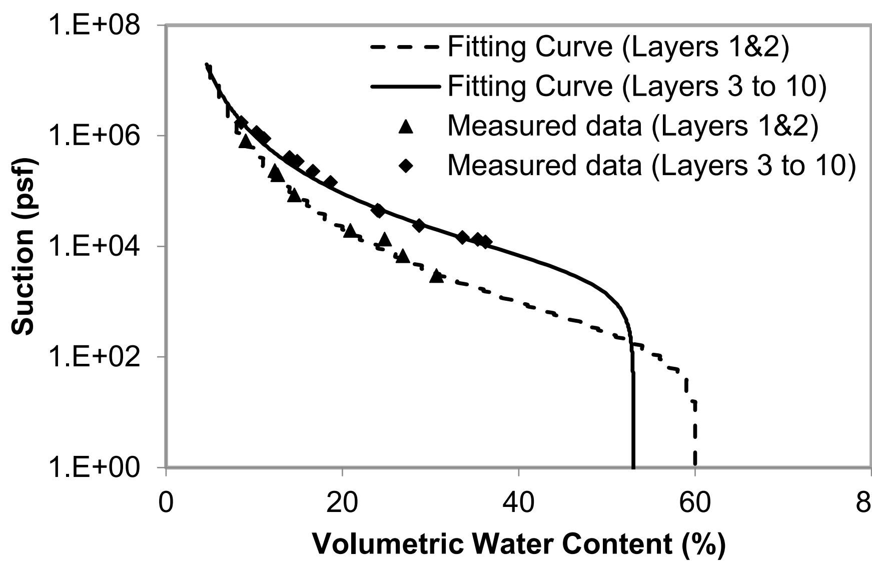

Figure 5.13. Chickasha: SWCC used in modeling.

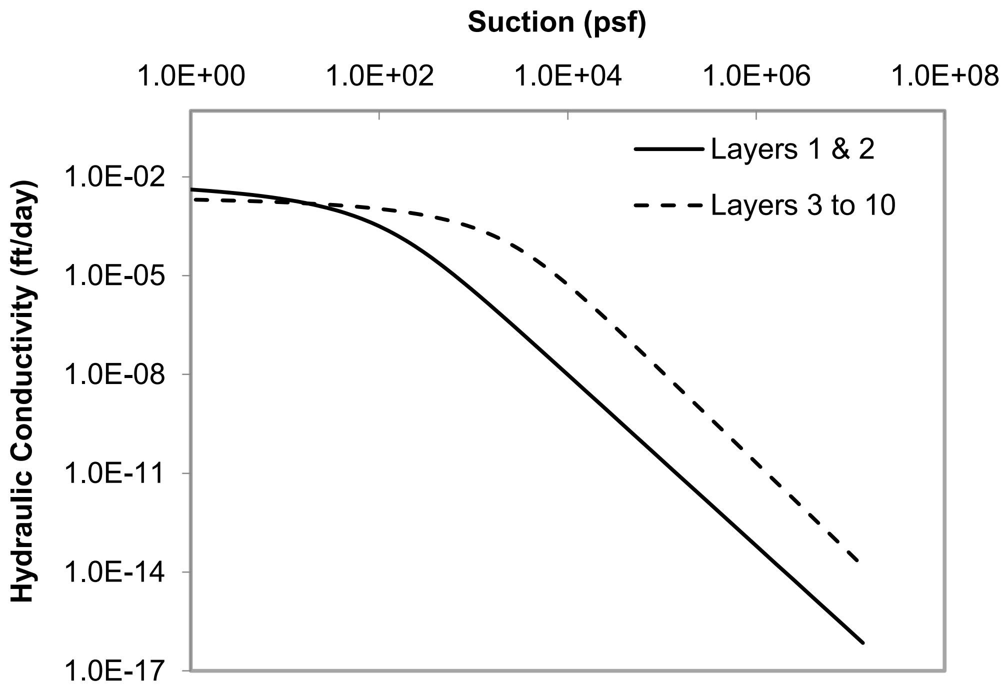

Figure 5.14. Chickasha: hydraulic conductivity versus suction.

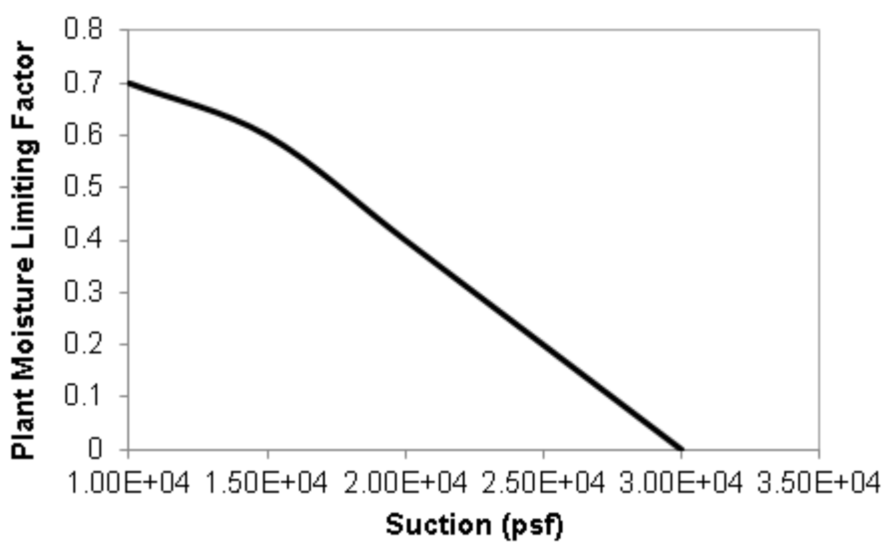

Figure 5.15. Plant moisture limiting factor versus suction.

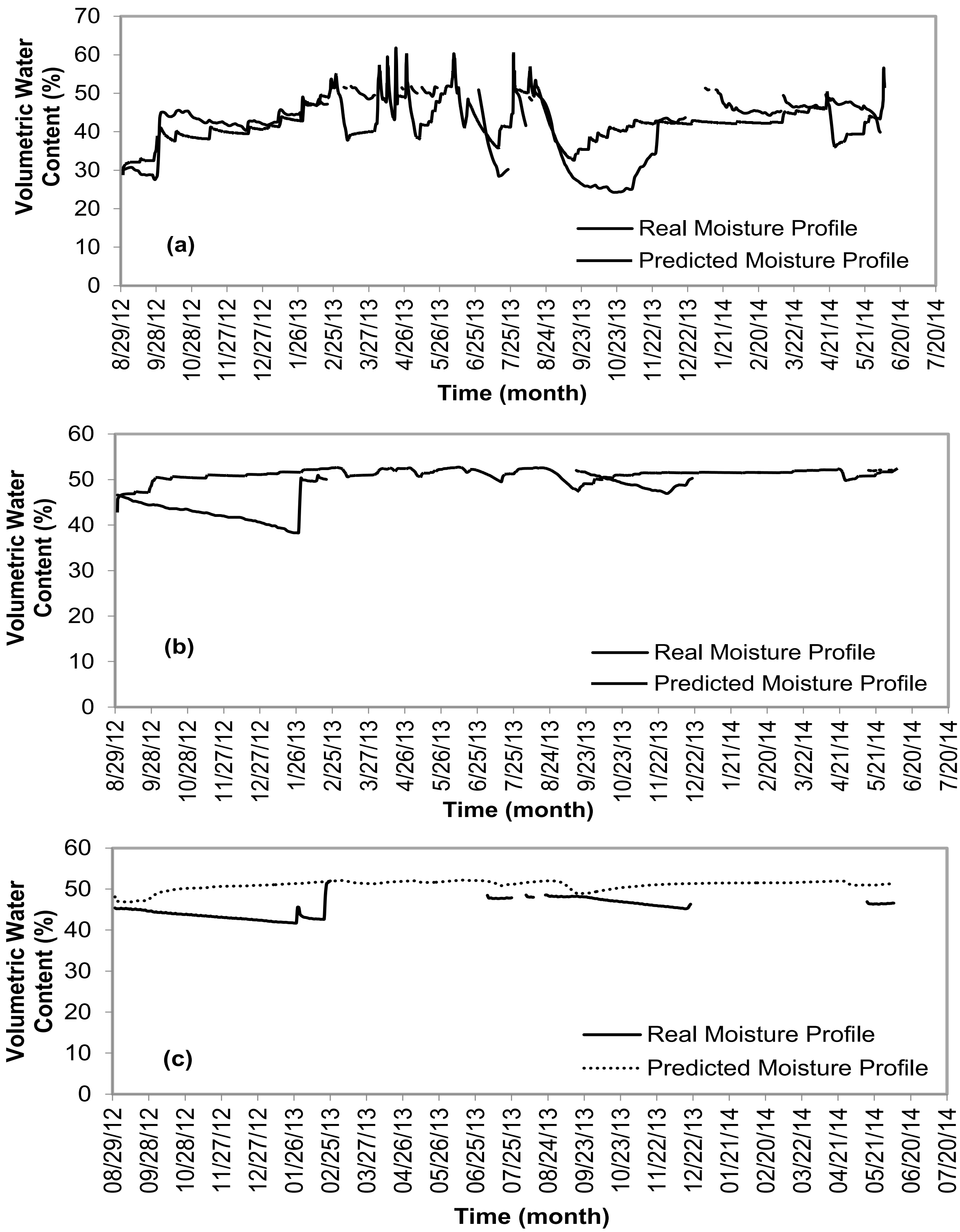

Figure 5.16. Chickasha: measured and predicted (SVFlux) moisture variations at depths of 1 ft. (a), 3 ft. (b), and 6 ft. (c).

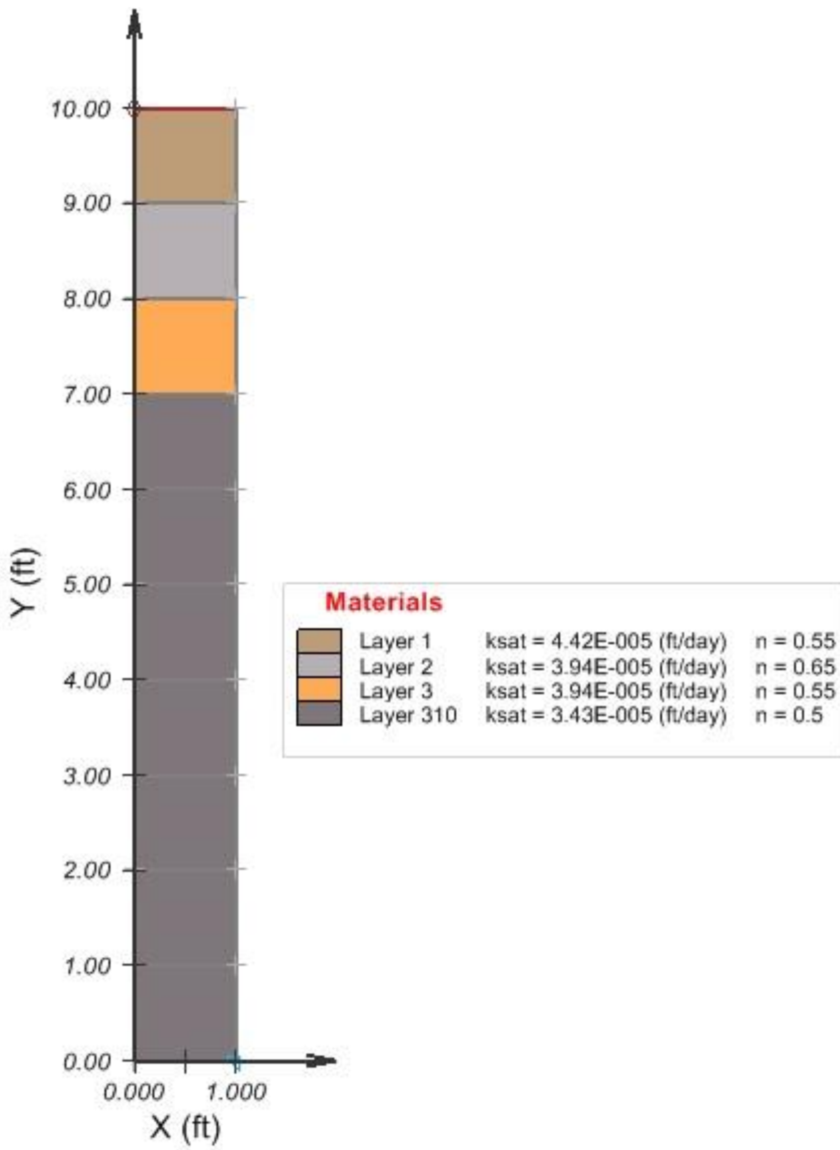

Figure 5.17. Idabel: SVFlux model soil profile.

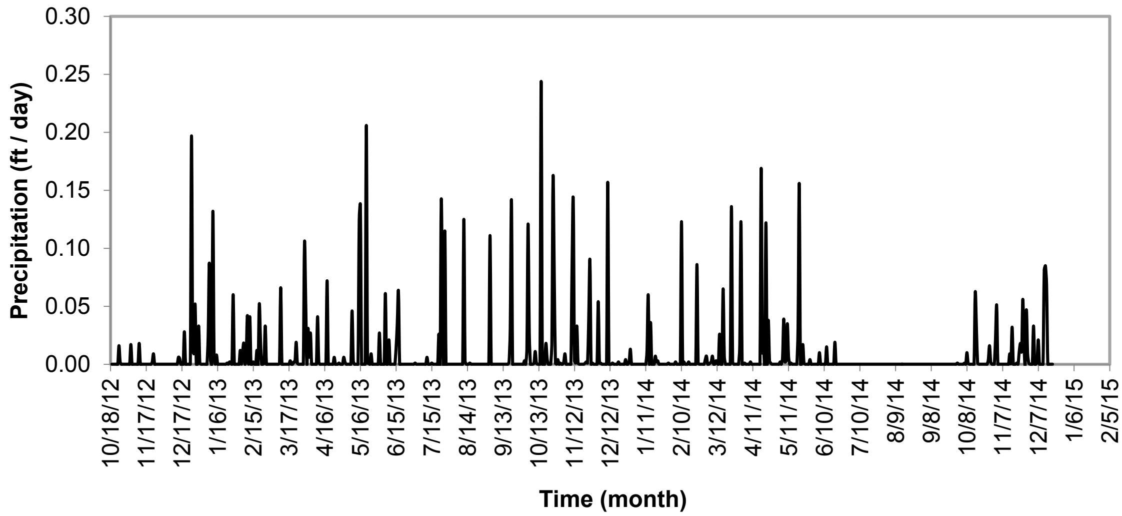

Figure 5.18. Idabel: rainfall data.

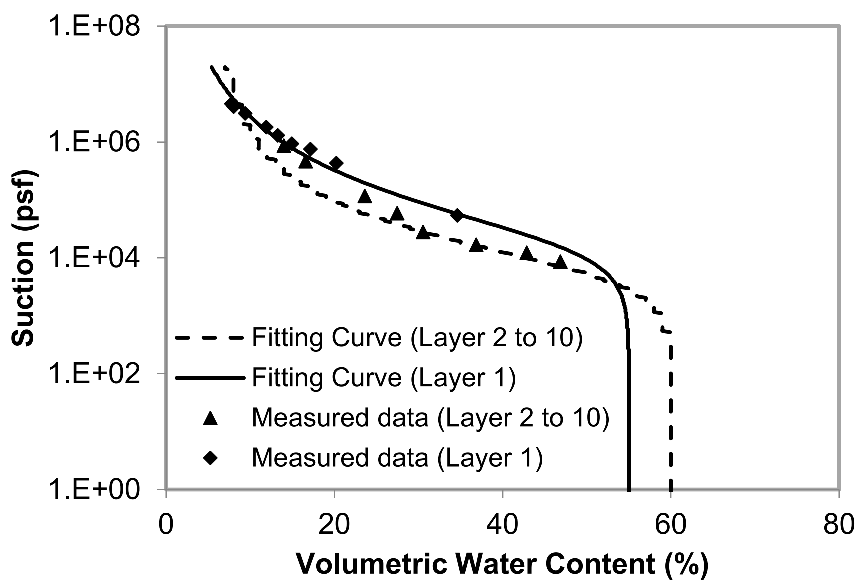

Figure 5.19. Idabel: SWCC used in the modeling.

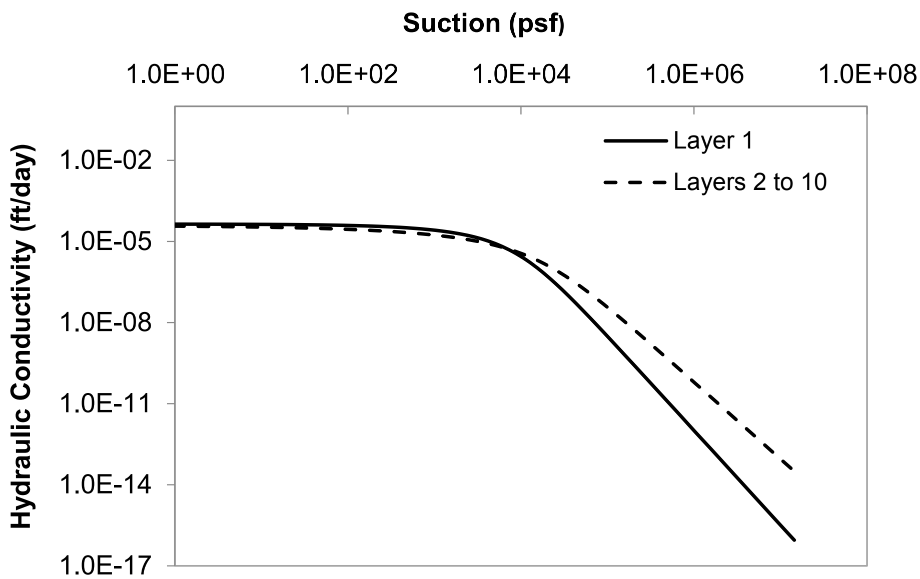

Figure 5.20. Idabel: hydraulic conductivity versus suction.

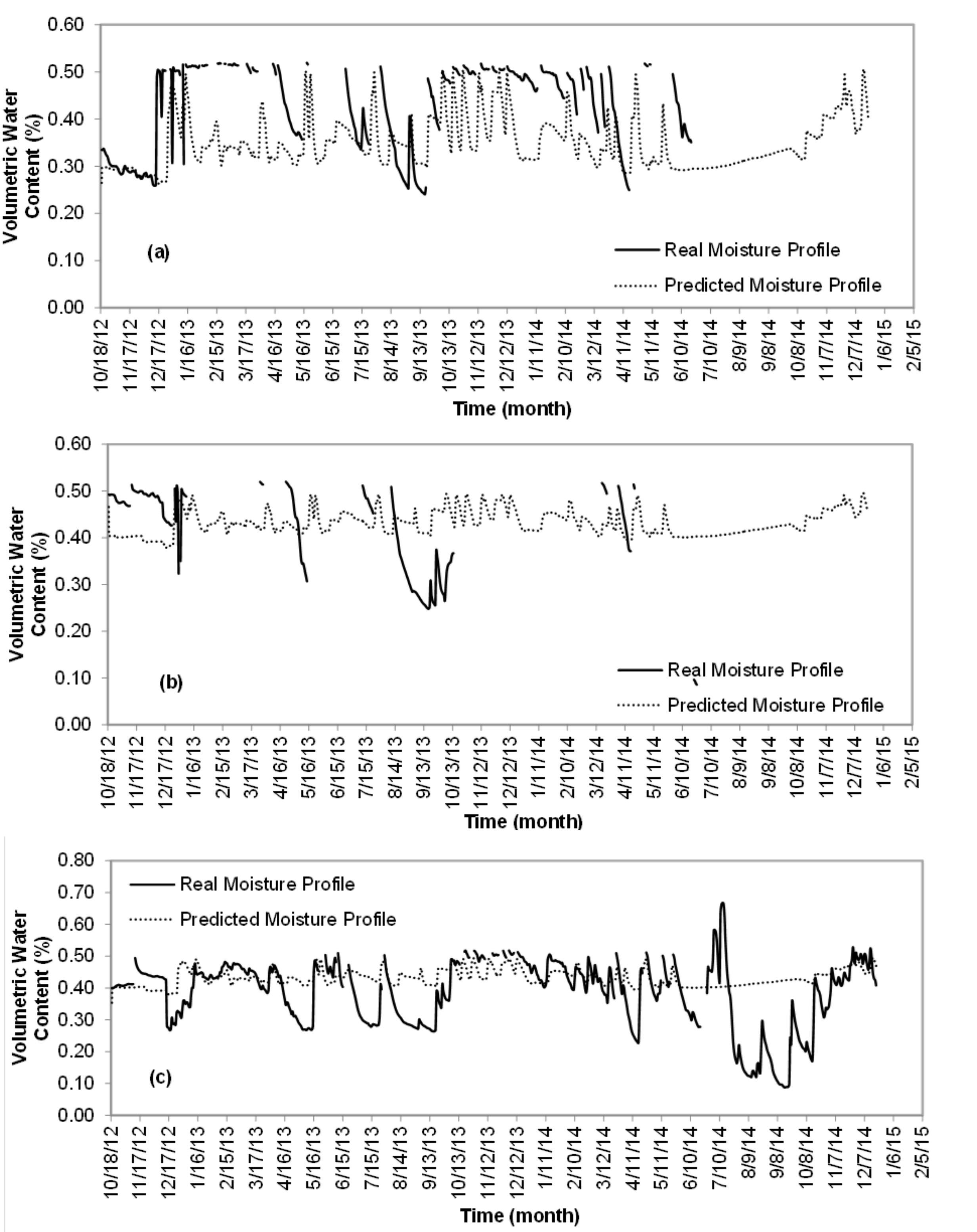

Figure 5.21. Idabel: measured and predicted (SVFlux) moisture variations at depths 0.5 ft. (a), 1 ft. (b), and 1.5 ft. (c).

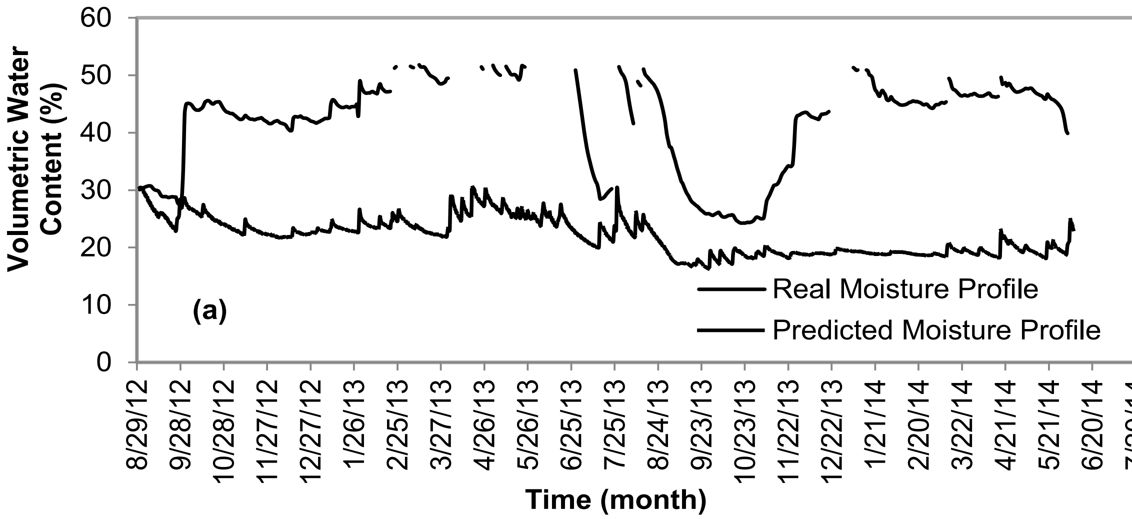

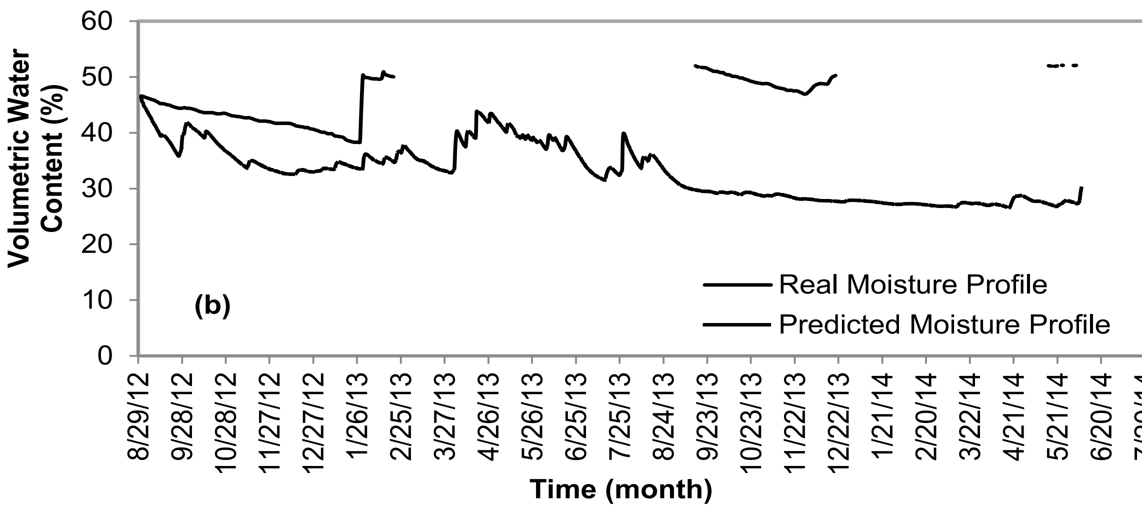

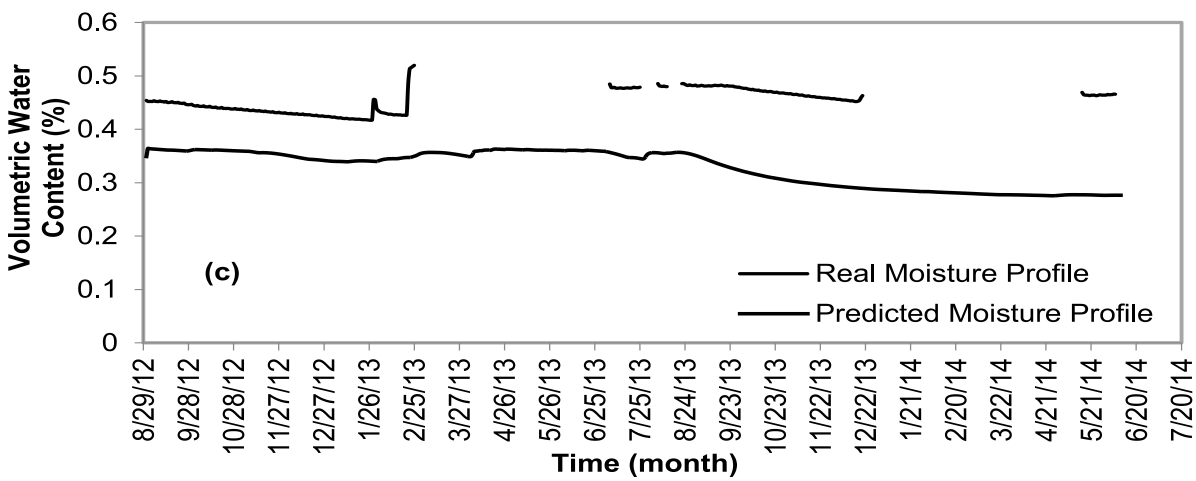

Figure 5.22. Chickasha: measured and predicted (VADOSE/W) moisture profiles at depths of 1 ft. (a), 3 ft. (b), 6 ft. (c).

Chapter 6 RESULTS OF LABORATORY TESTING

6.1 Basic Soil Properties

The variation in soil index properties with depth for each test site are summarized in Figures 6.1 and Figures 6.2. Stratigraphy of Idabel shows presence of clay in the composition of soil layers with the average activity of 0.3. Plasticity index (PI) and total suction for the first 6.0 feet depth show rather small fluctuation except for the depth of 10 inches as indicated in Figure 6.1.

The composition of Chickasha includes silt and clay particles having the average activity of 0.5. The total suction was constant for the first 6.0 feet depth except for the depth of 20 inches as indicated in Figure 6.2.

6.2 SWCC Test Results

Figures 6.3 and 6.4 show the wetting and drying branches of the Soil Water Characteristic Curve (SWCC) for soil compacted to the approximate dry density of field samples from the Chickasha and Idabel sites. The specimens were prepared at dry density and gravimetric water content equal to 88 pcf and 36%, 98 pcf and 31% related to Idabel and Chickasha sites, respectively. Total suction measurements were obtained using the WP4 Potentiometer and the axis translation method was used to determine matric suction in the low suction range during drying. At low suctions where the data from the two methods overlap, drying points from the axis translation method plot below the WP4 points at similar water content. This is likely due to the fact that the WP4 measures total suction, which is the sum of osmotic and matric suction components, while the axis translation method only detects matric suction.

From the SWCC for Idabel shown in Figure 6.3, the total suction (WP4 data) developed within a range of 100 psi to 50000 psi corresponding to a gravimetric moisture content range of 40% to 5%. These ranges were smaller for Chickasha soil as shown in Figure 6.4, which were 10 psi to 10000 psi corresponding to a gravimetric moisture content range of 25% to 5%. This is consistent with the higher fines content and plasticity index for the Idabel soil compared to Chickasha.

6.3 Soil Shear Strength

Shear strength of soil from both tests sites was determined from saturated, undrained triaxial compression tests on thin-walled tube samples and from direct shear tests on compacted samples. Direct shear testing involved saturated and unsaturated testing of compacted samples and samples that were subjected to wetting/drying cycles to estimate the fully softened strength. The goal was to define the in situ strength characteristics of the soil at the time of sampling and to determine the compacted soil strength characteristics expected shortly after construction of the embankments was complete. In addition, it was desired to explore how wetting/drying cycles impact the strength behavior in comparison to the other test methods.

6.3.1 CIUC Triaxial Test Results

6.3.1.1 Idabel: Triaxial Test Results

Five triaxial tests were run on thin-walled tube samples to estimate the in situ soil strength profile. For each test, the excess pore water pressures and deviatoric stresses were plotted versus the strain. The p-q diagram (MIT notation) was also plotted to assess the friction angle. The results of the tests from the Idabel site are summarized in Table 6.1. Effective stress friction angles vary between 19^o and 29^o with an average of 26^o while effective stress cohesion is low for all tests. A noticeable decrease in the friction angle occurs below a depth of 3 feet that is consistent with higher PI below this depth. In Table 6.1 the undrained shear strength (s_u) is normalized by the effective confining pressure (p_o) to provide the ratio (s_u/p_o). Normalized undrained strength values in Table 6.1 vary from 0.34 to 0.61 and are typical of slightly to moderately overconsolidated clayey soils. For reference, typical normally consolidated sedimentary clayey soils have s_u/p_o values around 0.22.

6.3.1.2 Chickasha: Triaxial Test Results

Results obtained from the triaxial tests on Chickasha samples are summarized in Table 6.2. Effective stress friction angles range from 18^o to 29^o with an average of 24^o. Effective stress cohesion intercepts range from 0 to 2.5 psi with an average around 1.3 psi. Normalized undrained shear strength values in a range of 0.78 to 1.7 indicate moderately to heavily overconsolidated behavior.

6.3.2 Saturated and Unsaturated Direct Shear Test Results

6.3.2.1 Idabel: Saturated and Unsaturated DST Results

Figure 6.5 shows the shear stress versus horizontal displacement while shearing in the saturated condition for Idabel soil. Initial water content and dry density for Idabel specimens were 36% and 88 pcf. Idabel specimens exhibited swelling during saturation due to high PI and a contraction during consolidation. Samples tended to contract during shearing with greater contraction occurring at higher normal stresses as observed in Figure 6.6.

Suction controlled direct shear testing occurred under net normal stress of 7.25, 14.5, and 21.75 psi, and suction values of 14.5 and 29.0 psi. For all tests, the compacted soil samples were prepared similarly to the saturated test samples. After equalization under the targeted state of stress, soil was sheared to a maximum horizontal displacement of 0.4 in. using a horizontal displacement rate was 0.0002 in/min. Shear stress and horizontal displacement were recorded typically at 1.0 min intervals.

Figures 6.7 and 6.8 show the change of water content with time during the equalization, consolidation, and shearing phases. As expected, for a given suction the magnitude of water content decreased with increase in net normal stress. Shear strength of soil increased with increase in net normal stress for a given suction value as shown in Figures 6.9 and 6.10.

The water volume controller pulled water from the soil specimen during shearing.

That water was being pulled out of the sample during the unsaturated test suggests that there was a tendency for increasing pore water pressure, consistent with volumetric contraction during shearing. It can be seen in Figs 6.11 and 6.12 that the amount of compression increased when the net normal stress increased and change in volume of water tended to decrease as the horizontal displacement increased. Shear strength envelopes based on net normal stress and suction variations are shown in Figs 6.13 and 6.14 and were used to obtain the basic shear unsaturated shear strength parameters.

6.3.2.2 Chickasha: Saturated and Unsaturated DST Results

Figure 6.15 shows the shear stress changes during shearing under saturated condition for Chickasha soil. Initial water content and dry density for Chickasha specimens were 31% and 98 pcf. Chickasha specimens showed a contraction during shearing as shown in Figure 6.16 with the amount of contraction increasing as net normal stress increased.

Similar to Idabel soil, net normal stresses of 7.25, 14.5, and 21.75 psi and matric suction of 7.25 and 14.5 psi was used for testing. In all tests, compacted samples were prepared similar to the saturated samples. After equalization under the targeted state of stress, soil was sheared to a maximum horizontal displacement of 0.4 in. Horizontal displacement rate was 0.0002 in/min; shear stress and horizontal displacement were recorded typically at 1.0 min intervals.

Figures 6.17 and 6.18 show plots of change in water content with time during the equalization, consolidation, and shearing phases. As expected, for a given suction the magnitude of water content decreased with increase in net normal stress. As shown in Figures 6.19 and 6.20, shearing resistance increased with increasing net normal stress and increasing suction. Similar to Idabel soil, contraction behavior during shearing and corresponding decreases in water content were greater for higher net normal stress. Strength envelopes based on net normal stress and suction variations are shown in Figs 6.23 and 6.24 and were used to obtain the unsaturated shear strength parameters.

6.3.3 Fully Softened Direct Shear Test Results

6.3.3.1 Idabel: Fully Softened DST Results

Table 6.3 summarizes the initial and final conditions (i.e., dry density and water content) of the samples that were subjected to cycles of wetting and drying to simulate fully softened conditions. The initial and final conditions correspond to the conditions before and after the cycles of wetting and drying. The final conditions given in Table 6.3 correspond to the initial conditions before shearing. Notice that the final water contents are similar for each sample even though initial water contents were different in some cases. The densities are all lower after wetting and drying cycles, but more variable from sample to sample. It was assumed that all the samples reached an equilibrium state by the end of the ten cycles, irrespective of the different initial conditions. Table 6.3 summarizes the initial and final conditions of the samples and Table 6.4 shows the normal stress and shear strength obtained from direct shear tests on the samples subjected to dry/wet cycles.

The shear stress and vertical displacement are plotted against horizontal displacement in Figures 6.26 and 6.27, respectively. Shear stress was greatest for the samples at the highest normal stress (Samples 3 and 5 at 5 psi) as expected.

Contractive volume changes during shearing were largest for higher normal stresses as well.

A representative final water content and dry density (33% and 88 pcf) from the artificially weathered samples subjected to wet/dry cycles was selected to recreate sample conditions at the end of wetting-drying cycles. The purpose was to see if samples prepared to the same water content and density as artificially weathered samples, but without being subjected to cycles of wetting and drying, would behave similarly. Having the same water content and density does not ensure similar behavior as the fabric and structure could be different due to the different stress histories. If however, the recreated and artificially weathered samples produced similar strength, then the fully softened strength could be reasonably estimated using the simple recreation method.

The results of the direct shear tests carried out on the recreated samples are summarized in Table 6.5 and comparison of failure envelopes from testing artificially weather (wet/dry cycles) and recreated samples is shown in Figure 6.27. As shown in Figure 6.27, the average failure envelopes from the two methods are similar. While the shear strength appears similar, the two methods produced different shearing behavior as shown in Figure 6.28. Artificially weathered samples gradually gain strength and undergo considerably more displacement before reaching peak shear stress. On the other hand, the recreated specimens reach a peak strength after relatively less displacement and then a post-peak decrease in strength. While the recreation method may be suitable for limit equilibrium analyses requiring estimates of shear strength, coupled strength-deformation analyses of fully softened soils should rely on testing of artificially weathered specimens to simulate actual soil behavior.

6.3.3.2 Chickasha: Fully Softened DST Results

Table 6.6 summarizes the initial and final conditions (i.e., before and after the cycles of wetting and drying) of the artificially weathered samples. Similar to Idabel, water contents are nearly the same for all samples at the end of wet/dry cycles, except for the first sample. Shear strengths and corresponding normal stresses are presented in Table 6.7. Shear stress and volume change versus horizontal displacement are shown in Figure 6.29 and 6.30, respectively. Similar to Idabel, the Chickasha soil gradually gained strength with increasing horizontal displacement, although it did not in most cases reach a maximum after 0.25 inches of horizontal displacement. The volume change remained strongly contractive throughout shearing as shown in Figure 6.30.

In a manner similar to Idabel, samples were recreated to achieve a final water content and dry density (29.5% and 91 pcf) representative of artificially weathered samples at the end of wet/dry cycles. Samples were sheared for comparison to results from artificially weathered samples. Results of the direct shear tests carried out on the recreated samples are summarized in Table 6.8. Failure envelopes resulting from the two sample preparation methods are shown Figure 6.31, while a comparison of shear stress-displacement curves are shown in 6.32. Similar to the Idabel soil, average failure envelopes were similar for artificially weathered and recreated samples, but shear stress-displacement behavior was significantly different.

6.3.4 Summary of Shear Strength Parameters

The average shear strength parameters, initial density and water content at the beginning of testing for each of the test methods are summarized in Tables 6.9 and 6.10 for Idabel and Chickasha soils, respectively. As shown in Tables 6.9 and 6.10 there are significant differences in strength parameters between the various test methods. These differences can be attributed to a number of factors:

1) The average unsaturated triaxial test results represent the averages of five tests on thin-walled tube samples from different depths within the soil profile. Results from these tests, as summarized in Tables 6.1 and 6.2, were quite variable due to the natural variability of tests samples. Thus, natural variability of the tests samples is a significant factor with respect to triaxial results.

2) Aside from differences in initial densities and water contents, field samples and newly compacted soil samples have significant differences in fabric and structure on account of significant differences in geologic and stress history.

3) Fully softened direct shear test represent compacted composite samples subjected to several cycles of wetting and drying during which the moisture content and density changed substantially before reaching somewhat of a constant value prior to testing. Wetting and drying cycles substantially changed the fabric and structure of the soil which has a significant impact on shearing behavior.

4) Saturated and unsaturated direct shear tests on composite compacted samples were prepared to target densities and water contents consistent with field measurements in the upper few feet of the test site. This was done since failure surfaces at the test sites were observed to be shallow.

5) Initial average densities and water contents were generally different for each test method on account of the factors just mentioned. Shear strength is dependent on initial density this is expected to play a role in the observed differences in average strength parameters.

6) The mode of testing was significantly different between direct shear and triaxial shearing. Imposed stress paths and drainage conditions were different, which is known to effect the interpretation of the effective stress strength parameters.

6.4 Hydraulic Conductivity Test Results

The standard test method for evaluating the movement of water through saturated highly plastic clays is to measure the hydraulic conductivity of a saturated specimen in a flexible wall permeameter. Since the clayey soils had low to high plasticity index and low hydraulic conductivity, the back-pressure saturation and consolidation of the specimen was time consuming. The permeability tests were conducted on undisturbed and disturbed specimens. The undisturbed samples were extruded from Shelby-tubes. The disturbed specimens were compacted at the maximum dry density and the optimum moisture content (OMC). Summaries of the hydraulic conductivity values at different depths for Idabel and Chickasha sites are shown in Tables 6.10 and 6.11, respectively. Hydraulic conductivity values are on average much lower for Idabel than Chickasha. This is consistent with the considerably higher plasticity of soils at the Idabel site.

6.5 Moisture Diffusivity Test Results

Results of drying diffusion tests are presented in Tables 6.12 and 6.13 for Idabel and Chickasha sites, respectively. These tests were conducted on thin-walled tube samples obtained from two different depths at each of the test sites. Results of moisture diffusivity tests provided drying diffusion coefficients of 5.1×10^{-5} in^2/sec and 1.8×10^{-5} in^2/sec for Idabel samples and 5.4×10^{-5} in^2/sec for both samples from Chickasha. Interestingly, the average drying diffusion coefficient from Idabel is the same as for Chickasha. These values are quite low and predicted active depths using the method of McKeen and Johnson (1990) are relatively shallow, on the order of 4 feet or less. This lower than active depths indicated by soil moisture sensors at the Chickasha site and is attributed to the fact that diffusivity tests on intact small laboratory samples do not accurately account for the influence of desiccation cracks in the field.

Table 6.1. Idabel: summary of triaxial test results.

Depth (in)	Avg. Depth (in)	Dry Unit Weight (pcf)	Gravimetric Water Content (%)	ϕ' (°)	c' (psi)	s_u/p_o
17 – 23	20	91.8	26.3	28.8	0.0	0.45
24 – 31	27	88.7	25.7	29.4	0.0	0.37
33 – 39	36	90.5	29.2	27.6	0.0	0.37
38 – 45	41	101.8	16.5	18.6	0.31	0.61
37 – 49	43	101.8	21.2	24.9	0.34	0.34

Table 6.2. Chickasha: summary of triaxial test results.

Depth (in)	Avg. Depth (in)	Dry Unit Weight (pcf)	Gravimetric Water Content(%)	ϕ' (°)	c' (psi)	s_u/p_o
10 - 16	13	98.0	25.0	23.7	2.46	0.78
17.5 - 23.5	21	98.0	31.0	21.5	1.88	1.42
24 - 32	28	89.3	29.8	28.2	0.00	1.15
30 - 36	33	95.5	26.1	29.2	0.40	1.13
35 - 45	40	101.8	22.6	18.4	1.81	1.70

Table 6.3. Idabel: summary of the conditions before and after the cycles of wetting and drying.

Sample #	Initial Conditions		Final Conditions	
	w (%)	Dry Unit Weight (pcf)	w (%)	Dry Unit Weight (pcf)
1	20.8	95.0	33.0	90.5
2	20.8	93.9	32.4	89.9
3	19.8	93.2	33.6	86.2
4	22.9	96.3	32.9	86.8
5	24.2	92.7	32.6	88.7

Table 6.4. Idabel: summary of direct shear tests conducted on samples subjected to wet/dry cycles.

Sample #	Initial Conditions		Final Conditions		Failure Stresses	
	w (%)	Dry Unit Weight (pcf)	w (%)	Dry Unit Weight (pcf)	Normal Stress (psi)	Shear Stress (psi)
1	33.0	90.5	36.5	83.1	2	1.70
2	32.4	89.9	36.0	86.8	2	1.76
3	33.6	86.2	35.8	86.2	5	2.75
4	32.9	86.8	36.0	81.8	2	1.70
5	32.6	88.7	35.7	84.9	5	2.76

Table 6.5. Idabel: summary of results from reconstituted softened samples.

Recreated Sample #	Initial Conditions		Final Conditions		Failure Stresses		
	w (%)	Dry Unit Weight (pcf)	w (%)	Dry Unit Weight (pcf)	Normal Stress (psi)	Peak (psi)	Post-Peak (psi)
1	34.0	85.6	41.1	79.3	2	2.02	1.58
2	38.5	85.6	44.4	79.3	2	1.70	1.16
3	30.6	92.4	37.0	84.9	5	3.45	2.27
4	29.1	94.9	36.6	86.8	5	2.87	2.10

Table 6.6. Chickasha: summary of the conditions before and after the cycles of wetting and drying.

Sample #	Initial Condition		Final Condition	
	w (%)	Dry Unit Weight (pcf)	w (%)	Dry Unit Weight (pcf)
1	25.5	91.4	25.8	95.5
2	24.8	88.8	29.5	92.4
3	23.2	86.4	29.9	88.7
4	23.4	85.1	29.6	88.5

Table 6.7. Chickasha: summary of direct shear tests conducted on samples subjected to wet/dry cycles.

Sample #	Initial Conditions		Failure Stresses	
	w (%)	Dry Unit Weight (pcf)	Normal Stress (psi)	Shear Stress (psi)
1	25.8	95.5	2	2.27
2	29.5	92.4	5	3.74
3	29.9	88.7	2	1.92
4	29.6	88.5	5	3.34

Table 6.8. Chickasha: summary of DST results from reconstituted softened samples.

Recreated Sample #	Initial Condition		Final Condition		Failure Stresses		
	w (%)	Dry Unit Weight (pcf)	w (%)	Dry Unit Weight (pcf)	Normal Stress (psi)	Peak (psi)	Post-Peak (psi)
1	32.4	88.6	33.1	92.4	5	3.74	--
2	25.3	96.8	34.8	91.1	5	3.70	--
3	25.9	93.0	31.7	90.5	2	2.04	2.00
4	27.2	93.6	30.8	91.1	5	3.63	3.49
5	28.6	93.6	31.6	91.8	2	2.95	2.15

Table 6.9. Idabel: summary of average strength parameters and initial states.

Test Type	*w* (%)	γ_d (pcf)	ϕ' (deg.)	c′ (psi)	ϕ^b (deg.)
Sat./Unsat. DST	36.0	88.0	15.1	1.8	12.2
Fully Softened DST	32.9	88.4	18.8	1.04	---
Undisturbed Triaxial	23.8	94.9	25.9	0.13	---

Table 6.10. Chickasha: summary of average strength parameters and initial states.

Test Type	*w* (%)	γ_d (pcf)	ϕ' (deg.)	c′ (psi)	ϕ^b (deg.)
Sat./Unsat. DST	31.0	98.0	29.7	1.1	11.1
Fully Softened DST	28.7	91.3	25.6	1.13	---
Undisturbed Triaxial	26.9	96.5	24.2	1.31	---

Table 6.11. Idabel: summary of saturated hydraulic conductivity values.

Depth (in)	γ_d (pcf)	Effective Confining Stress (psi)	Hydraulic Gradient	Saturated Hydraulic Conductivity (in/sec)
17-24	86.8	6.0	35.9	6.14e-9
27-35.5	94.7	6.3	40.8	5.47e-9
Compacted	96.8	5.0	12.7	4.76e-9

Table 6.12. Chickasha: summary of saturated hydraulic conductivity values.

Depth (in)	γ_d (pcf)	Effective Confining Stress (psi)	Hydraulic Gradient	Saturated Hydraulic Conductivity (in/sec)
14-25	91.1	5.0	21.5	1.11e-6
35-48	99.2	5.0	22.3	3.35e-7
Compacted	108.9	5.0	13.3	2.53e-7

Table 6.13. Idabel: results of moisture diffusivity tests.

Sample Depth (inches)	Drying Diffusion Coefficient (cm^2/sec)	Drying Diffusion Coefficient (in^2/sec)
1.5-10	5.11E-05	7.92E-06
15-23	1.81E-05	2.81E-06

Table 6.14. Chickasha: results of moisture diffusivity tests.

Sample Depth (inches)	Drying Diffusion Coefficient (cm^2/sec)	Drying Diffusion Coefficient (in^2/sec)
4-10	3.46E-05	5.36E-06
30-36	3.46E-05	5.36E-06

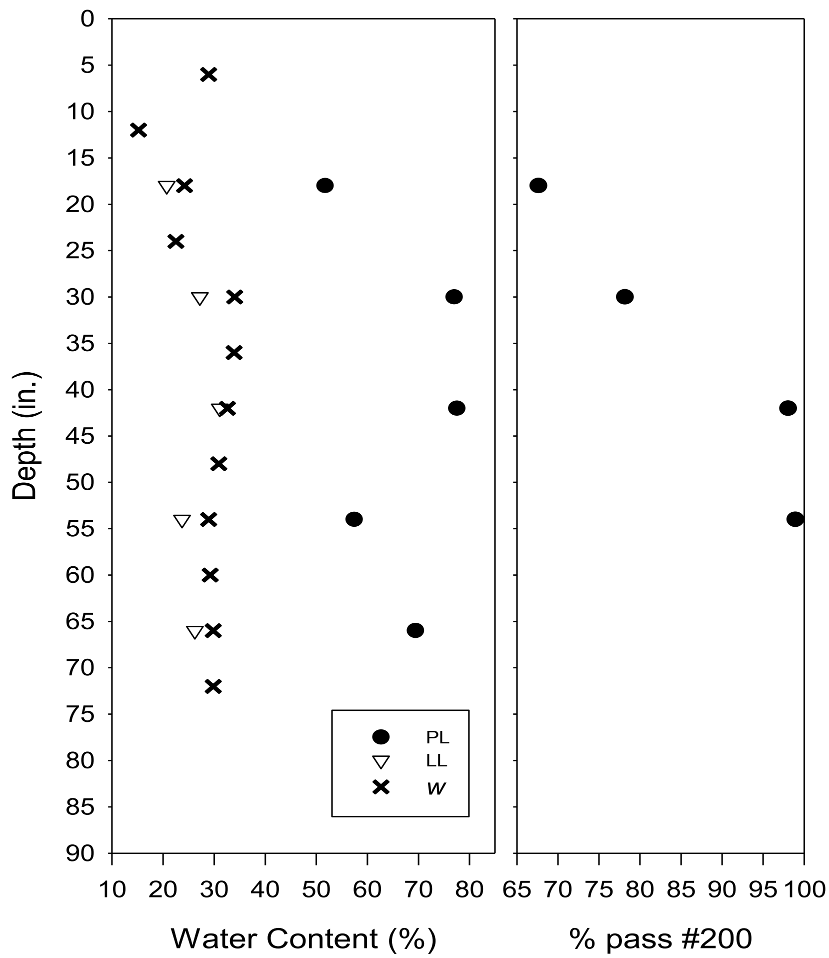

Figure 23. Idabel: Atterberg limits and grain size data from field samples.

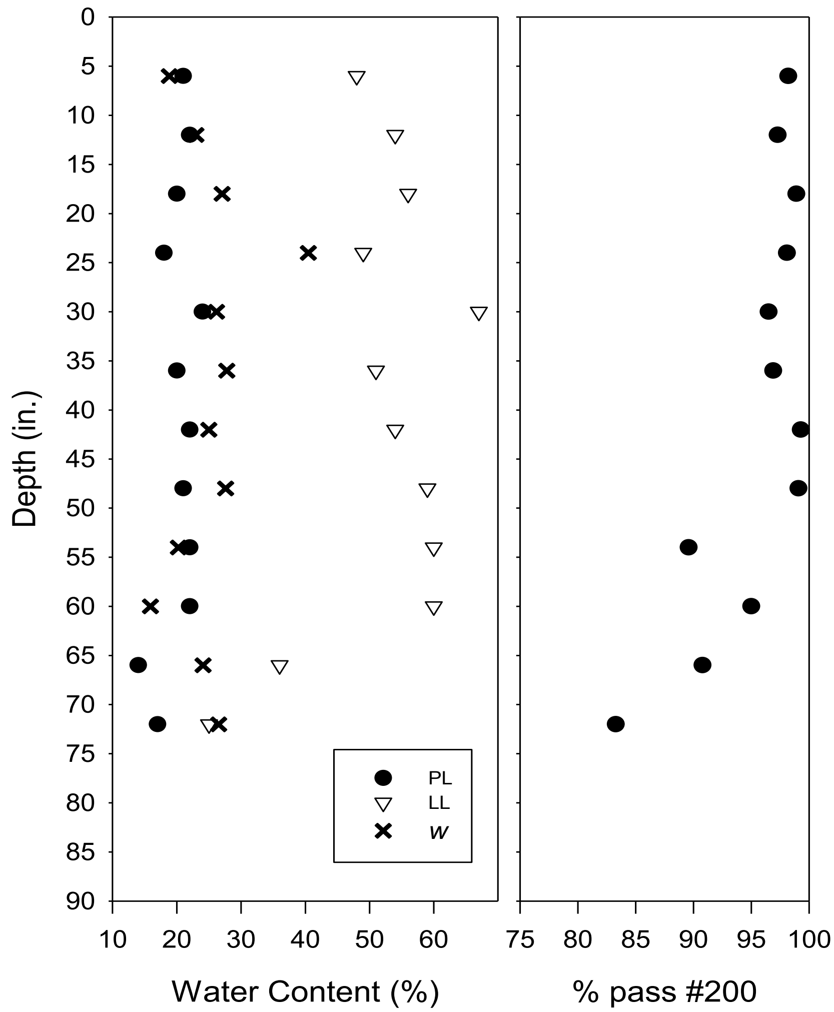

Figure 24. Chickasha: Atterberg limits and grain size data from field samples.

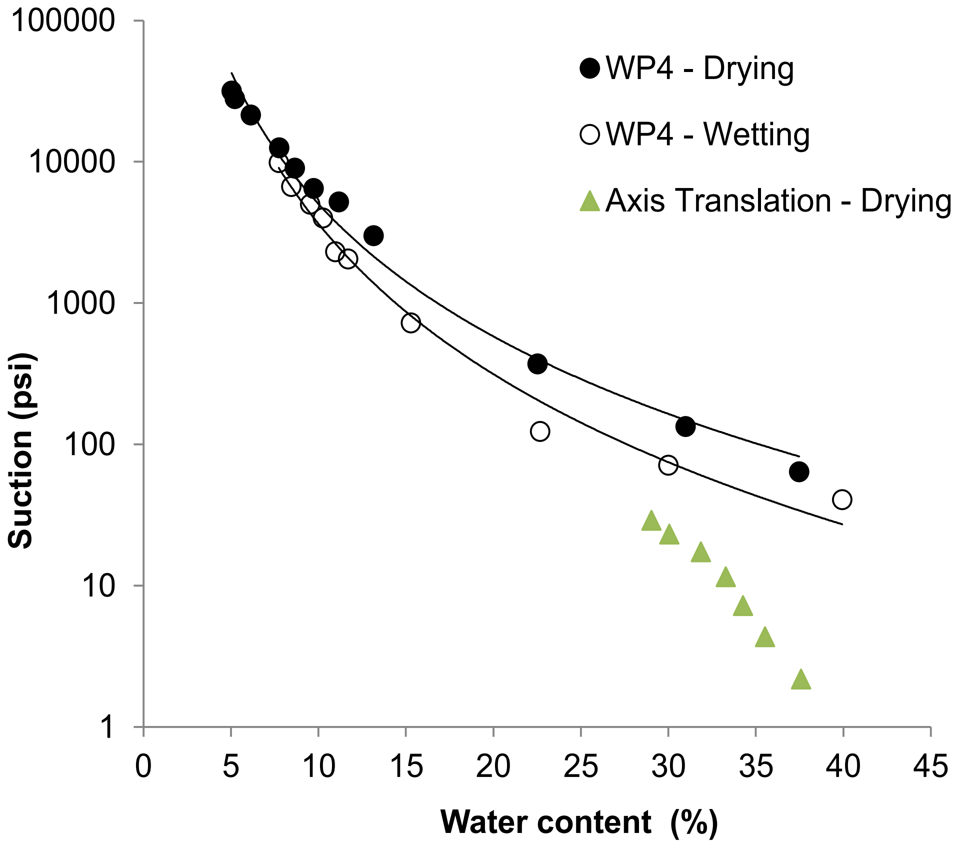

Figure 6.25. Idabel: SWCC based on gravimetric water content measurements and suction determined using WP4 apparatus and axis translation device.

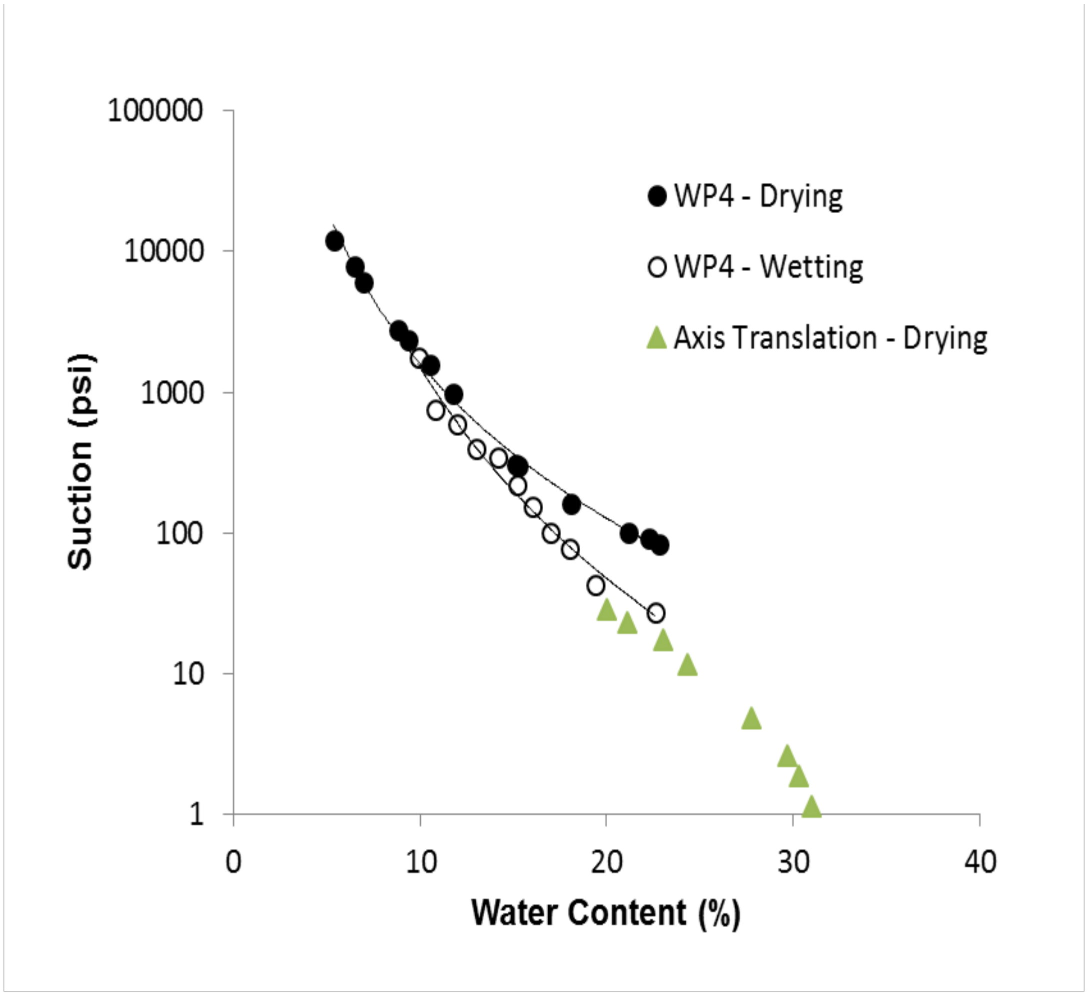

Figure 6.26. Chickasha: SWCC based on gravimetric water content measurements and suction determined using WP4 apparatus and axis translation device.

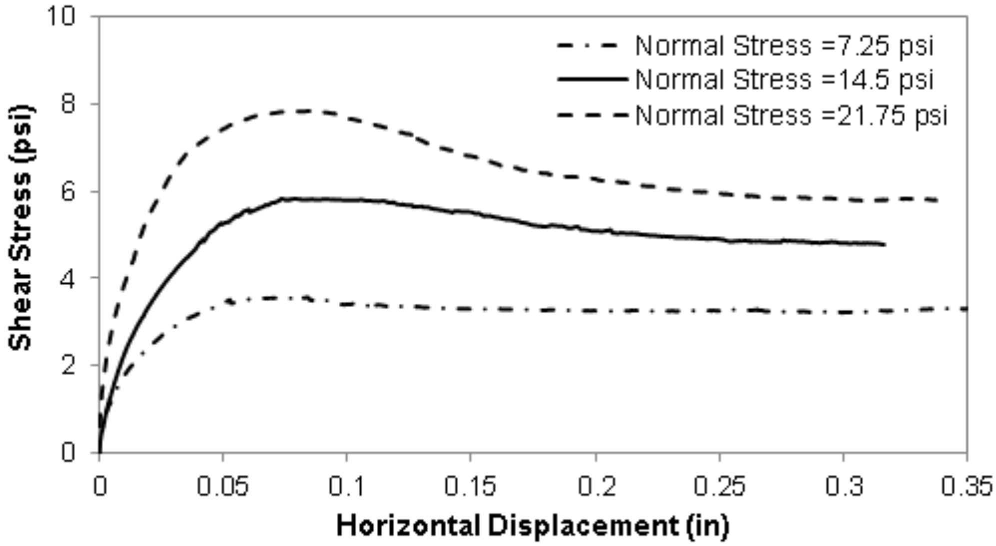

Figure 6.27. Idabel: shear stress versus horizontal displacement under saturated conditions.

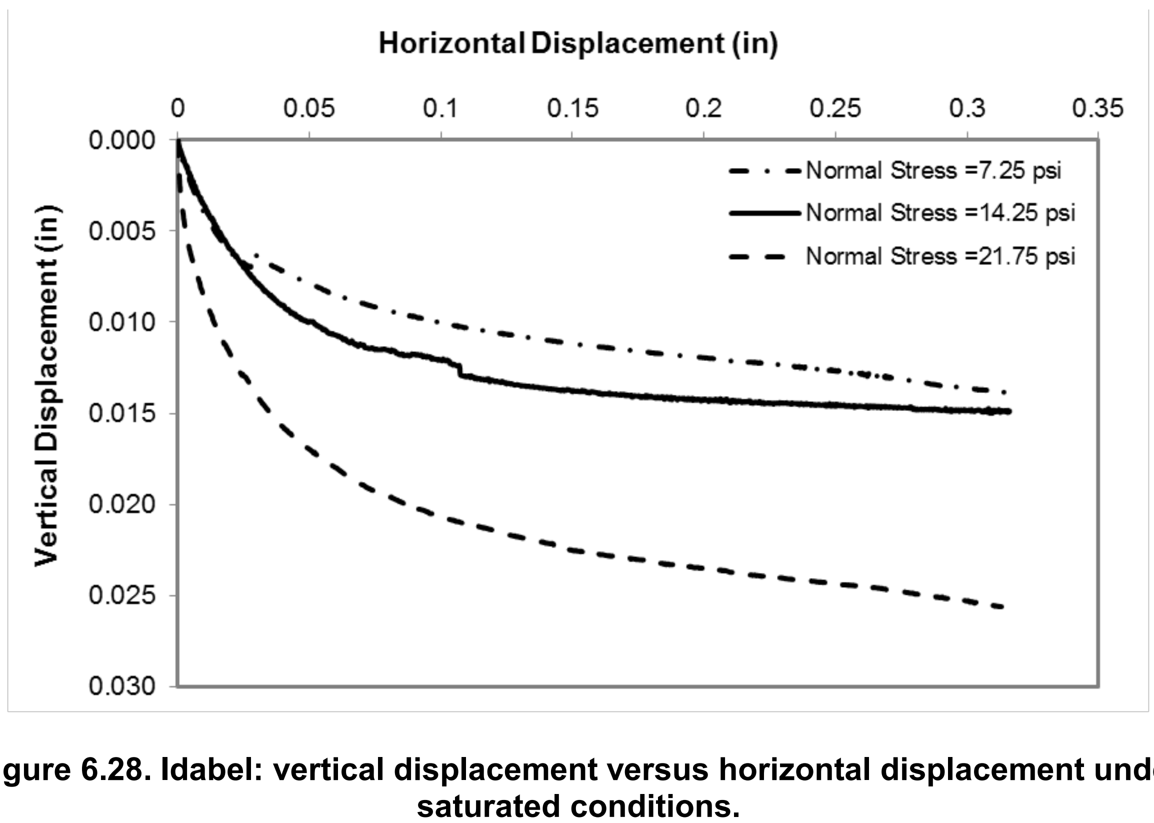

Figure 6.28. Idabel: vertical displacement versus horizontal displacement under saturated conditions.

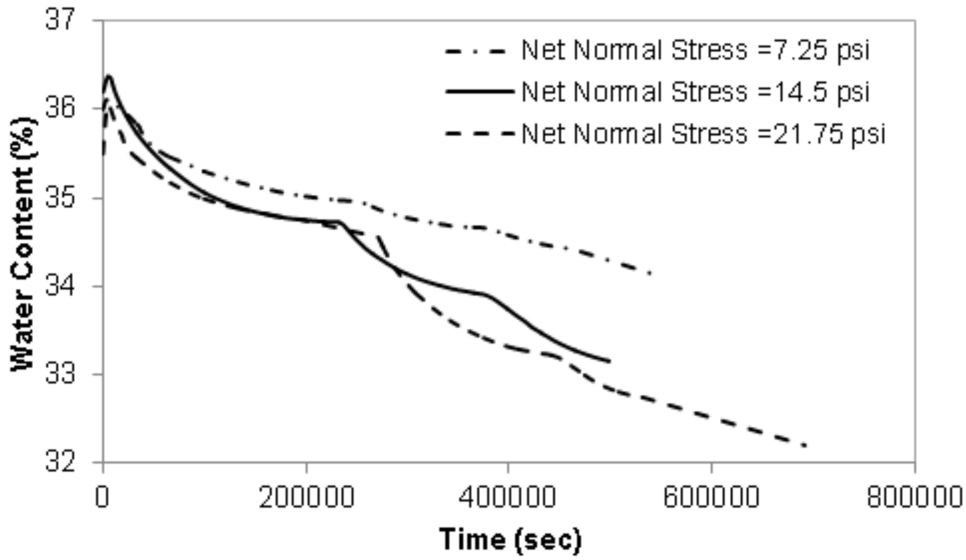

Figure 6.29. Idabel: water content changes under different net normal stresses and constant suction (14.5 psi) during equalization and shearing.

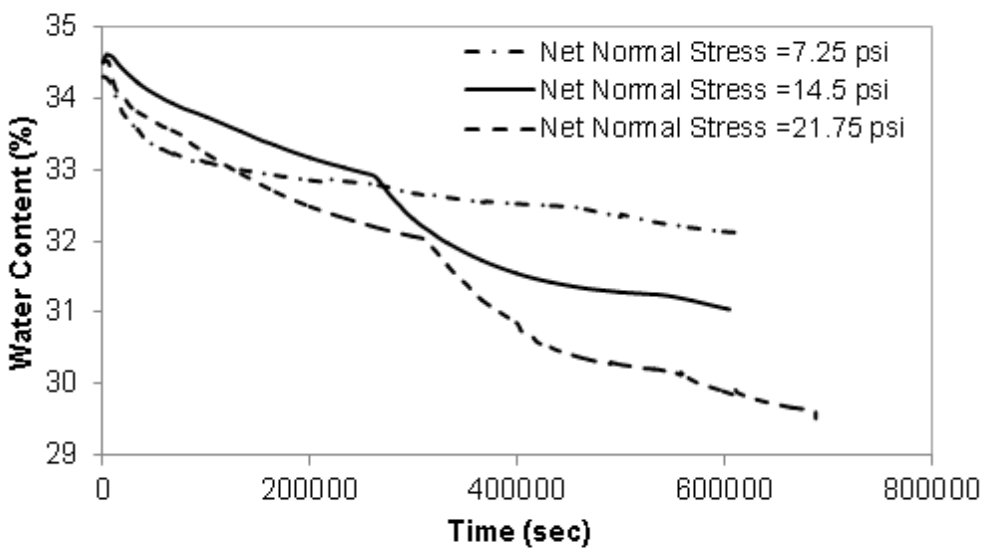

Figure 6.30. Idabel: water content changes under different net normal stresses and constant suction (29.0 psi) during equalization and shearing.

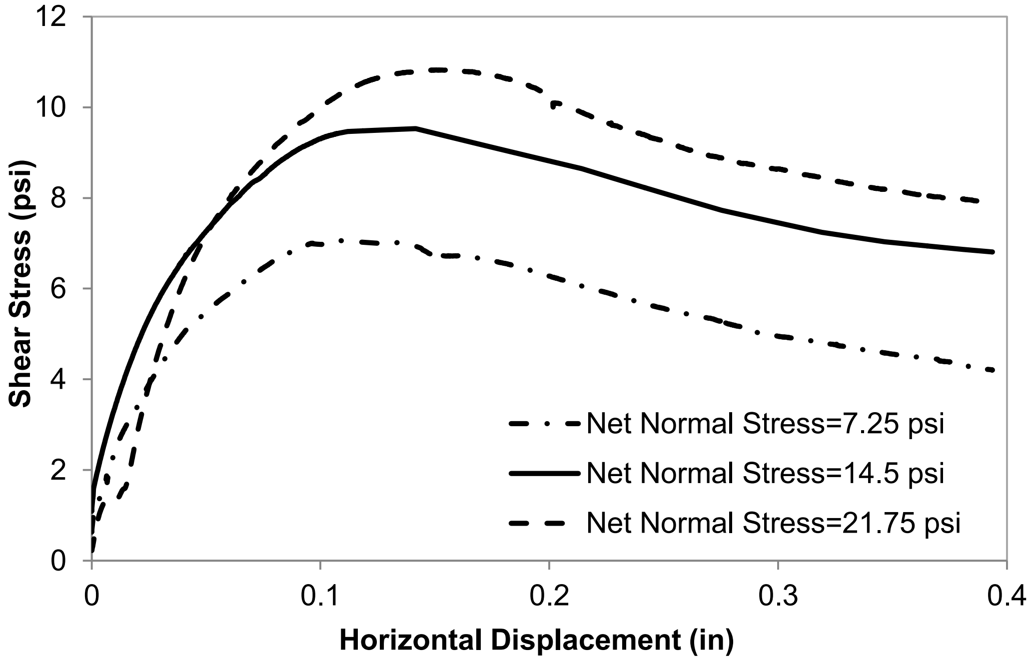

Figure 6.31. Idabel: shear stress changes under different net normal stresses and constant suction (14.5 psi) during shearing.

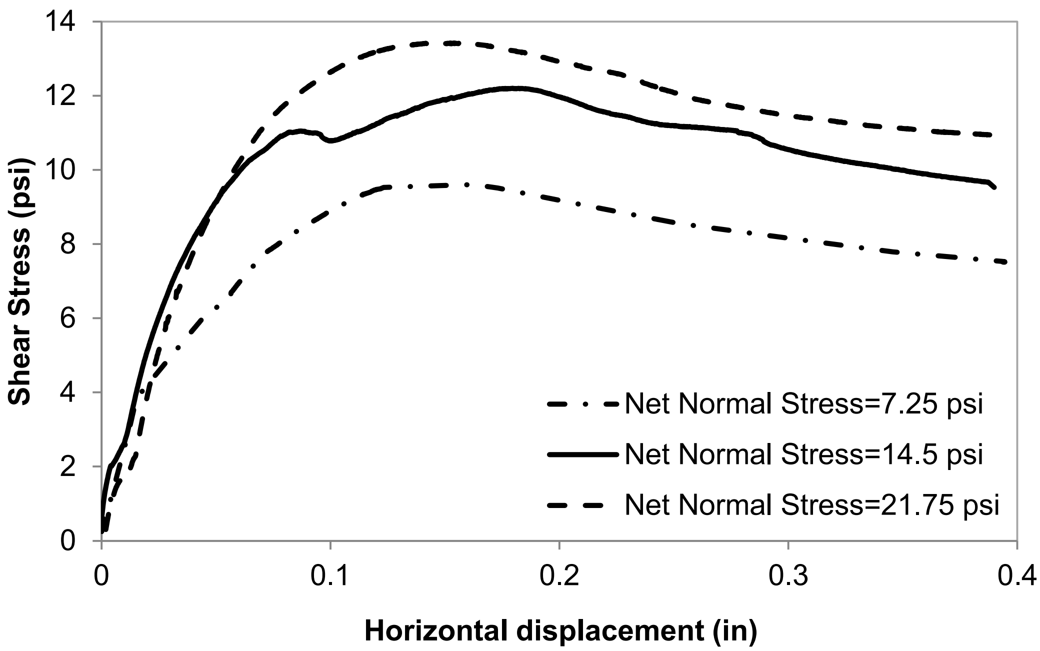

Figure 6.32. Idabel: shear stress changes under different net normal stresses and constant suction (29.0 psi) during shearing.

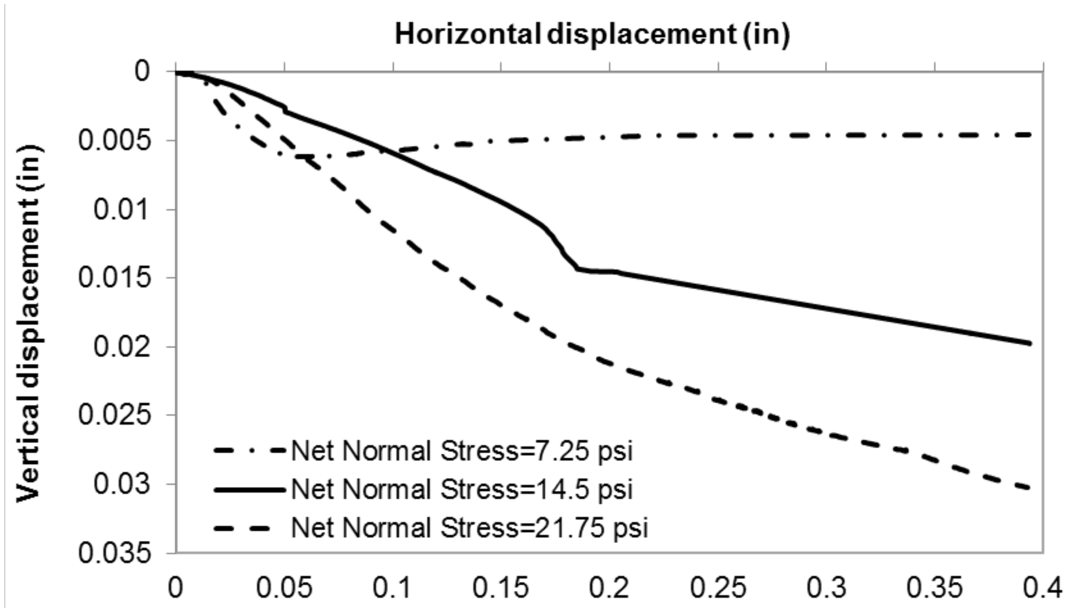

Figure 6.33. Idabel: vertical displacement changes during shearing under different net normal stresses and suction (14.5 psi).

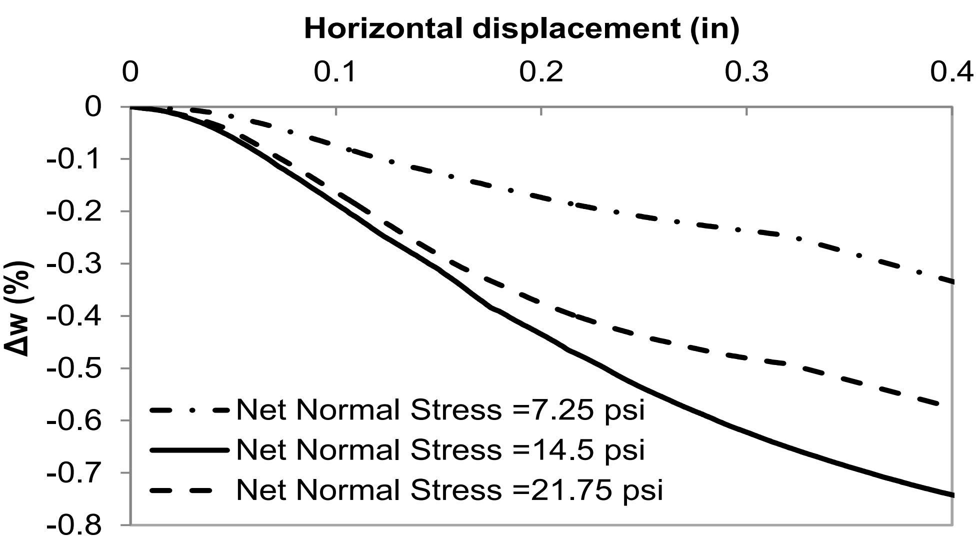

Figure 34. Idabel: water volume changes during shearing under different net normal stresses and suction (14.5 psi)

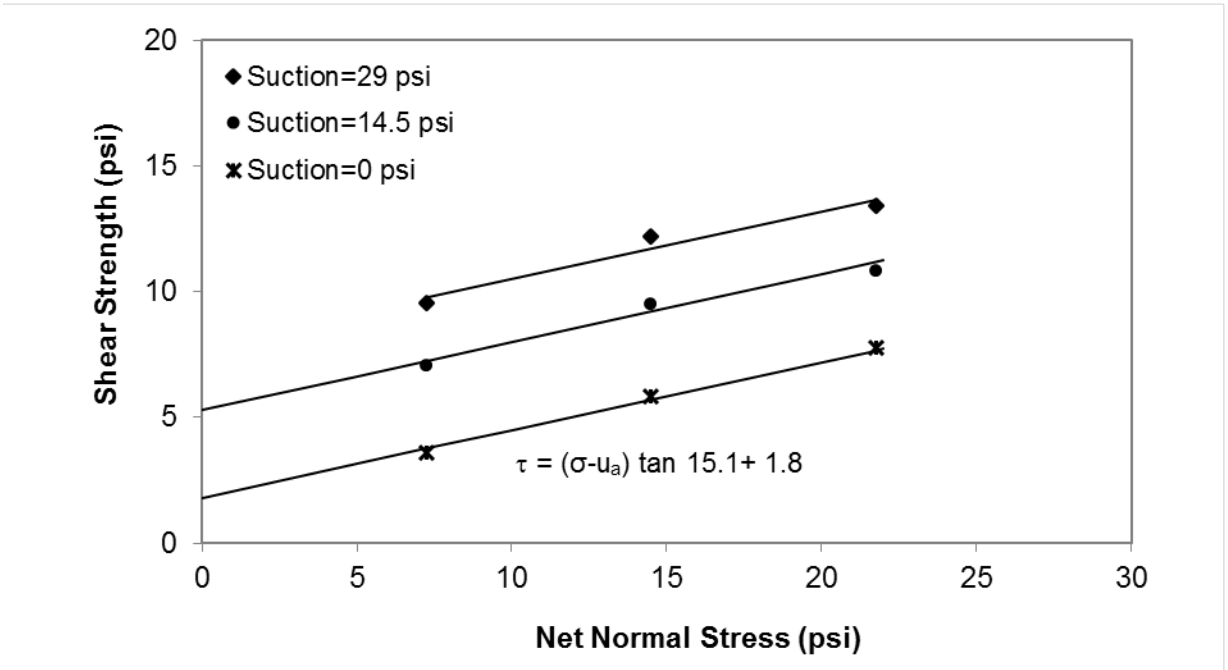

Figure 6.35. Idabel: shear strength envelope under different net normal stresses and suctions (0, 14.5, and 29.0 psi).

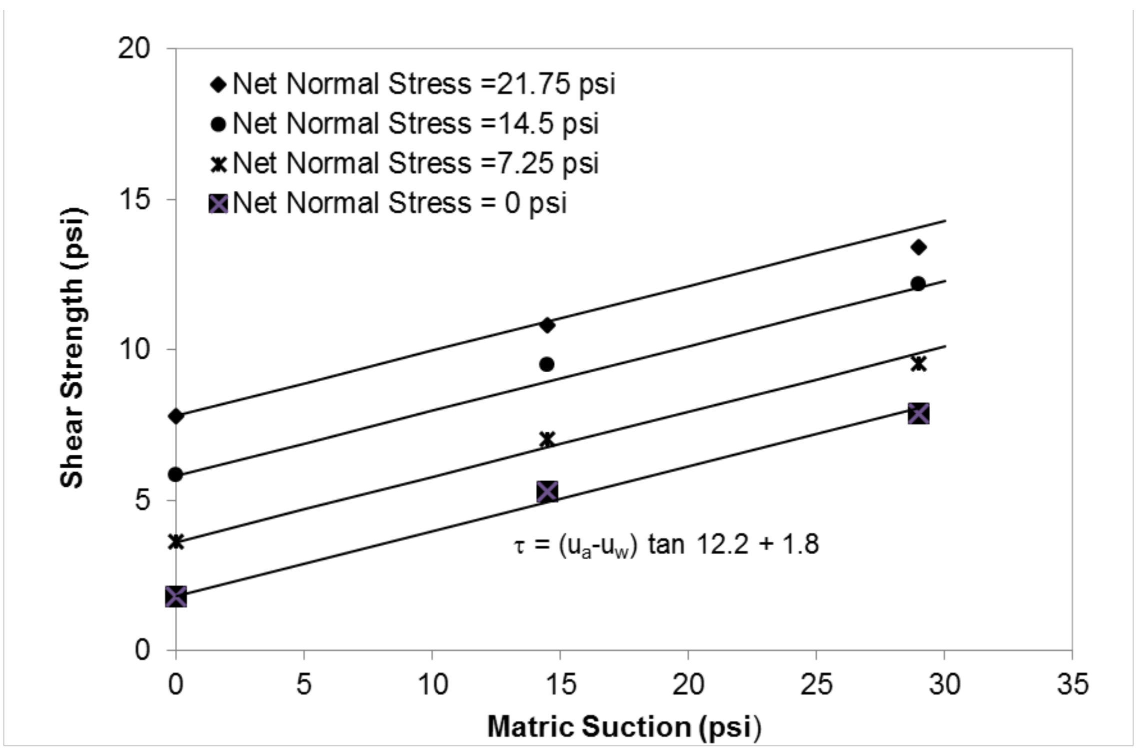

Figure 6.36. Idabel: shear strength envelope under different matric suctions and net normal stresses (0, 7.25, 14.5, and 21.75 psi).

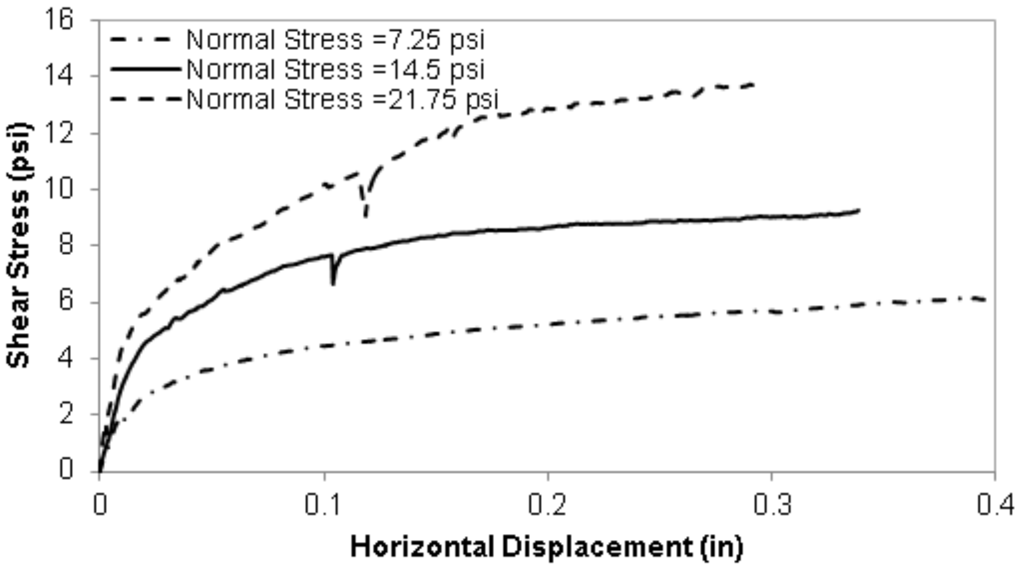

Figure 6.37. Chickasha: shear stress versus horizontal displacement under saturated conditions.

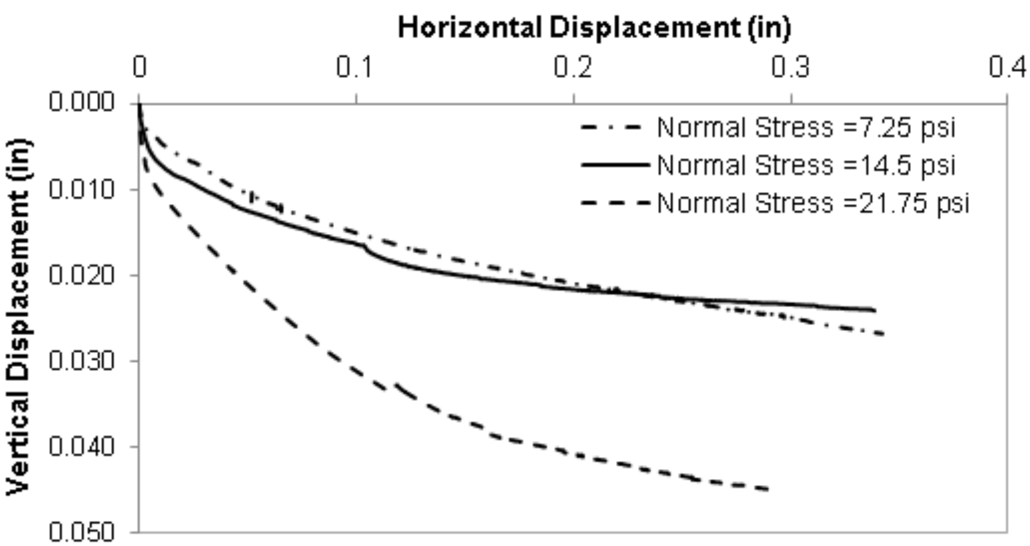

Figure 6.38. Chickasha: vertical displacement versus horizontal displacement under saturated conditions.

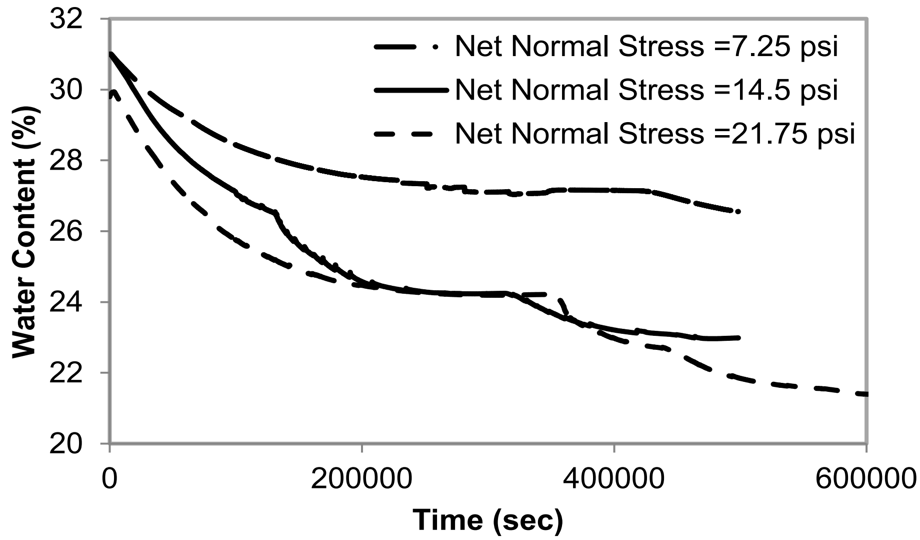

Figure 6.39. Chickasha: water content changes under different net normal stresses and constant suction (7.25 psi) during equalization and shearing.

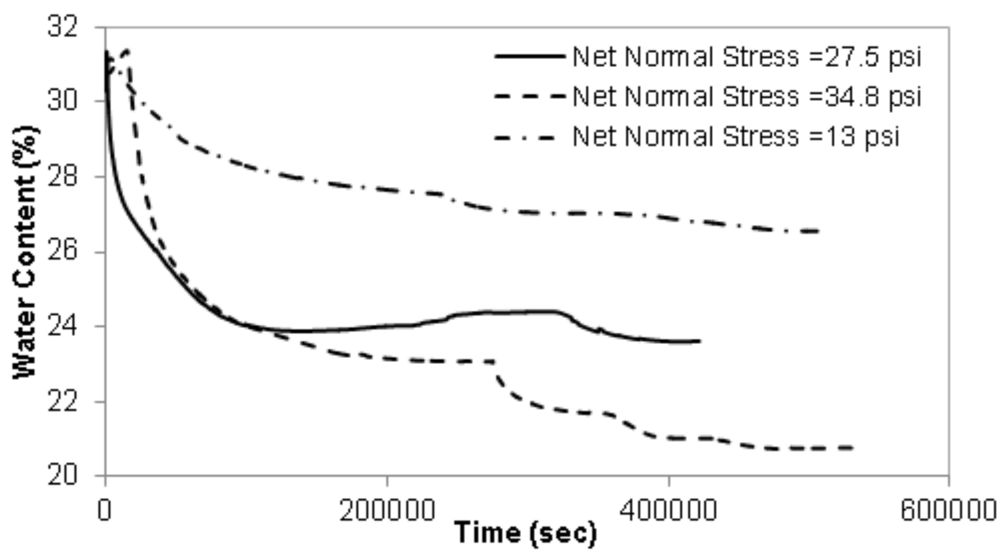

Figure 6.40. Chickasha: water content changes under different net normal stresses and constant suction (14.5 psi) during equalization and shearing.

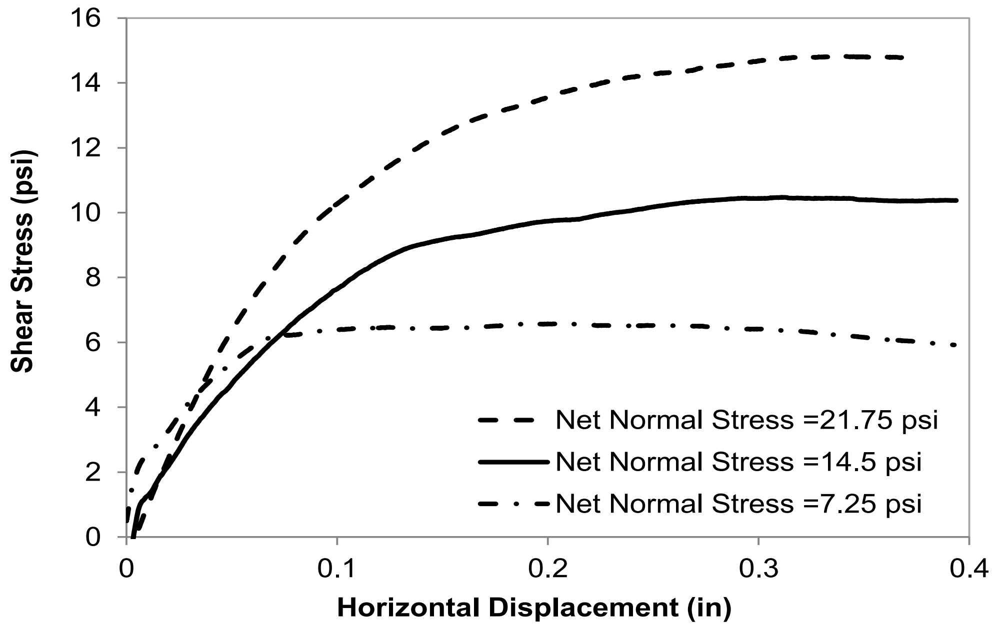

Figure 6.41. Chickasha: shear stress changes under different net normal stresses and constant suction (7.25 psi) during shearing.

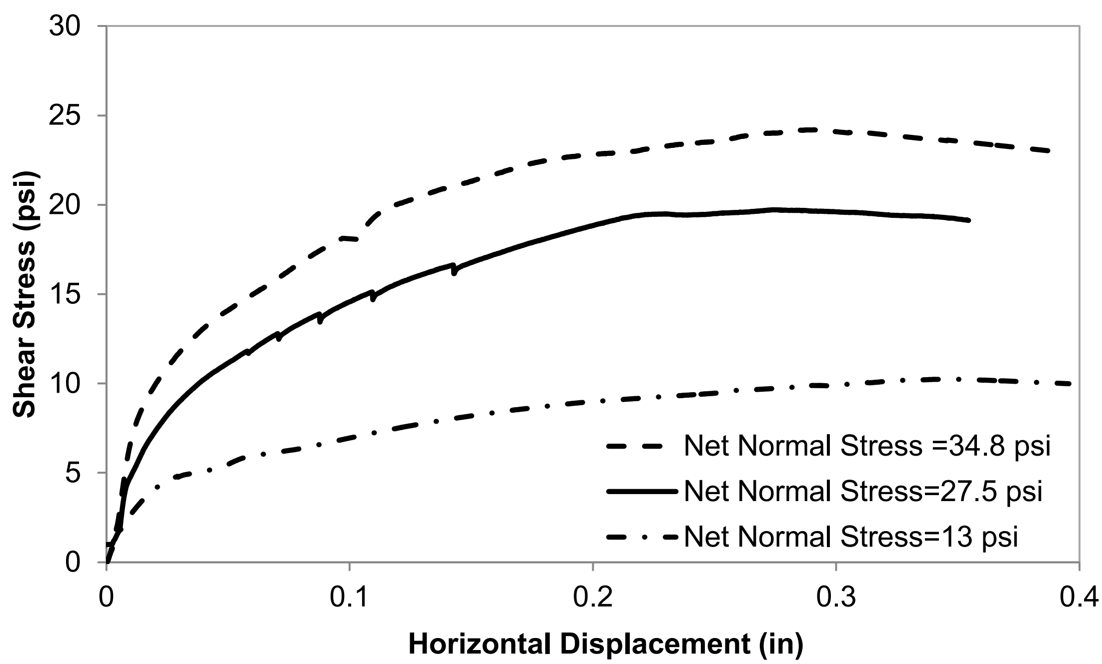

Figure 6.42. Chickasha: shear stress changes under different net normal stresses and constant suction (14.5 psi) during shearing.

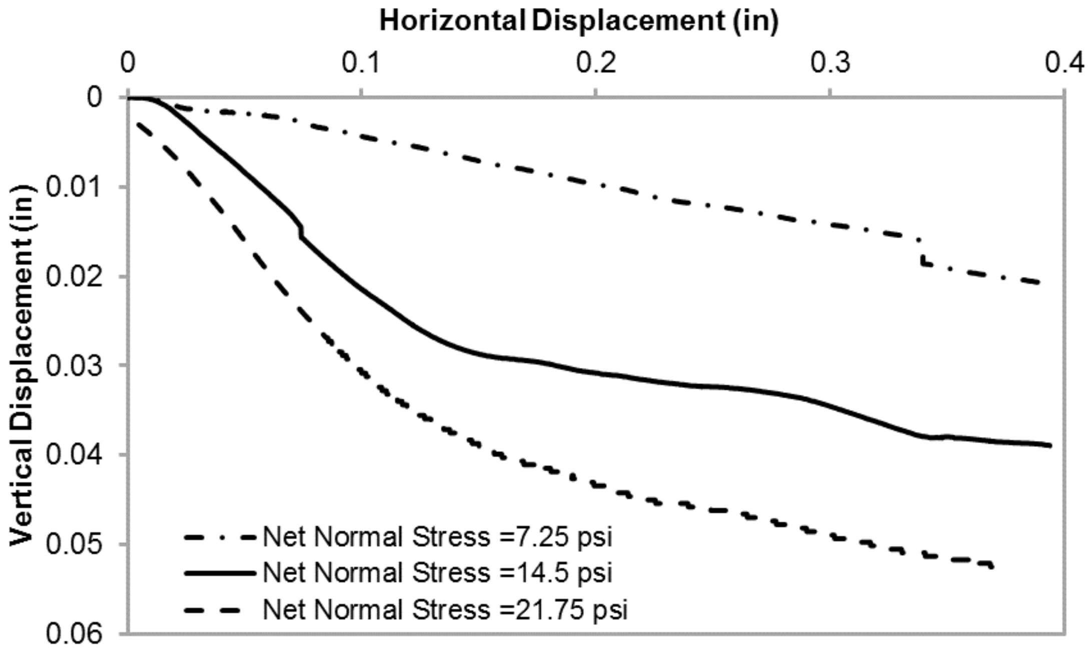

Figure 6.43. Chickasha: vertical displacement changes during shearing under different net normal stresses and suction (7.25 psi).

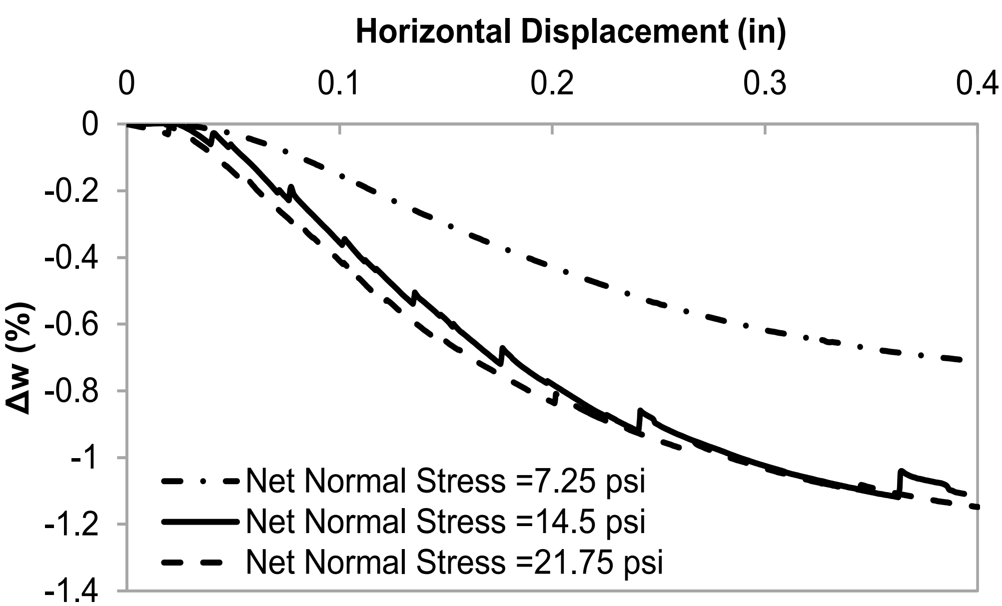

Figure 6.44. Chickasha: water volume changes during shearing under different net normal stresses and suction (7.25 psi).

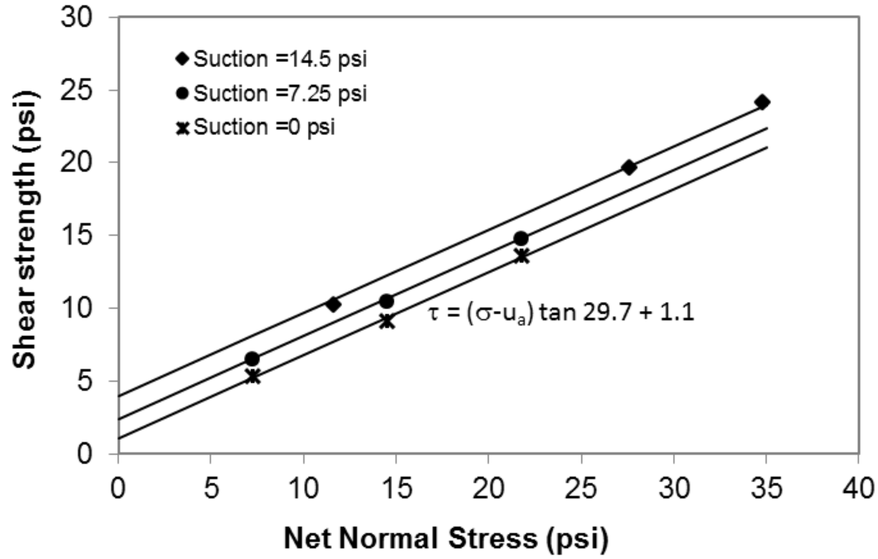

Figure 6.45. Chickasha: shear strength envelope under different net normal stresses and suctions (0, 7.25, and 14.5 psi).

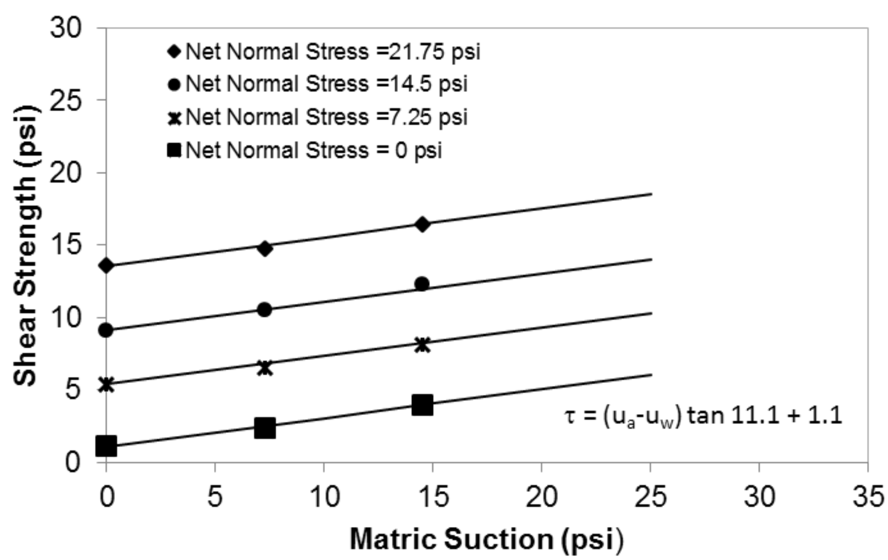

Figure 6.46. Chickasha: shear strength envelope under different matric suctions and net normal stresses (0, 7.25, 14.5, and 21.75 psi).

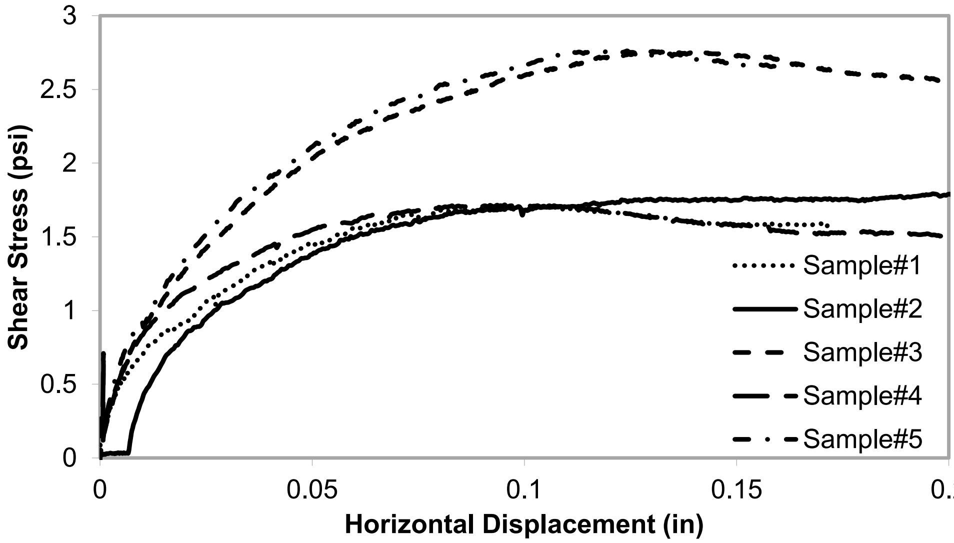

Figure 6.47. Idabel: shear stress versus displacement during shearing of samples artificially weathered by wet/dry cycles.

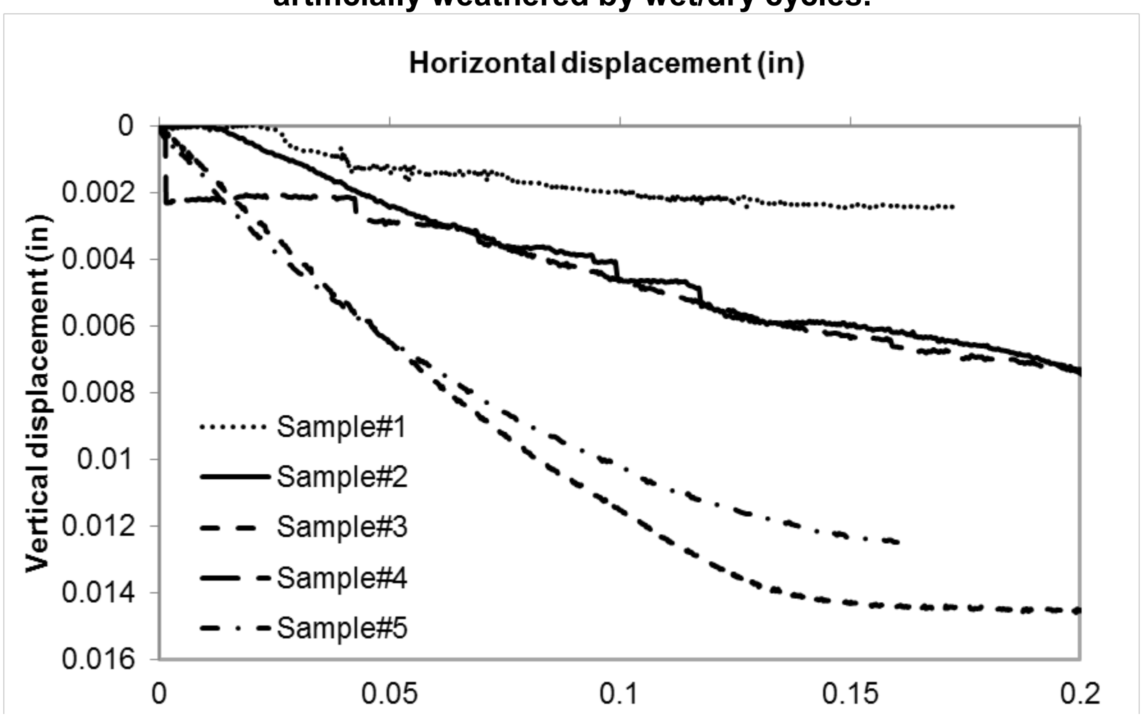

Figure 6.48. Idabel: vertical versus horizontal displacement during shearing of samples artificially weathered by wet/dry cycles.

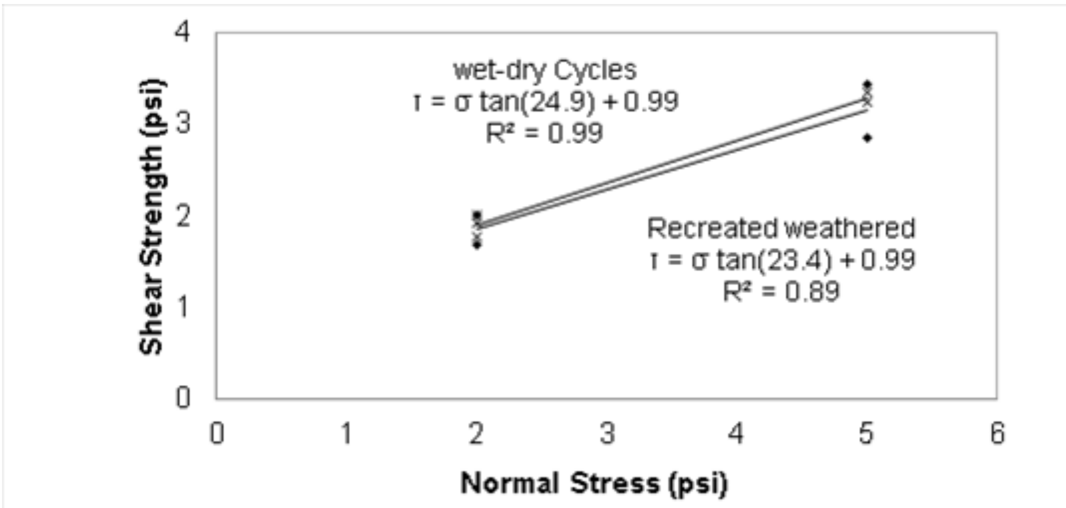

Figure 6.49. Idabel: comparison of failure envelopes between artificially weathered and recreated samples.

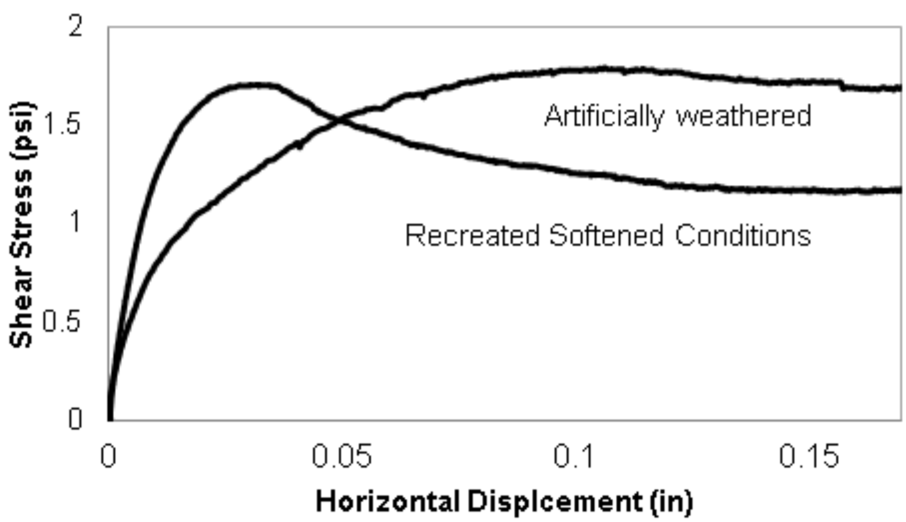

Figure 6.50. Idabel: comparison of shear stress-displacement curves for artificially weathered and recreated samples at a normal stress of 2 psi.

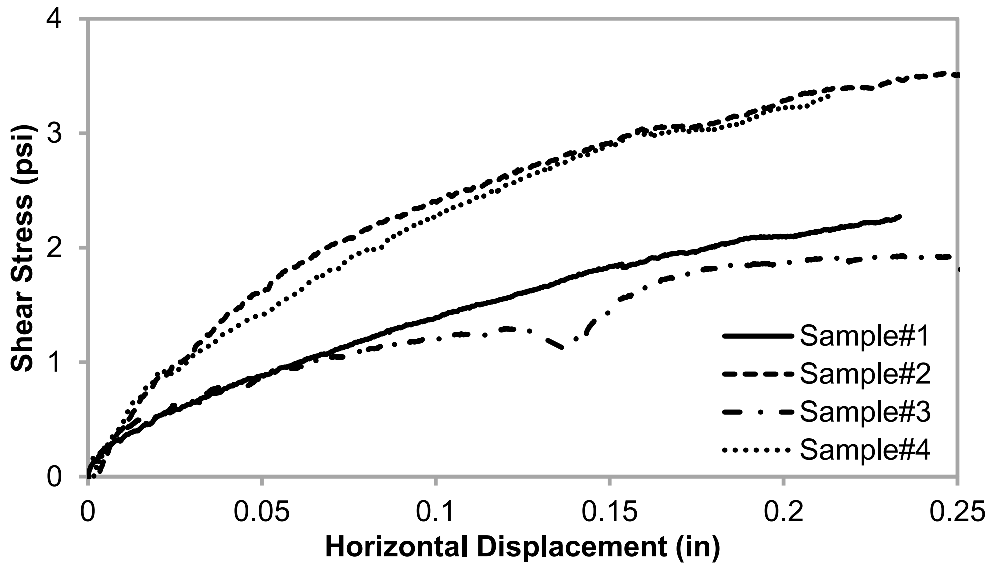

Figure 6.51. Chickasha: shear stress versus displacement during shearing of samples artificially weathered by wet/dry cycles.

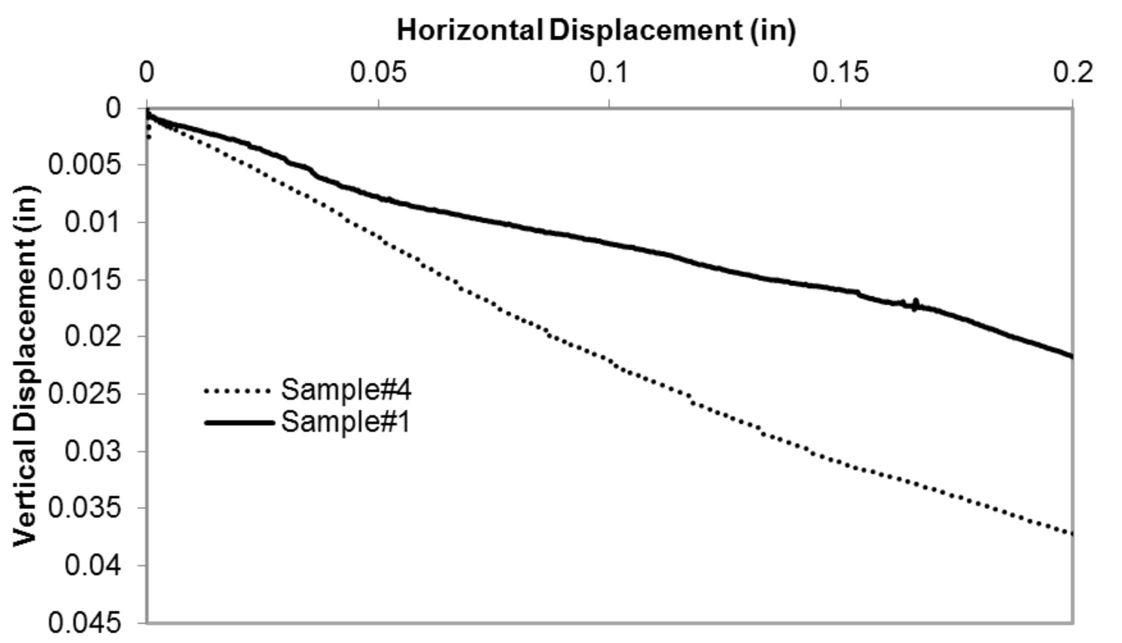

Figure 6.52. Chickasha: vertical versus horizontal displacement during shearing of samples artificially weathered by wet/dry cycles.

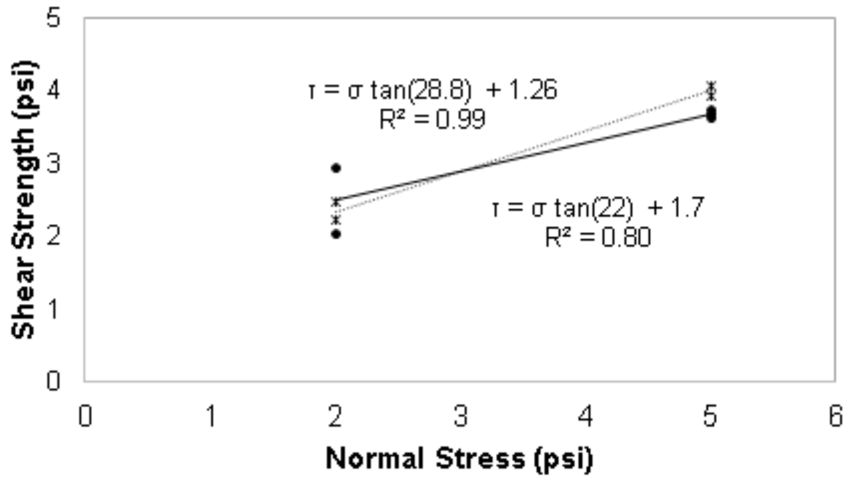

Figure 6.53. Chickasha: comparison of failure envelopes between artificially weathered and recreated samples.

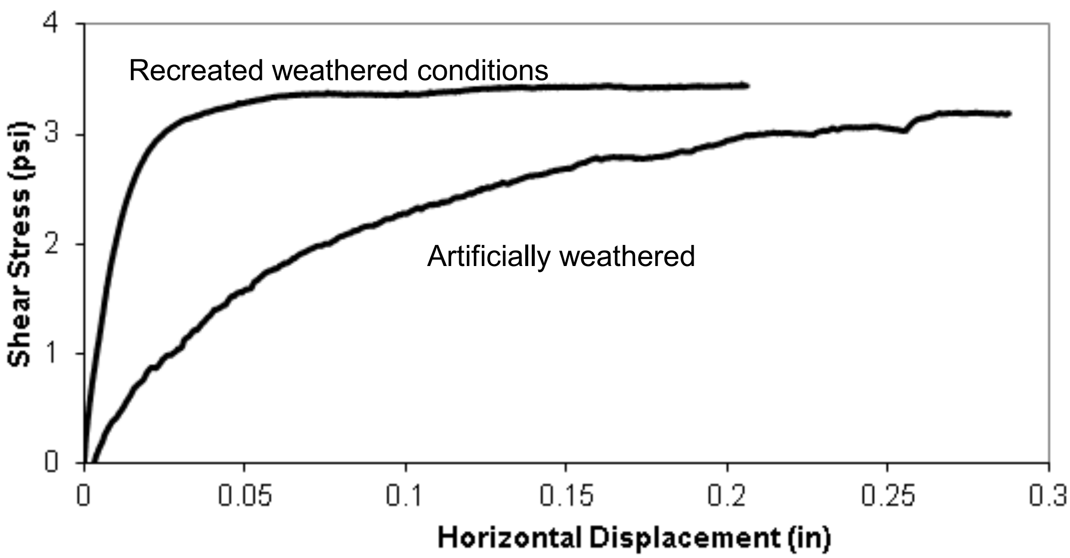

Figure 6.54. Chickasha: comparison of shear stress-displacement curves for artificially weathered and recreated samples at a normal stress of 5 psi.

Chapter 7 SLOPE STABILITY ANALYSES

7.1 Software and Model Set Up

To analyze the slope stability at the sites the program SVSlope by Soil Vision Ltd. was utilized because it allows for limit equilibrium analysis using traditional drained or undrained approaches as well as analysis using a suction dependent unsaturated strength model. A significant advantage of this software is that results of modeling moisture flow during wet weather events using SVFlux provide suction profiles that can be incorporated directly into the slope stability analysis using the SVSlope program.

Generally, in the limit equilibrium approaches, the slope is discretized into a number of slices that are bounded by the ground surface at the top and the failure surface at the bottom. Stability is examined by comparing forces emanating from shearing resistance along the base of a slice to forces produced by gravity in the downslope direction. The factor of safety defined by the limit equilibrium method is a factor by which the shear strength must be reduced to bring a material mass into a state of force equilibrium along a specified slip surface. In other words, limit equilibrium is achieved when the resisting forces just equal the forces driving failure.

Factor of safety was used as the basis of interpreting the slope stability analyses conducted in this study. Considering that slope failures have occurred at the test sites, a correctly modeled stability analysis should result in a factor of safety of unity. In other words, with the correct determination of strength parameters and pore water pressure conditions, the stability analysis should reveal a critical surface similar to that observed in the field and produce a factor of safety close to one.

Two general approaches to analyzing the slope stability were used. First, a more traditional limit equilibrium approach was used where drained behavior was assumed and pore water pressures were estimated using the pore pressure ratio, R_u. The pore pressure ratio, R_u, is the ratio of pore water pressure to total overburden pressure at some point along the failure surface. Incorporating the total unit weight of the soil, R_u is used to calculate pore water pressure and effective stress at the base of slices. The resisting shear stresses at the base of slices can then be calculated using effective stress normal to the failure surface and a Mohr-Coulomb strength law. The difficulty in using this approach is that R_u is not known and a typical value must be assumed. To analyze slope stability for each site, a parametric analysis was performed since R_u can vary over a wide range and since friction angles determined by various methods for each site varied significantly as well. Thus, factors of safety were computed using a range of friction angles and R_u values consistent with conditions at each site.

The second approach to modeling slope stability is inherently more complicated but potentially more realistic. In this approach, the pore pressure conditions in the slope were predicted using the unsaturated seepage modeling via SVFlux and the critical pore pressure distributions were used in the limit equilibrium slope stability analyses incorporating a suction dependent unsaturated strength model. Resulting pore pressures may be positive or negative, with negative pore pressures representing the soil suction. Pore pressure distributions are a function of initial slope conditions, soil hydraulic properties, vegetation and weather variations used as input for the seepage modeling, as discussed in Chapter 5. The daily pore water pressure variations through the depth of the slope were predicted and the critical state was determined on the rainfall day in which the factor of safety was at the minimum value. Finding the critical value of factor of safety was possible through several trials using the link between SVSlope and SVFlux.

To run the stability analyses, a simple geometric model was created. The geometries of the slopes for Idabel and Chickasha sites are shown in Figures 7.1 and 7.2, respectively, and were based on optical survey measurements. In this study, the shape of the potential slip surface was assumed to be shallow and circular to simulate failures that occurred at each tests site. Preliminary analysis using non-circular shallow linear surfaces revealed similar results to shallow circular failure surfaces. Further, observations of failures at each test site suggested the slip surface tended to be curved. Typical critical shallow slip surfaces for Idabel and Chickasha sites are shown if Figures 7.3 and 7.4. Unit weights used in stability analyses were based on field measurements from thin-walled samples provided in previous chapters. Within a range of reasonable values, unit weight values had a minor effect on results of slope stability analyses.

7.2 Stability Analyses using Pore Pressure Ratio, R_u

In Figure 7.5, results of stability analyses for different combinations of effective stress friction angle and pore pressure ratio are shown for the Idabel site. Effective stress cohesion was assumed to be zero in these analyses. It has been suggested that a reasonable value of R_u is between 0.2 and 0.4 (e.g. Mesri and Shahien 2003). Using this range as a guide suggests that operative friction angles in the absence of cohesion at failure should be between 20 and 27 degrees based on Figure 7.5 for the Idabel site. As presented in Chapter 6, average friction angles were about 15, 19, and 26 degrees based on DSTs on compacted soil, fully softened DSTs and triaxial tests on field samples, respectively. Thus, it would seem that a combination of fully softened strength and R_u=0.2 or triaxial strength from field samples and R_u=0.4 would provide reasonable estimates of slope stability. It is noted that for the lowest friction angle of about 15 degrees obtained from saturated/unsaturated strength testing on compacted remolded soil, the factor of safety is less than one for R_u equal to zero (i.e. no positive pore water pressure). If the operative friction angle was actually 15 degrees, some additional component of cohesion, such as from matric suction, would be necessary to maintain stability of the slope. Interestingly, Cerato and Nevels (2007) reported that the back-calculated friction angle for a previous failure at the site was equal to about 14.5 degrees and that the slope failed after a significant precipitation event. Their analysis assumed pore water pressures were zero. This supports the presumption that the operative friction angle was likely close to 15 degrees and that the slope was stable under the influence of suction. The rain event likely reduced the suction close to zero, which triggered the failure. The unsaturated analysis presented subsequently lends additional support for this hypothesis.

There is much uncertainty as to the proper selection of strength parameters and R_u values for stability analyses. This results from the different friction angles and pore pressure conditions that can be used to predict a similar factor of safety for a situation as demonstrated by the previous discussion. Furthermore, there is the question as to whether the effective stress cohesion intercept represents a true component of shear strength operating under field conditions. If cohesion is incorporated into the analysis, the factors of safety go up considerably and result in unrealistic values of R_u (>1) needed to produce instability. Cohesion intercepts from multistage triaxial tests appear unreliable and vary considerably and should therefore be neglected. For fully softened conditions, cohesion intercepts are assumed to be zero as the soil is believed to approach a normally consolidated condition and should also be neglected in the stability analysis. In the case of direct shear testing on saturated and unsaturated compacted clays, the applicability of effective cohesion intercept is uncertain. In fact, for the friction angle of 15 degrees determined from unsaturated strength testing the slope would be unstable without cohesion unless pore water pressures were negative (i.e. $R_u<0$), as discussed previously. This will be further explored in a subsequent section on unsaturated stability analyses.

In Figure 7.6, results of stability analyses for different combinations of effective stress friction angle and pore pressure ratio are shown for the Chickasha site. Effective stress cohesion was assumed to be zero in these analyses. Similar to the analysis for Idabel, for R_u in the range of 0.2 to 0.4, the operative friction angles in the absence of cohesion at failure should be between 23 and 31 degrees based on Figure 7.6. As presented in Chapter 6, average friction angles were about 30, 26, and 24 degrees based on DSTs on compacted soil, fully softened DSTs and triaxial tests on field samples, respectively. Interestingly, the largest average friction angle for Chickasha soil corresponds to the DSTs on compacted soil while the average of triaxial tests represents the lowest value. This is opposite to observations for Idabel soil. In this case, a combination of triaxial strength and R_u=0.2 or DST strength from compacted samples and R_u=0.4 would provide reasonable estimates of slope stability. In addition, since the fully softened strength is intermediate to the DST and triaxial strengths, using the fully softened friction angle and R_u around 0.25 would provide reasonable estimates of stability. The questions raised with respect to Chickasha soil are similar to those raised with regard to the Idabel soil.

7.3 Unsaturated Stability Analyses

Highway embankment and cut slopes are exposed to numerous cycles of drying and wetting. Invariably, the upper reaches of these slopes within the soil active zone exist in an unsaturated condition much of the time, especially during extended drying periods. Failures often occur during significant wetting periods due to reductions in matric suction, soil softening and increased soil weight. The presence of desiccation cracks may contribute to the cause of failures by providing rapid access for water to the soil beneath the ground surface. In Oklahoma, many slope failures in unsaturated soils are triggered by heavy rainfall that usually occurs between May through October. These failures are characterized by relatively shallow failure surfaces that develop parallel to the original slope.

To model the unsaturated slope stability, first unsaturated seepage analyses were conducted for each site using SVFlux to estimate moisture variation and pore water pressures in a slope due to changing seasonal weather patterns. The predicted pore water pressure profiles were then imported into SVSlope for limit equilibrium analysis using an unsaturated strength model. The advantages of this approach are that pore water pressures are estimated from seepage analysis based on known or predicted weather variables and the model can handle both positive and negative (suction) pore water pressures.

Results of the analysis, discussed subsequently, suggest that slopes may fail with significant portions of the failed mass under unsaturated conditions with negative pore pressures. Implicit in the use of traditional slope stability analyses using typical R_u values is that the slope is saturated and pore water pressures are positive. Realistic modeling of slope stability should account for the real possibility that many slopes may fail in a partially or completely unsaturated state. There are however, disadvantages with unsaturated slope stability analyses. Not least of which is the added complexity of conducting unsaturated seepage analysis, determination of a weather pattern for design and determining unsaturated strength parameters and other needed soil properties including SWCC parameters. Another complicating factor is how to include the impact that desiccation cracks may have on the slope stability. In light of the added complexity, it could be argued that a traditional saturated analysis with a conservative estimate of positive pore water pressures is preferred, especially since it should represent a worst case relative to unsaturated conditions. However, in some cases this may be a poor representation of actual worst case conditions in a slope. It may be adequate to use a simplified traditional approach to slope stability analysis to get a reasonable representation of actual conditions; however, it is important to first understand and quantify to the degree possible the actual worst case conditions. In this way, engineers will have some understanding of the implications of their simplifying assumptions relative to likely actual worst case conditions. The unsaturated seepage and slope stability analysis conducted for the two test sites where shallow failures have occurred provides a better understanding of possible mechanisms leading to failure.

7.3.1 Unsaturated Seepage Analysis

Using the water content variation in different layers for Idabel soil and Chickasha soils, the negative pore water pressures (suctions) corresponding to the water contents at specified depths was determined as the initial condition. The ground surface was a flux boundary receiving rainfall infiltration simulated by that obtained by the weather station installed on the slope. The left and right boundaries were assumed to be impermeable. The boundary on the bottom was a unit hydraulic gradient boundary. The physical meaning of this boundary condition is that the amount of flux that passes through the boundary at a particular suction is equal to the coefficient of permeability of the soil corresponding to that suction.

To assess the impact of desiccation cracking the slope at each site was divided into an upper layer and a lower layer as shown in Figures 7.7 and 7.8. The upper layer extended from the ground surface to a depth where desiccation cracking was expected to reach. This also corresponds to the depth near the bottom of the expected failure surface. All of the assigned material parameters were the same for two layers except for hydraulic conductivity. That is the two layers were assigned the same shear strength parameters, the same unit weight, and the same SWCC; however, the hydraulic conductivity of the upper layer was increased to account for the presence of desiccation cracks.

Three cases of unsaturated seepage analyses were conducted for each site: 1) $K_1=K_2$, 2) $K_1=10K_2$ and 3) $K_1=100K_2$; where K_1 and K_2 represent the saturated hydraulic conductivity of the upper and lower layers, respectively. For the purpose of this study, the saturated hydraulic conductivity was determined from flexible wall permeameter tests presented in Chapter 6. Unsaturated hydraulic conductivities were computed using an unsaturated permeability function, where K_{unsat} is a function of the saturated permeability, current suction and the SWCC. Since the SWCC was assumed to be the same for the upper and lower layers, the scaling factor on the saturated permeability was the same for the unsaturated permeability. In other words, if $K_1=10K_2$, then $K_{1unsat}=10K_{2unsat}$ for the same suction. While this does not properly model the flow through and adjacent to desiccation cracks, it does allow for investigation of the influence of an enhanced hydraulic conductivity using a continuum approach. It is a first step in examining the impact of desiccation cracks on slope stability.

Unsaturated seepage analyses were conducted using weather parameters observed at the test sites during the monitoring period for three hydraulic conductivity cases described above. Plots of initial pore water pressures (i.e. suction) and critical pore pressure distributions for hydraulic conductivity Cases 1, 2 and 3 are shown in Figures 7.9 to 7.12 for Idabel and Figures 7.13 to 7.16 for Chickasha. These analyses indicate that enhanced flow of water in the upper layer can cause significantly more reduction of suction within the slope compared to the non-cracked case ($K_1=K_2$). Generally more water is observed to build up in the slope as the hydraulic conductivity of the upper layer increases. For the cases with $K_1=100K_2$, significant water builds up in the upper cracked layer as shown in Figures 7.12 and 7.16. This actually provides some justification for conducting a traditional drained stability analysis with a conservative R_u value.

7.3.2 Results of Unsaturated Slope Stability Analysis

Critical pore water pressure distributions for the three hydraulic conductivity cases discussed above ($K_1=K_2$, $K_1=10K_2$, and $K_1=100K_2$) were used to conduct slope stability analyses. Basically, the critical cases represent the pore pressure distributions with the lowest predicted suctions. A linear unsaturated strength model was used in the stability analyses where the shear strength is given as:

$$\tau = c' + (\sigma - u_a)\tan\phi' + (u_a - u_w)\tan\phi^b \quad \textbf{(7.1)}$$

The unsaturated strength parameters reported in Chapter 6 for each site were used in the analysis. Net normal stress (σ-u_a) and suction (u_a-u_w) represent the stress conditions along the failure surface. Since the air pressure is assumed to remain at atmospheric pressure or zero gage pressure, the suction is equivalent to the opposite of the negative pore water pressures predicted from the unsaturated seepage analysis (Figures 7.10-7.12, 7.14-7.16).

Results of the stability analyses are presented in Tables 7.1 and 7.2 for the Idabel and Chickasha sites, respectively. The two variables that were varied in the analysis were the pore pressure distributions corresponding to the different seepage scenarios and the effective stress cohesion intercept (c'). Analyses were run using c' as determined from the laboratory direct shear tests and with c' equal to zero.

It is clear from the analysis that the simulated effect of the desiccation cracks is significant to the resulting factors of safety. Factors of safety decrease dramatically from the non-cracked state ($K_1=K_2$) to the cracked states ($K_1>K_2$). Furthermore, the factors of safety were very sensitive to whether or not the effective stress cohesion intercept is considered. A perfect simulation of the failures that have occurred would result in a factor of safety equal to 1.0. Based on the results presented for Idabel, a factor of safety equal to 1.0 would occur for the analysis with $c'=0$ and for pore pressure distributions simulated using K_1 between $10K_2$ and $100K_2$. For Chickasha, the lowest factor of safety, close to 1, occurs for $K_1=100K_2$. Generally, there was a much wider range in predicted factors of safety for Idabel in comparison to Chickasha for the range of parameters used. While there is a significant amount of work needed to further develop and enhance the unsaturated approach for modeling slope stability used in this study, these preliminary results suggest that this method is viable.

7.4 A Simple Model for Predicting Desiccation Crack Depth

In the previous section, the depth of the zone of enhanced hydraulic conductivity was assumed to extend approximately to the bottom of the failure surface that was approximately 5 feet and 6 feet below the surface of the slope for Idabel and Chickasha sites. A simple formulation for estimating depth of desiccation cracking generally supports this assumption. The method is preliminary in the sense that additional validation and refinements are needed; however, it appears to be a reasonable and promising starting point. It is presented in this section and demonstrated for the Chickasha test site.

7.4.1 Desiccation Crack Depth Based on Elastic Theory

Following on the work of Morris et al. (1992), a simple preliminary approach for predicting desiccation crack depth in compacted soil was developed. The equation for predicting crack depth based on elastic theory involves the following simplifying assumptions:

1. The crack depth corresponds to a point below the ground surface where the final horizontal stress equals the tensile strength of the soil.
2. Depth of cracks is based on a formulation for a horizontal ground surface. As a starting point for analyzing slopes, it will be assumed the depth of cracks measured normal to face of the slope will be similar to the depth of cracks for a horizontal surface.
3. Cracks form in one direction along a linear plane.
4. The crack has zero thickness and vertical stress remains constant at the bottom of the crack.
5. Horizontal stress at a given depth is the same in all directions up to the point of cracking.
6. Pore air pressures remain at atmospheric pressure (zero gage pressure).
7. The horizontal strain is zero up to the point of cracking.
8. The soil behaves as a linear elastic material up to the point of cracking.

Based on the equations presented by Fredlund and Rahardjo (1993), the incremental elastic equation for strain in a horizontal direction for isotropic unsaturated soil can be written as follows:

$$\varepsilon_x = \frac{\Delta(\sigma_x - u_a)}{E} - \frac{\mu}{E}\left(\Delta\sigma_y + \Delta\sigma_z - 2\Delta u_a\right) + \frac{\Delta(u_a - u_w)}{H} \qquad \textbf{(7.2)}$$

where, ε_x = is taken as strain normal to the long axis of the crack prior to cracking, $\Delta(\sigma_i - u_a)$ is the change in net normal stress in the x, y, and z (vertical) directions, u_a is the air pressure, u_w is water pressure, $\Delta(u_a\text{-}u_w)$ is the change in matric suction, and E and H are the elastic moduli with respect to net normal stress and suction. A schematic of assumed initial and final stress conditions during development of a desiccation crack are shown in Figure 7.17.

Incorporating the assumptions, ε_x=0, Δu_a=0, u_a=0, $\Delta\sigma_z$=0 and $\Delta\sigma_x=\Delta\sigma_y$; Equation 7.2 simplifies to:

$$\Delta\sigma_x = \frac{E}{H(1-\mu)}\Delta(u_a - u_w) \tag{7.3}$$

The initial horizontal stress, σ_{xo} is equal to $K_o\sigma_{vo}=K_o\gamma z_c$, and the final horizontal stress, σ_{xf}, is assumed to be equal to the tensile strength of the soil, σ_t; thus, $\Delta\sigma_x=K_o\gamma z_c-\sigma_t$. The vertical total stress is σ_{vo}, γ is the total unit weight, K_o is the ratio of the horizontal to vertical total stress before desiccation, and z_c is the depth of cracking. Substituting these expressions into Equation 7.3 leads to an expression for the desiccation crack depth:

$$z_c = \frac{E}{K_o\gamma H(1-\mu)}\Delta(u_a - u_w) + \frac{\sigma_t}{K_o\gamma} \tag{7.4}$$

Equation 7.4 can be used to predict the crack depth for a given set of initial conditions and change in suction during drying. Alternatively, the equation can be rearranged to solve for the change in suction needed to produce cracking for a particular depth.

7.4.2 Estimating Soil Properties for Predicting Cracking Depth

To use Equation 7.4 requires determining several important soil properties. For the purpose of analysis demonstrated here, it is assumed that the soil starts from an initial compacted state corresponding to the end of construction. Initial lateral stresses are unknown; however, since compacted cohesive soils can experience lateral stress ratios approaching unity or greater (e.g. Duncan and Seed 1986), as a first approximation, a value of 1.0 was selected. A Poisson's ratio of 0.35 and E/H ratio of 0.3 were selected as a starting point based on work of Morris et al. (1992) and suggestions in Fredlund and Rahardjo (1993). The tensile strength of the soil was determined by direct measurement while the soil was undergoing desiccation from an initial condition corresponding to the initial conditions of the embankment soil. The method for determining tensile strength is was presented in Chapter 4. Model parameters used to model desiccation crack depth at the Chickasha site are summarized in Table 7.3.

7.4.3 Cracking Depth Based on Field Suction Estimates

Based on field observations at sites in Australia, Morris et al. (1992) suggested that desiccation cracks generally occur within the active zone of a soil profile. This is consistent with Equation 7.4 in that only values of z_c greater than zero are valid and this only occurs when $\Delta(u_a\text{-}u_w)$ is greater than some critical value with z_c=0. Rearranging Equation 7.4, it is possible to solve for the change in suction needed to produce cracking at a given depth:

$$\Delta(u_a - u_w) = \frac{\sigma_t H(\mu - 1)}{E} + \frac{\gamma Z_c H}{E}(K_o - K_o\mu) \qquad \textbf{(7.5)}$$

Equation 7.5 provides a more useful estimation of depth of cracking as demonstrated in Figure 7.18. In Figure 7.18 the estimated changes in suctions at various depths based on extreme values of moisture content determined at the embankment site and the SWCC are shown. The bottom of the active zone is the point where the estimated change in suction is zero; this point is at a depth of 2.3 m and was extrapolated from the previous two measurement depths (0.9 and 1.8 m). Superimposed on the profile of estimated field changes in suction are lines showing the changes in suction required to produce cracking at various depths based on Equation 7.5. The “best estimate” line is based on model parameters in Table 7.3. The ± 25% lines were obtained by increasing and/or decreasing the model parameters in Table 7.3 (not including $\Delta(u_a\text{-}u_w)$ which was calculated in Equation 7.5) by 25% such that the lowest and highest values of predicted changes in suction resulted. The purpose of this was to show the range of predicted crack depths that might result due to uncertainty in estimating model parameters. Crack depths are estimated by the intersection of the line of measured suction changes with theoretical lines relating suction change to crack depth. Based on the field estimates of suction changes shown, the range of estimated crack depths considering uncertainty in model parameters is 5.3 to 7.2 ft. with the best estimate at about 6.4 ft. From a practical point of view, this range of cracks depths seems reasonable especially considering the significant variation of model parameters. This range is consistent with the assumed thickness of the layer having enhanced hydraulic conductivity for the unsaturated seepage analysis of the Chickasha site. Although not shown in Figure 7.18, different field estimates of suction change can also be investigated based on soil-climate modeling results and/or to account for uncertainty in field determined suction values due to extreme weather conditions different from those encountered during field monitoring. The method shows promise as a means of predicting desiccation crack depths; although, as mentioned, additional validation and possible refinement of the method is needed.

Table 7.1. Idabel: summary of unsaturated slope stability analyses.

Conditions	Effective Friction Angle, ϕ'	c' (psi)	ϕ^b (deg.)	Factor of Safety
Unsaturated	15.1	1.8	12.2	7.37
Unsaturated, cracked (K_1=10K_2)	15.1	1.8	12.2	5.19
Unsaturated, cracked (K_1=100K_2)	15.1	1.8	12.2	3.89
Unsaturated without cohesion	15.1	0	12.2	4.30
Unsaturated without cohesion, cracked (K_1=10K_2)	15.1	0	12.2	1.60
Unsaturated without cohesion, cracked (K_1=100K_2)	15.1	0	12.2	0.52

Table 7.2. Chickasha: summary of unsaturated slope stability analysis.

Conditions	Effective Friction Angle, ϕ'	c' (psi)	ϕ^b (deg.)	Factor of Safety
Unsaturated	29.7	1.1	11.1	2.84
Unsaturated,Cracked (10$K_{uncracked}$)	29.7	1.1	11.1	2.39
Unsaturated,Cracked (100$K_{uncracked}$)	29.7	1.1	11.1	2.02
Unsaturated without cohesion	29.7	0	11.1	1.92
Unsaturated without cohesion, Cracked (10$K_{uncracked}$)	29.7	0	11.1	1.46
Unsaturated without cohesion, Cracked (100$K_{uncracked}$)	29.7	0	11.1	1.09

Table 7.3. Model paramters used to predict desiccation crack depth.

Parameter	Value	Determined by:
E/H	0.3	estimated
μ	0.35	estimated
K_o	1	estimated
σ_{tu}, psi	-2.5	measured
σ_t, psi	-3.9	calculated

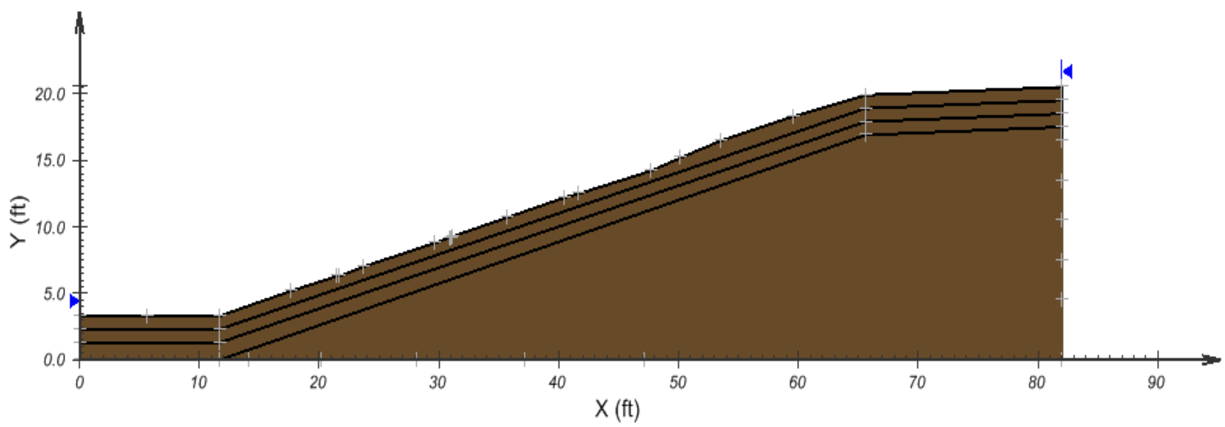

Figure 7.1. Idabel: slope geometry.

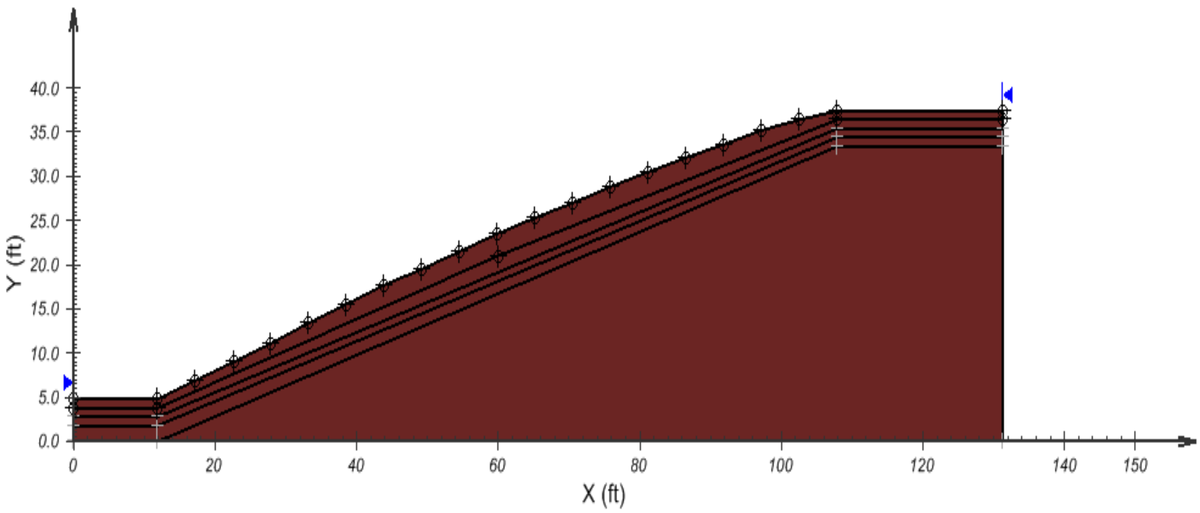

Figure 7.2. Chickasha: slope geometry.

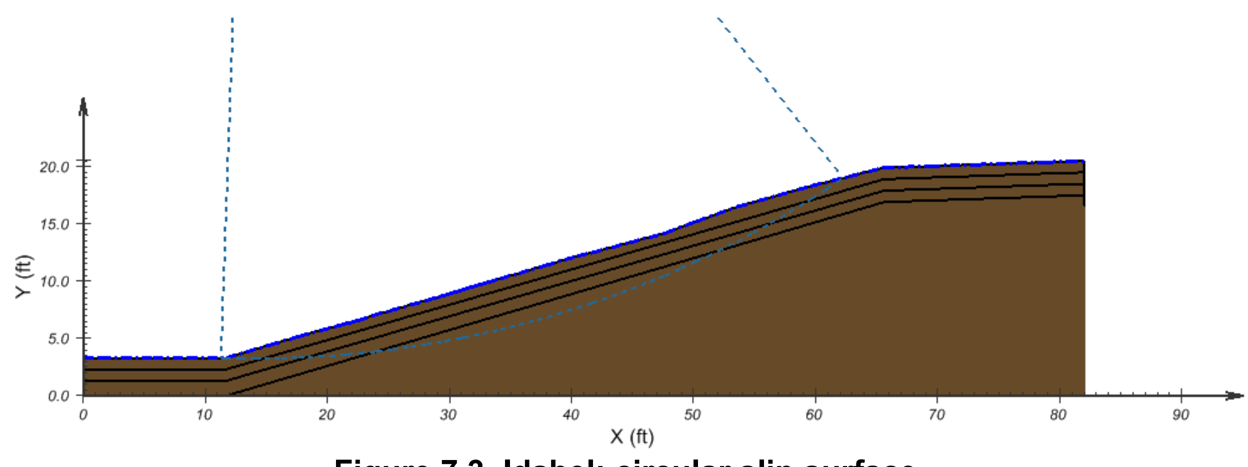

Figure 7.3. Idabel: circular slip surface.

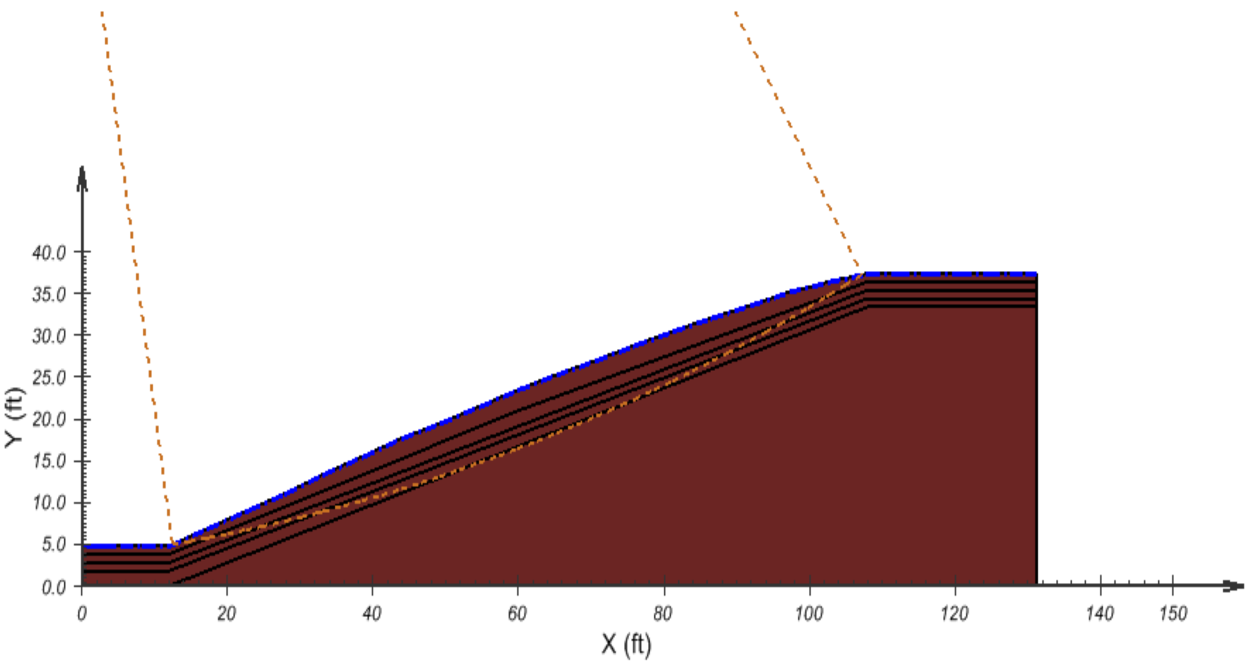

Figure 7.4. Chickasha: circular slip surface.

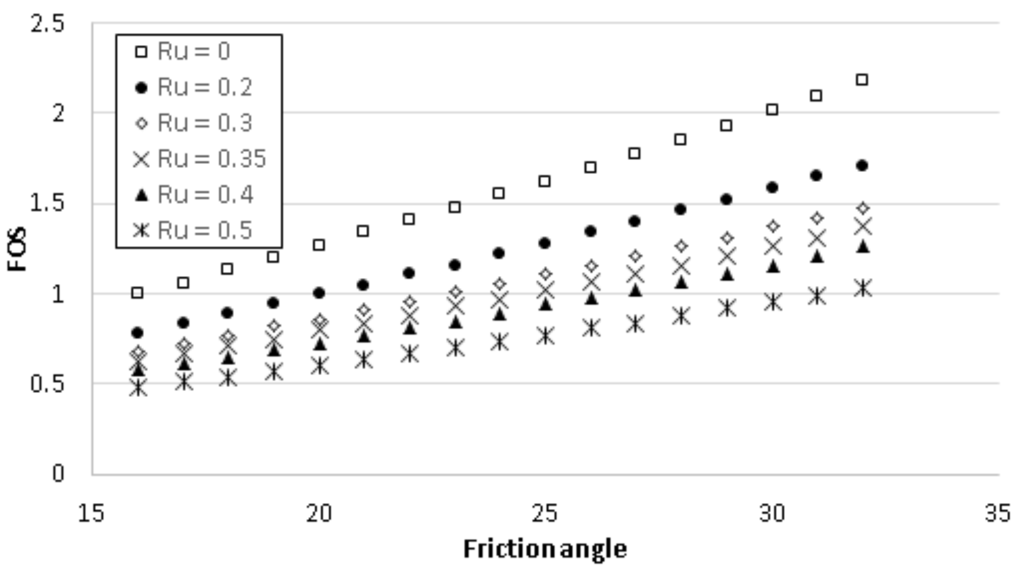

Figure 7.5. Idabel: factor of safety (FOS) as a function of friction angle and pore pressure ratio

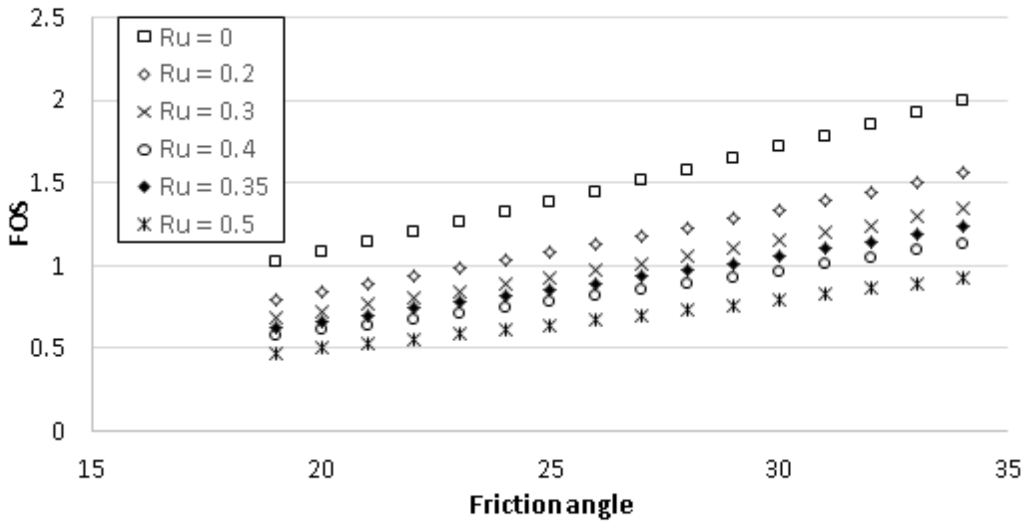

Figure 7.6. Chickasha: factor of safety (FOS) as a function of friction angle and pore pressure ratio.

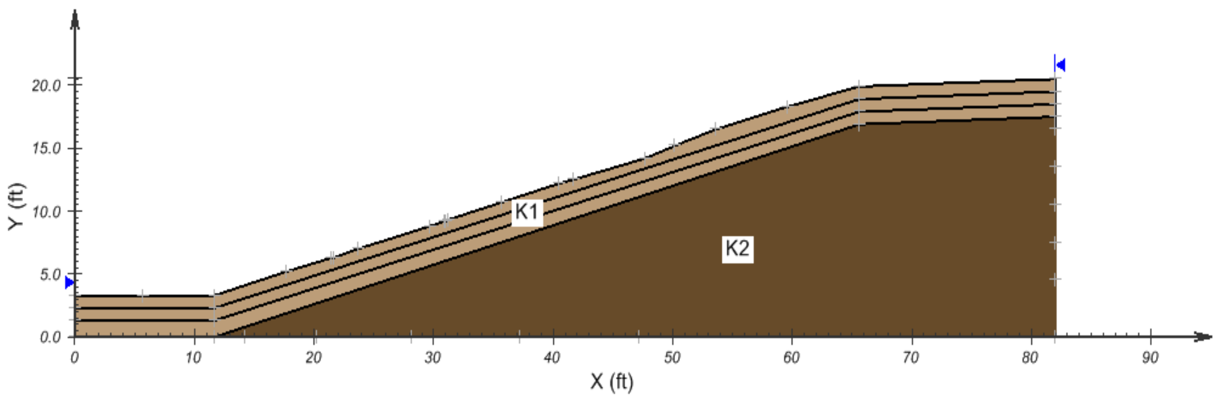

Figure 7.7. Idabel: soil layers in unsaturated seepage model.

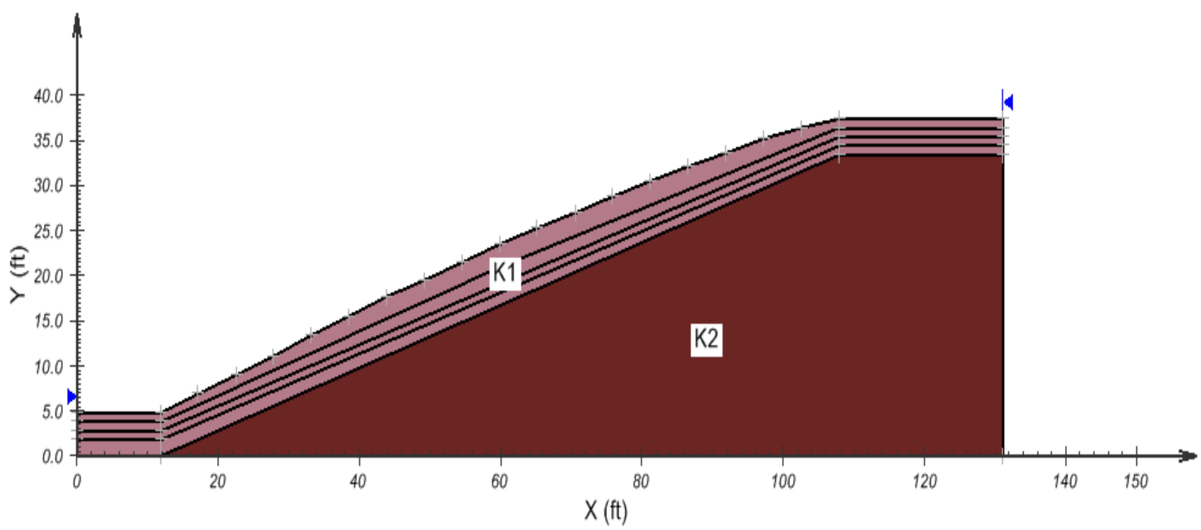

Figure 7.8. Chickasha: soil layers in unsaturated seepage model.

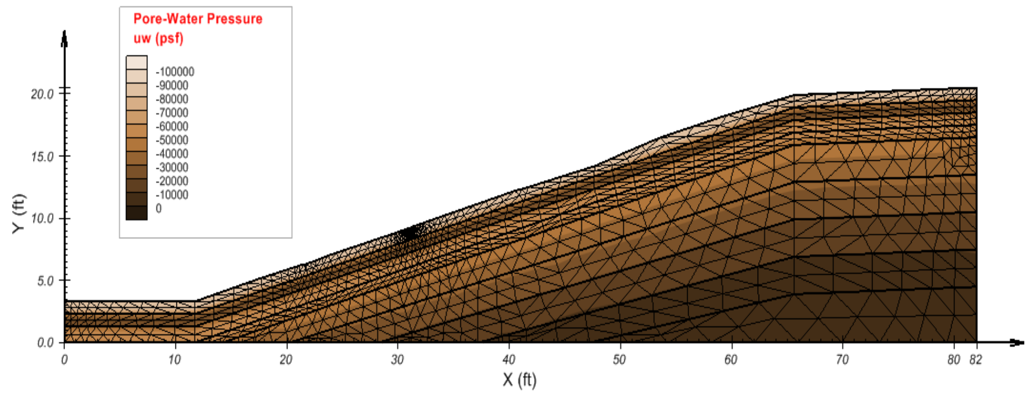

Figure 7.9. Idabel: initial pore water pressure distribution in the slope prior to unsaturated seepage modeling.

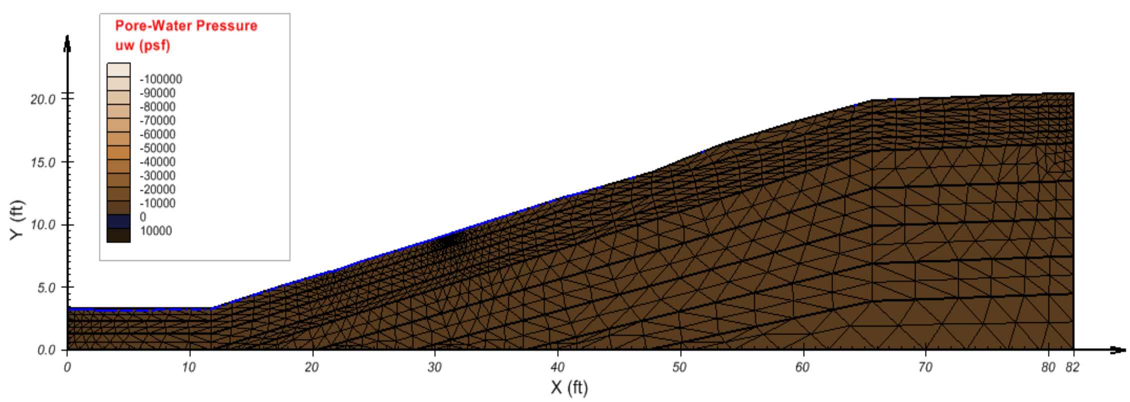

Figure 7.10. Idabel: pore water pressure distribution at the critical situation from unsaturated seepage modeling for K_1=K_2= 5.5e-9 in/sec.

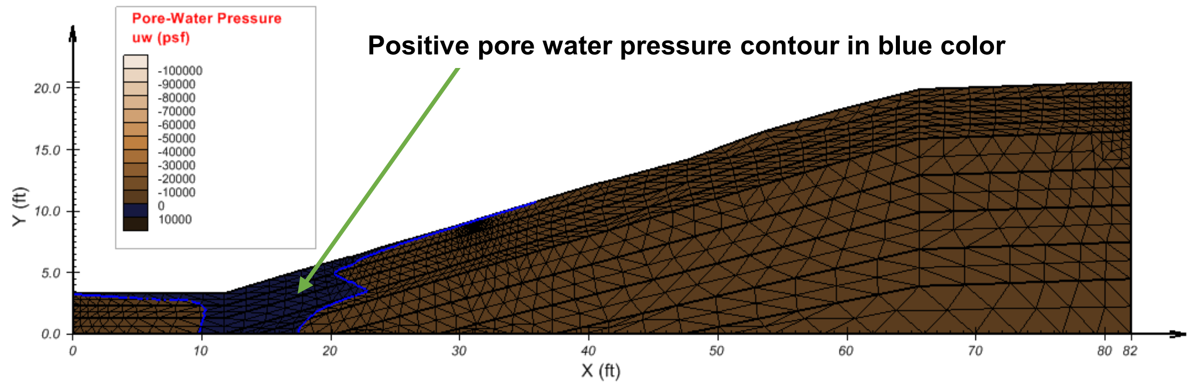

Figure 7.11. Idabel: pore water pressure distribution at the critical situation from unsaturated seepage modeling for K_1=10K_2= 5.5e-8 in/sec.

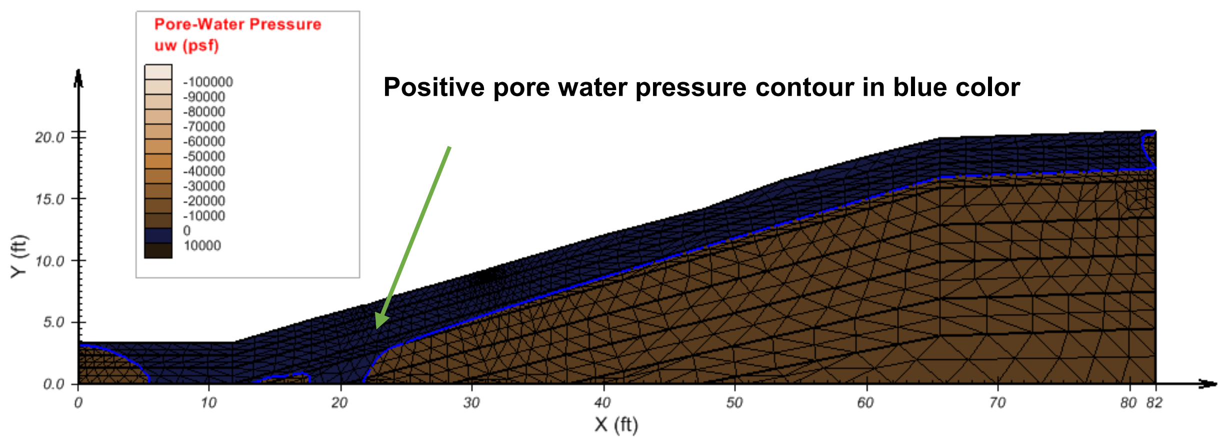

Figure 7.12. Idabel: pore water pressure distribution at the critical situation from unsaturated seepage modeling for K1=100K2= 5.5e-7 in/sec.

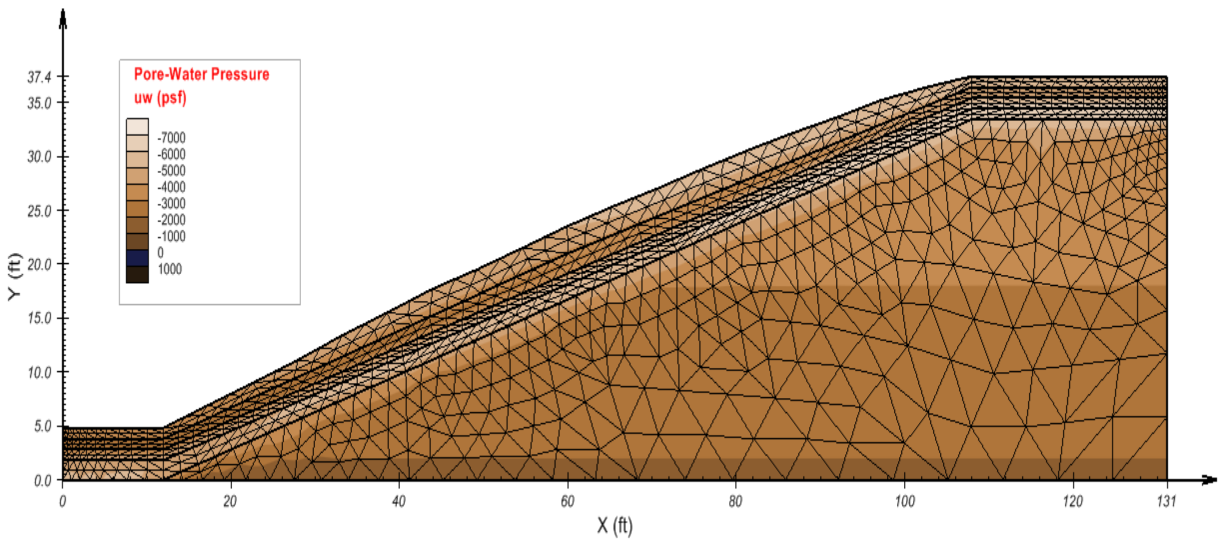

Figure 7.13. Chickasha: initial pore water pressure distribution in the slope prior to unsaturated seepage modeling.

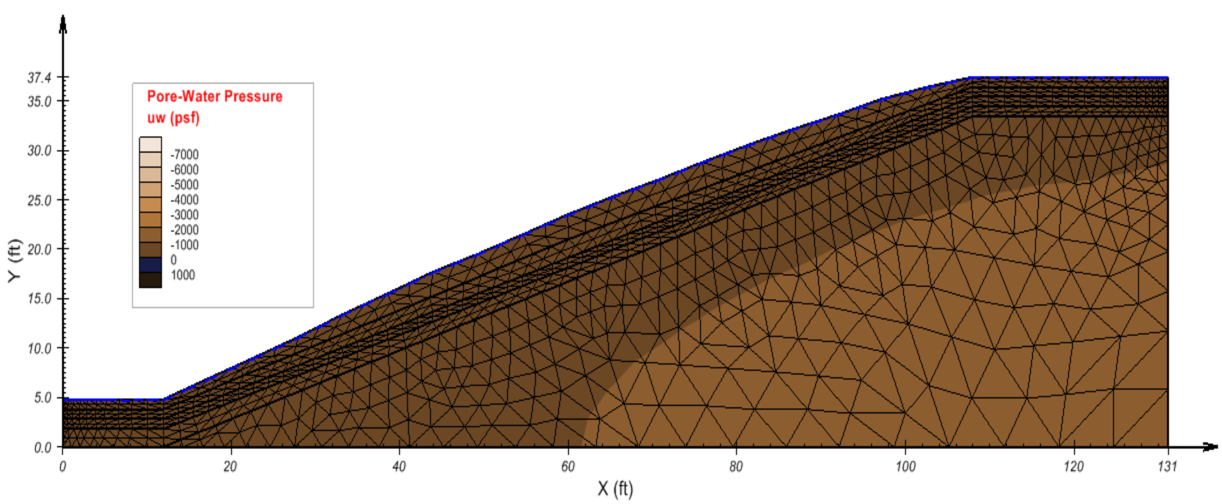

Figure 7.14. Chickasha: pore water pressure distribution at the critical situation from unsaturated seepage modeling for K1=K2= 5.7e-7 in/sec.

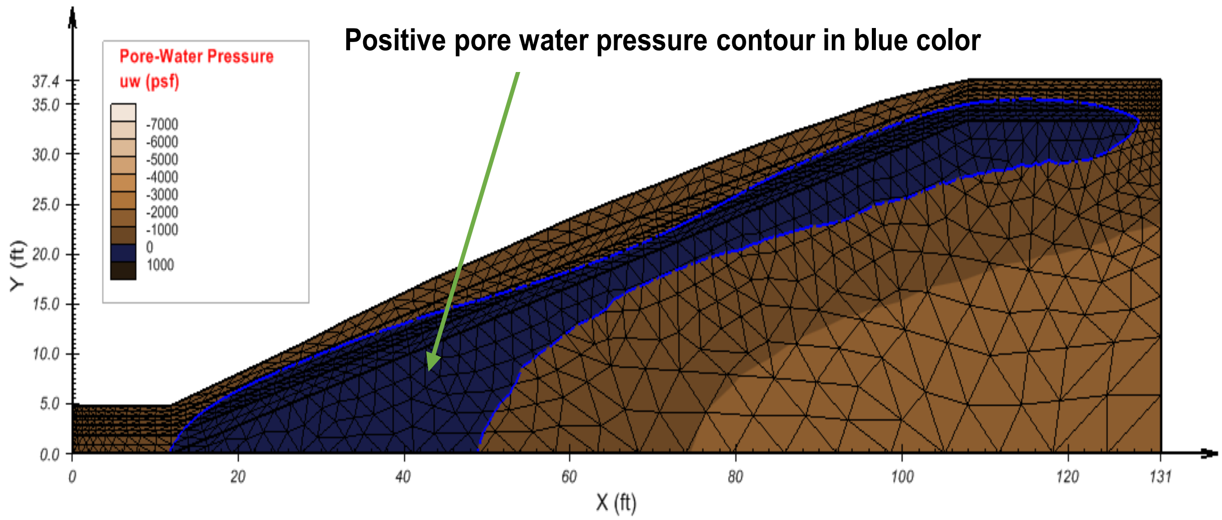

Figure 7.15. Chickasha: pore water pressure distribution at the critical situation from unsaturated seepage modeling for K1=10K2= 5.7e-6 in/sec.

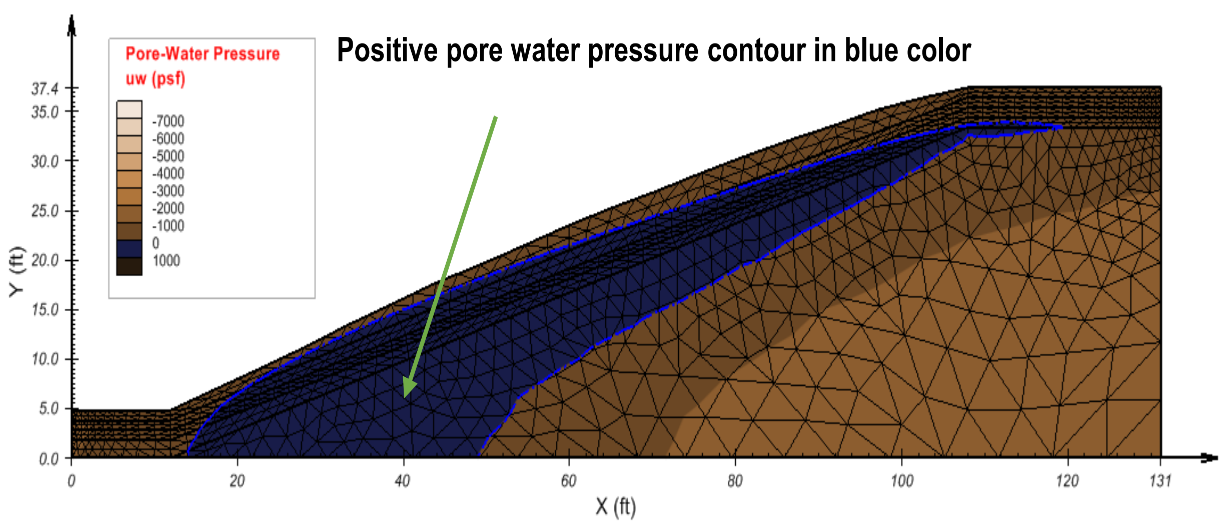

Figure 7.16. Chickasha: pore water pressure distribution at the critical situation from unsaturated seepage modeling for K1=100K2= 5.7e-5 in/sec.

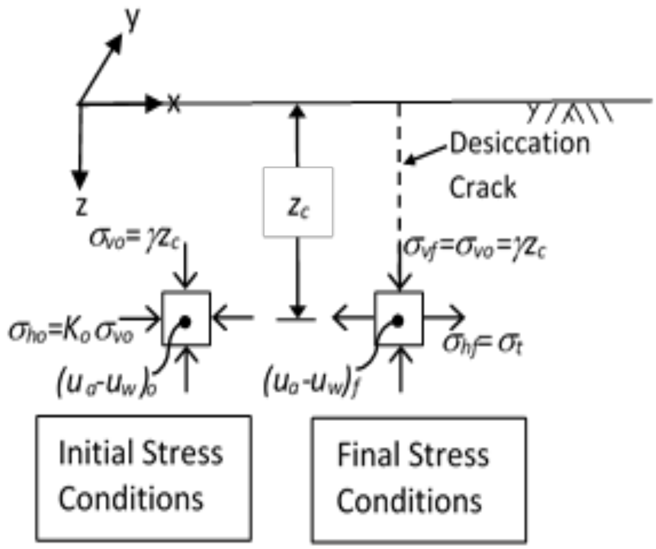

Figure 7.17. Schematic of assumed stress conditions in desiccating compacted soil.

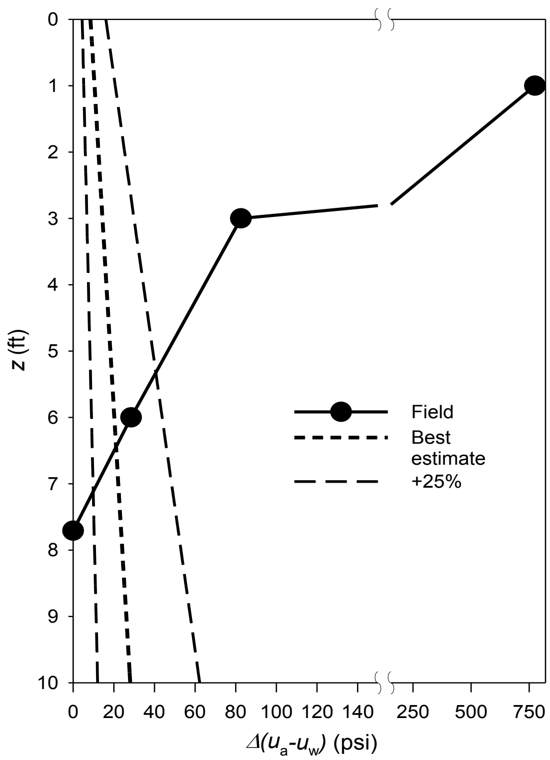

Figure 7.18 Change in suction based on extreme variations in field measured water contents and theoretical change in suction to produce cracking.

Chapter 8 CONCLUSIONS AND RECOMMENDATIONS

An extensive field and laboratory investigation and modeling of shallow slope stability was conducted. The research involved installing weather monitoring stations and soil moisture sensors at two test sites where shallow slope failures had occurred. Laboratory testing was conducted to determine soil shear strength, soil water characteristic curves, and moisture flow properties. A new apparatus for measuring the tensile strength of desiccating soil was developed and used to perform an extensive investigation of soil parameters that affect the tensile strength. Numerical modeling was conducted using SVFlux and Vadose/W to predict moisture content changes in soil profiles using measured weather data as input for comparison to measured moisture contents during the monitoring period. Limit equilibrium slope stability analyses were conducted using the program SVSlope; two types of analyses were conducted. First using a traditional drained approach with a range of friction angles encompassing those determined from various laboratory strength tests. Pore pressure ratios were also varied, which provided positive pore water pressure ranging from zero to 50% of the overburden pressure. The second type of slope stability analysis involved first predicting pore water pressures using an unsaturated seepage program, SVFlux, with weather data used for input. Three unsaturated seepage analyses were conducted for each site. In the first case, the hydraulic conductivity was assumed to be uniform throughout the slope while in the second and third cases, an upper layer of soil with enhanced hydraulic conductivity was assumed. The thickness of this layer was assumed to correspond to roughly the bottom of the slope failure surface and consistent with the depth of desiccation cracking. Pore water pressures predicted by this method were both positive and negative, the latter reflecting the presence of matric suction. Stability analyses were then performed using the predicted pore pressure distributions. In addition, a simple analytical model was developed for predicting desiccation crack depth. Following are some of the important conclusions and recommendations from this study.

8.1 Conclusions

1. Average friction angles determined by direct shear testing on fully softened soil, saturated triaxial shear testing on thin-walled tube samples, and saturated/unsaturated direct shear testing on compacted soil samples varied significantly at each test site. For the Idabel site the respective average friction angles were 18.8, 25.9, and 15.1 degrees. For the Chickasha site the respective average friction angles were 25.6, 24.2, and 29.7 degrees.
2. Unsaturated strength parameters, ϕ', ϕ^b, and c' determined with saturated/unsaturated direct shear testing of composite samples of compacted soil were 15.1^o, 12.2^o, and 1.8 psi for Idabel and 29.7^o, 11.1^o, and 1.1 psi for Chickasha.
3. Results of flexible wall hydraulic conductivity tests on two thin walled tube samples and one compacted sample from each site provided a range of saturated hydraulic conductivity of $4.8x10^{-9}$ in/sec to $6.2x10^{-9}$ in/sec for the Idabel site and $2.5x10^{-7}$ in/sec to $1.1x10^{-6}$ in/sec for the Chickasha site. Average values were assumed to represent the intact saturated hydraulic conductivity for use in unsaturated seepage analyses. Unsaturated hydraulic conductivity functions

were determined using soil water characteristic curves and saturated hydraulic conductivities. Hydraulic conductivities determined in this manner seemed to provide reasonable results from unsaturated seepage analyses.

4. Results of moisture diffusivity tests on two thin walled tube samples from each test site provided drying diffusion coefficients of 5.1×10^{-5} in^2/sec and 1.8×10^{-5} in^2/sec for Idabel samples and 5.4×10^{-5} in^2/sec for both samples from Chickasha. Interestingly, the average drying diffusion coefficient from Idabel was the same as for Chickasha. These values are quite low and predicted active depths using the method of McKeen and Johnson (1990) are relatively shallow, on the order of 4 feet or less. This is lower than active depths indicated by soil moisture sensors at the Chickasha site and is attributed to the fact that diffusivity tests on intact small laboratory samples do not accurately account for the influence of desiccation cracks in the field.
5. A new device, the desiccation box, was developed to measure tensile strength of compacted soil during desiccation. The box was successfully used to measure tensile strength of composite samples from Idabel and Chickasha sites under various initial dry densities and water contents.
6. Tensile strength determined in the desiccation box was observed to generally increase with increasing density, increasing initial water content, and increasing soil plasticity. However, the tensile strength only increased up to a point where the water content was well beyond optimum and then it decreased with increasing water content.

7. A theoretical model for tensile strength based on a Mohr-Coulomb failure law and that incorporates a microstructural representation of effective stress for unsaturated soil (Alonso et al. 2010) was used to predict tensile strengths as a function of water content. Comparisons of theoretical tensile strengths with those measured in the desiccation box were quite favorable. Of particular note was that the model was able to capture the increase and decrease of tensile strength observed with increasing water content.
8. A simple model, based on linear elastic theory, for predicting depth of desiccation cracks in compacted clayey soil was developed. The model was used to predict the change in suction required to produce cracking as a function of depth. Predicted changes in suction necessary to produce cracking at a particular depth were compared to maximum changes in suction estimated from moisture sensors at the Chickasha site. The cracking depth is assumed to be the depth where the trend of predicted cracking suction changes and the trend of measured suction changes meet. The depth of desiccation cracks predicted for the Chickasha site using the simplified model and accounting for some uncertainty in the model parameters was in the range of 5.3 to 7.2 feet with the best estimate around 6.4 feet. This is consistent with observations of moisture changes with depth and the estimated depth of the failure surface at the site.
9. Weather data obtained from instrumentation installed at each of the test sites was compared to weather data obtained from the nearest Mesonet station. While there were some differences on a day to day basis in measured parameters,

generally the trends of the two data sets were quite similar. Some differences are expected on account of differences in topography and location.

10. Trends of soil moisture variations observed with moisture sensors at each test site were predicted reasonably well using the software SVFlux. However, predictions generally did not capture well the abrupt changes in moisture content recorded by the sensors. These abrupt changes occur mainly at the shallowest sensor locations and may be partly the result of desiccation cracking that allows more rapid wetting and drying at sensor locations.
11. Although input soil properties and weather data were similar in each case, predictions using Vadose/W were not as favorable as those using SVFlux. Predicted trends of moisture contents at all depths using Vadose/W were significantly lower than measured trends.
12. A traditional approach to slope stability analyses using drained strength parameters and pore pressure ratio, R_u, was conducted. Since the slopes at each test site had experienced shallow failure, it was assumed that shallow stability analyses providing a factor of safety of one would be closest to representing the actual soil and pore water pressure conditions at failure. For Idabel, for the friction angles of 19, 26 and 15 degrees determined by direct shear testing on fully softened samples, triaxial testing on field samples and saturated/unsaturated direct shear tests on compacted samples, the corresponding R_u values needed to produce a factor of safety of one are 0.2, 0.4, and less than 0.0, respectively. A R_u less than zero indicates the presence of negative pore pressures (matric suction) at failure. For the Chickasha site the

corresponding friction angles were 26, 24, and 30 degrees with associated R_u values of 0.3, 0.2, and 0.4.

13. Unsaturated seepage analyses using SVFlux were performed using weather data as input to estimate worst case pore water pressure profiles in the slopes at each site. The pore pressure profiles were incorporated into a limit equilibrium slope stability analyses that used a linear unsaturated strength model. Unsaturated strength parameters presented previously were used. The analysis was run with and without considering the effective stress cohesion intercept, c′. Analyses with c′ resulted in unusually high factors of safety. The influence of desiccation cracks was modeled by incorporating an upper layer of soil having an enhanced hydraulic conductivity. Three cases were analyzed: first with the hydraulic conductivity of the upper (k_1) and lower (k_2) layers equal (k_1=k_2), second with k_1=10k_2 and third with k_1=100k_2. The first case represents a slope with no cracks. Results of the stability analyses for both sites show a significant reduction in factor of safety for shallow slope failure as the hydraulic conductivity of the surface layer increases. Results show that the factor of safety approached one when k_1 of the surface layer was one to two orders of magnitude greater than k_2 of the underlying soil. The cohesion intercept c′ was assumed to be zero in the analysis.
14. Results of the unsaturated seepage analysis for k_1 approaching 100k_2 indicate significant buildup of water in the surface layer of the slope. This supports the idea of performing a traditional drained stability analysis with Ru on the order of 0.4 or so.

8.2 Recommendations

Some recommendations based on this research project are presented below. These are based on observations and analyses involving two test sites in Oklahoma. These recommendations should thus be used with due consideration of the uncertainty associated with studying only two sites.

1. Unsaturated seepage modeling provides a fundamentally sound and systematic means of evaluating moisture profiles and suction in slopes in response to varying weather. This provides a rational way to determine pore water pressures, both positive and negative (matric suction), for use in unsaturated slope stability analyses. However, it requires considerable effort to learn the software and underlying concepts, determine the model parameters, format the input weather data, calibrate and run the numerical models. There is also much uncertainty associated with the influence of desiccation cracks and determination of several model parameters. Nevertheless, the analysis conducted in the study provided significant insight into the problem, and despite the uncertainties provided realistic simulations of conditions leading to shallow slope failure. Therefore, whenever possible in the course of investigating shallow slope failures, it is recommended that unsaturated seepage modeling be conducted using historical weather data from nearby Mesonet stations. Some additional related recommendations are:
    a. Unsaturated seepage modeling should be conducted using SVFlux.
    b. The depth of the upper cracked layer should be estimated using the simplified analysis presented in this report and/or based on field

observations and other information. The simplified analysis of predicting crack depth will require an estimate of the maximum changes in suction expected in the slope soil profile.

c. An upper layer of uniform thickness equal to the predicted depth of desiccation cracks with enhanced hydraulic conductivity should be used in the unsaturated seepage model. At least three cases should be investigated as described previously ($k_1=k_2$, $k_1=10k_2$, $k_1=100k_2$), including the non-cracked case. If possible, the intact hydraulic conductivity should be based on flexible wall permeability tests conducted on thin-walled samples obtained from the slope site.

d. If possible, unsaturated strength tests should be conducted to determine the unsaturated strength parameters. However, it is recognized that this is impractical for many situations. Thus, unsaturated strength parameters can be estimated from widely available empirical methods in combination with conducting high quality saturated strength tests to determine the effective stress friction angle ϕ'.

e. The effective stress cohesion intercept c' should be assumed equal to zero in the slope stability analyses.

2. For the purpose of evaluating shallow slope stability using a traditional drained analysis it is recommended to use fully softened strengths and pore pressure ratio, R_u, of 0.4. Fully softened strengths can be estimated using methods

described in this report or some other suitable method described in the literature. This analysis should be run for comparison even if the unsaturated analysis is conducted.

3. Conducting slope stability analyses using the recommendations provided should provide a reasonable approach to anticipate whether a given slope may fail at some point following construction due to drying and wetting cycles. If a slope is found to likely become unstable at some point in time, measures can be taken to improve the stability such as: changing the slope geometry, improving soil properties (such as using chemical additives or by reinforcement), or taking measures to reduce the likelihood of desiccation cracking (such as by adding a protective surface layer).

ACKNOWLEDGEMENTS

The authors are grateful for the financial support of the Oklahoma Department of Transportation and the Oklahoma Transportation Center, and for the logistical support and guidance of ODOT personnel in the Materials and Research Division. Thanks is extended to Michael Schmitz for his assistance with manufacturing and maintaining the equipment and to Wassim Tabet for his assistance with field work and laboratory desiccation experiments at the start of this project. Graduate students Tommy Bounds and Bo Zhang played a significant role in the field work and laboratory testing near the beginning of the project, for which the authors are grateful. Gratitude is further extended to all of the numerous other graduate and undergraduate students who contributed to the project through laboratory and/or field work.

REFERENCES

Li, A.G., Yue, Z.Q., Tham, L.G., Lee, C.F., and Law, K.T., (2005), "Field monitored variations of soil moisture and matric suction in saprolite slope," Can. Geotech J., 42: 13-26.

Albrecht, B., and Benson, C., (2001), "Effect of Desiccation on Compacted Natural Clays," Journal of Geotechnical and Geoenvironmental Engineering, 127(1): 67-75.

Al-Hussaini, M.M., and Townsend, F.C., (1974), "Investigation of Tensile Testing of Compacted Soils," U.S. Army Engineer Waterways Experiment Station, Soil and Pavement Laboratory, Vicksburg, Mississippi, USA.

Alonso, O.S., Vaunat, J., and Pereira, J.M. (2010), "A Microstructurally Based Effective Stress for Unsaturated Soils," Géotechnique, 60(12): 913-925.

Aubeny, C., and Lytton, R., (2004), "Shallow Slides in Compacted High Plasticity Clay Slopes," Journal of Geotechnical and Geoenvironmental Engineering, 130(7): 717-727.

Aubeny, C., and Lytton, R., (2002), "Properties of High Plasticity Clays," Technical Report.

Barzegar, A.R., Oades, J.M., Rengasamy, P., and Murray, R.S., (1995), "Tensile Strength of Dry Remoulded Soils as Affected by Properties of the Clay Fraction," Geoderma, 65(1–2): 93-108.

Briggs, K.M. (2010), "Changing embankment: climate change impacts on embankment hydrology," Ground Engng. 43(6): 28-31.

Cerato, A.B. and Nevels, J.B. (2007), "Shallow Slope Failure Analysis: McCurtain County, Oklahoma," Proc. 1st North American Lanslide Conference, Vail, Colorado, CD Proceedings.

Duncan J.M., Brandon T.M., and VandenBerge, D.R., (2011), "Report of the workshop on shear strength for stability of slopes in highly plastic clays," Center for Geotechnical Practice and Research, Blacksburg.

Fang, H.Y., and Fernandez, J., (1981), "Determination of tensile strength of soils by unconfined-penetration Test," ASTM STP 740, American Society for Testing and Materials, 130-144.

Florinsky, I., Eilers, R., Manning, G., Fuller, L., (2001), "Prediction of soil properties by digital terrain modelling," Environmental Modelling and Software 17, 295-311.

Fredlund D.G., and Rahardjo H., Soil Mechanics for Unsaturated Soils, John Wiley & Sons, 1993.

Hamid, T.B. and Miller, G.A. (2009), "Shear Strength of Unsaturated Soil Interfaces," Canadian Geotechnical Journal, 46, 595-606.

Hossain, K. (2010). "Effect of Rainfall on Matric Suction and Stability of a Residual Granite Soil Slope," Journal of Dhaka University of Engineering and Technology, 1(1).

Jones, E.W., Koh, Y.H., Tiver, B.J., and Wong, M.A.H., (2009), "Modelling the behaviour of unsaturated, saline clay for geotechnical design," School of Civil, Environmental and Mining Engineering, University of Adelaide.

Kayyal M.K., and Wright, S.G., (1991), "Investigation of Long-Term Strength Properties of Paris, and Beaumont Clays in Earth Embankments," Research Report 1195-2F, Center for Transportation Research, The University of Texas at Austin.

Khoury, C.N., and Miller G.A., (2012), "Influence of Hydraulic Hysteresis on the Shear Strength of Unsaturated Soils and Interfaces," Geotechnical Testing Journal, 35(1):135-149.
Kim, T., Kim, T., Kang, G., and Ge, L., (2012), "Factors Influencing Crack-Induced Tensile Strength of Compacted Soil," Journal of Materials in Civil Engineering, 24(3): 315-320.
Kim, T.H., and Hwang, C., (2003), "Modeling of Tensile Strength on Moist Granular Earth Material at Low Water Content," Engineering Geology, 69(3-4): 233-244.
Kim, Y.K., and Lee, S.R. (2010), "Field Infiltration Characteristics of Natural Rainfall in Compacted Roadside Slope," Journal of Geotechnical and Geoenvironmental Engineering, ASCE, 136(1): 248-252.
Yang, L., Wei, W., Chen, L. Jia, F., and Mo, B., (2012), " Spatial variations of shallow and deep soil moisture in the semi-arid Loess Plateau China," Hydrol. Earth Syst. Sci., 16 (9): 3199-3217.
Lakshmikantha, M.R., Prat, Pere C., and Ledesma, A. (2012), "Experimental Evidence of Size Effect in Soil Cracking," Canadian Geotechnical Journal, 49(3): 264-284.
McKeen, R.G., and Johnson, L. (1990), "Climate-Controlled Soil Design Paramters for Mat Foundations," ASCE Journal of Geotechnical Engineering, 116: 1073-1094.
Mesri, G., and Cepedia-Diaz A.F., (1986), "Residual shear strength of clays and shales," Geotechnique.
Mesri, G., and Shahien, M., (2003), "Residual Shear Strength Mobilized in First-Time Slope Failures," Journal of Geotechnical and Geoenvironmental engineering, January.
Miller, G.A., and Hamid, T.B., (2007), "Interface Direct Shear Testing for Unsaturated Soil," Geotechnical Testing Journal, 3(30).
Mohanty, B.P., and Skaggs, T.H., (2001), "Spatio-temporal evolution and time stable characteristics of soil moisture within remote sensing footprints with varying soil, slope, and vegetation," Advances in Water Resources, 24: 1051-1067.
Morris, P.H., Graham, J., and Williams, D.J., (1992), "Cracking in Drying Soils," Canadian Geotechnical Journal, 29(2): 263-277.
Penman, H.L., (1948), "Natural Evapotranspiration from Open Water, Bare Soil and Grass," Proc. R. Soc. London, Ser. A., 193: 120-145.
Qiu, Y., Fu, B., Wang, J., Chen, L., (2000), "Soil moisture variation in relation to topography and land use in a hillslope catchment of the Loess Plateau," China. Journal of Hydrology 240: 243-263.
Rahardjo, H., Ong, T., Rezaur, R., Leong E., (2007), "Factors Controlling Instability of Homogeneous Soil Slopes under Rainfall," Journal of Geotechnical and Geoenvironmental Engineering, ASCE December.
Ray, R.L., Jacobs, J.M., Ballestero, T.P. (2011), "Regional landslide susceptibility: Spatiotemporal variations under dynamic soil moisture conditions," Natural Hazards, 59: 1317-1337.
Rayhani, M. H., Yanful, E. K., and Fakher, A., (2007), "Desiccation-Induced Cracking and Its Effect on the Hydraulic Conductivity of Clayey Soils from Iran," Canadian Geotechnical Journal, 44(3): 276-283.

Salciarini, D., Godt, J.W., Savage, W.Z., Conversini, P., Baum, R.L., Michael, J.A., (2006), "Modeling regional initiation of rainfall induced shallow landslides in the eastern Umbria Region of central Italy," Landslides, 3: 181-194.
Simoni S, Zanotti F, Bertoldi G, Rigon R. (2008), "Modelling the probability of occurrence of shallow landslides and channelized debris flows using GEOtop-FS," Hydrological Processes, 22(4): 532-545
Skempton, A.W., (1970), "First time slides in over-consolidated clays," Geotechnique.
Skempton, A.W., (1977), "Slope stability of cuttings in Brown London clay," 9th International Conference on Soil Mechanics and Foundation Engineering.
Stark T.D., and Duncan J.M., (1991), "Mechanisms of strength loss in stiff clays," J. Geotech. Eng., 117: 139-154.
Stark T.D., and Hussain M., (2012), "Empirical correlations – drained shear strength for slope stability analyses," Paper# GTENG-2476 – Revision#2, ASCE Journal of Geotechnical and Geoenvironmental Engineering.
Stark, T., and Eid, H., (1997), "slope stability analyses in stiff fissured clays," Journal of Geotechnical and Geoenvironmental Engineering.
Tamrakar, S., Mitachi, T., Toyosawa, Y., and Itoh, K., (2005), "Development of a new soil tensile strength test apparatus," Site Characterization and Modeling, American Society of Civil Engineers, 1-10.
Trabelsi, H., Jamei, M., Zenzri, H., and Olivella, S., (2012), "Crack patterns in clayey soils: Experiments and modeling," International Journal for Numerical and Analytical Methods in Geomechanics, 36(11): 1410-1433.
Vanapalli, S.K., Fredlund, D.G., and Pufahl, D.E., (1996), "The relationship between the soil-water characteristic curve and the unsaturated shear strength of a compacted glacial till," American Society for Testing and Materials.
Van-Genuchten, M.T., (1980), "Closed-form equation for predicting the hydraulic conductivity of unsaturated soils," Soil Science Society of America Journal, 44(5): 892-898.
Wang, Z.F., Li, J.H., and Zhang, L.M., (2011), "Influence of Cracks on the Stability of a Cracked Soil Slope," 5th Asia-Pacific Conference on Unsaturated Soils, 2: 594-600.
Wheeler, S.J., Sivakumar, V., (1995), "An elasto-plastic critical state framework for unsaturated soil," Géotechnique, 45(1): 35-53.
Wilson, G.W., Fredlund, D.G. and Barbour, S.L., (1994), "Coupled soil-atmosphere modeling for soil evaporation," Canadian Geotechnical Journal, 31: 151-161.
Wright, S.G., Zornberg J.G., and Kuhn J., (2007), "Determination of Field Suction Values, Hydraulic Properties and Shear Strength in High PI Clays," Technical Report, The University of Texas at Austin.
Yeakley, J.A., Swank, W.T., Swift, L.W., Hornberger, G.M., Shugart, H.H., (1998), "Soil moisture gradients and controls on a southern Appalachian hillslope from drought through recharge," Hydrol Earth Syst Sci, 2 (1): 41-49.